國立台灣大學醫學院生物化學暨分子生物學研究所

博士論文

Graduate Institute of Biochemistry and Molecular Biology

College of Medicine

National Taiwan University

Doctoral Thesis

肝細胞癌之相關研究：

一、肝型脂肪酸結合蛋白促進肝細胞癌之血管新生及細胞移行

二、科羅索酸針對 VEGFR2/Src/FAK 路徑抑制肝細胞癌之細胞移行

Studies on Hepatocellular Carcinoma (HCC)：

I. Liver Fatty Acid-Binding Protein (L-FABP) Promotes Cellular Angiogenesis and Migration in Hepatocellular Carcinoma

II. Corosolic Acid Inhibits Hepatocellular Carcinoma Cell Migration by Targeting the VEGFR2/Src/FAK Pathway

辜琮祐

Chung-Yu Ku

指導教授：呂紹俊 博士(Shao-Chun Lu, Ph.D.)

林榮耀 博士(Jung-Yaw Lin, Ph.D.)

中華民國 104 年 6 月

June, 2015

國立臺灣大學博士學位論文
口試委員會審定書

中文題目：肝細胞癌之相關研究

一、肝型脂肪酸結合蛋白促進肝細胞癌之血管新生及細胞移行

二、科羅索酸針對 VEGFR2/Src/FAK 路徑抑制肝細胞癌之細胞移行

英文題目： **Studies on Hepatocellular Carcinoma (HCC)**

I. Liver Fatty Acid-Binding Protein (L-FABP) Promotes Cellular Angiogenesis and Migration in Hepatocellular Carcinoma

II. Corosolic Acid Inhibits Hepatocellular Carcinoma Cell Migration by Targeting the VEGFR2/Src/FAK Pathway

本論文係 辜琮祐 君（學號 D97442007）在國立臺灣大學生物化學暨分子生物學研究所完成之博士學位論文，於民國一百零四年六月二十四日承下列考試委員審查通過及口試及格，特此證明

口試委員：

林俊宏 博士（指導教授）

呂紹俊 博士（指導教授）

方剛 博士

李德章 博士

李明學 博士

系主任、所長 林敬哲 （簽名）

致 謝

首先，誠摯的感謝我的指導教授：林榮耀教授與呂紹俊教授，兩位老師悉心的教導使我得以一窺癌症生物學及抗癌藥物機轉領域的深奧，並不時的討論指點我正確的方向，使我在唸博士班的這些年中獲益匪淺，老師對於學問及實驗態度上的嚴謹更是我學習的典範。感謝李明學教授及李德章教授在進度報告以及論文修改上的建議；感謝方剛教授在口試前熱心幫忙讓口試能順利進行；感謝詹迺立教授在結構生物學上提供幫助；感謝周綠蘋教授推薦我加入 R942 這個大家庭，並且總是很關心我的博士生涯；感謝游偉絢教授樂於分享他研究的成果，還不嫌棄我的排球技術；最後要感謝台大醫學院生化分生所上的每位老師，不論在專題報告或研究中，都啟發了我在實驗設計及邏輯思考的能力。

七年的日子，不論是在 R942 或 D208，實驗室裡共同的生活點滴，學術上的討論，當然還有不能讓老師知道的奇幻旅程以及每周固定的活動筋骨。感謝各位學長姐、同學、學弟妹的陪伴，讓這些日子能過得多采多姿。

感謝郁蕙學姐給我許多實驗上的協助，以及讓我了解如何與老師溝通的技巧；感謝玄原學長總是一肩扛起實驗室大大小小的事情，讓我能心無旁騖的進行研究；感謝賽文學長讓我見識到國境之南及蓬萊之巔的景色，學長爽朗又滄桑的笑聲道盡了實驗生涯的一切；感謝子玲學姐總是在見面時給我一個溫暖的微笑，並一起體驗了難得的總區助教經驗；感謝我的好同學：志強、俊榮、郁鈴、昭圻、雅姿以及很少見面的曹甯與婕伶，在之後的人生中我相信大家一定都能在自己的領域找到一片天；感謝台大與師大的學弟妹們：孟倫、詩瑾與銘得，雅月與柏均，綱緒、銘亨與賀培，柏劭、瑀萱與蕭甄，還有喬偉與庭瑋，大家一起見識了 R942 到 D208 的演變，太多的回憶無法一一細數；感謝芬如學姐辛苦的報帳，並讓大家每次都能一飽口福；感謝瓊瑛學姐與所辦的長輩們分享許多處事的經驗；秀儀、慶桂、怡伶、嘉嬣、啟榮，喜甄與和惠，你們在實驗上的幫忙與協助讓我銘感在心。

特別感謝我的老婆—佳純與她的老師—顧記華教授；佳純一路上陪著我，從中國醫，北醫，再到台大，要同時兼顧老婆、媳婦、及母親的角色，蠟燭多頭燒的辛苦我都看在眼裡；而顧老師除了在我投稿論文階段給予很大的幫助之外，也讓我很放心佳純在實驗及工作上，能一路順遂；如果沒有你們，我不可能撐得過這些日子。宗佑、丞斌與鄉民保護協會的大家，是與你們的歡樂時光讓我能在一天辛苦的實驗結束後，至少還能笑著繼續明天的挑戰。

最後，謹以此文獻給我摯愛的父母，這段時間我沒能好好的陪伴你們，你們是我能安心求學最大的後盾；我的岳父岳母，感謝你們肯將女兒嫁給當時還沒畢業的我，而現在我也終於不用再拒絕你們釣遊四海的邀約了；我的妹妹—千芬，希望我這個哥哥還能不讓妳覺得失望；還有在最後趕著來報到，讓我能沾上許多好運的女兒—曼姿，是妳可愛的照片讓我在實驗室能度過許多寂寞的夜晚。

感謝一路上每一位幫助我、陪伴我的親人、朋友與同學，謝謝大家！

琮祐 謹上 中華民國一百零四年七月一日

Contents

Page

Abbreviations 1

中文摘要 3

Abstract 5

Introduction

Hepatocellular carcinoma 7
Vascular endothelial growth factor and HCC 7
Liver fatty acid-binding protein (L-FABP) 8
Lipid rafts, receptor tyrosine kinases (RTKs) and non-receptor tyrosine kinases 9
Chinese herbal medicines and *Actinidia chinensis* 10
Corosolic acid (CA) 11

Materials and methods

Part I

Antibodies used for western blot analysis and chemical inhibitors 12
Tissue microarray construction and immunohistochemistry 12
Cell culture 13
Creation and culture of L-FABP overexpressed stable clones 13
Western blot analysis and immunoprecipitation 14
Cell migration assay 14
Angiogenesis activity assay 15
Short interference RNA (siRNA) and short hairpin RNA (shRNA) 16
Lipid rafts isolation 17
Confocal microscopy analysis 18
Small GTPase binding assay 18
Construction of human VEGF-A promoter 19
Luciferase reporter assay 19
Animals 20
Cloning of L-FABP mutants 21
Statistical analysis 21

Part II

Plant extracts 22
HPLC analysis 22
Reagents 22
Cell culture 23
Cytotoxicity assay 23
Migration assay 24
Immunoprecipitation 24
Western blot analysis 25
Kinase activity assay 25
Rho GTPase activity assay 26
G-actin/F-actin activity assay 26
Confocal microscopy analysis 27
Animal model 27
Immunohistochemistry 29
Synergistic analysis 29
Molecular docking 29
SRB cell growth assay 30
Statistical analysis 30

Results

Part I

1. Up-regulation of L-FABP expression in HCC tissues is correlated with VEGF-A overexpression 31
2. L-FABP induces VEGF-A expression and angiogenic potential in immortalized Hus and Huh7 cells 31
3. Association of L-FABP with VEGFR2 in membrane rafts 33
4. L-FABP increases VEGFR2/Src phosphorylation and cell migration by FAK/cdc42 pathway 34
5. L-FABP induced VEGF-A expression by Akt/mTOR/P70S6K/4EBP1 in translation level 35
6. L-FABP promoted tumor growth and metastasis *in vivo* 36
7. Cholesterol binding and membrane interacting properties are essential for L-FABP induced cell migration and angiogenesis 37

Part II

8. Corosolic acid significantly decreases the migration activity of Huh7 cells 38
9. Corosolic acid inhibits VEGFR2 kinase activity 39

10. Corosolic acid decreases cell motility by inhibiting VEGFR2/Src/FAK/cdc42 activity and actin rearrangement 40
11. Corosolic acid exhibits anti-tumor effect *in vivo* 41
12. Synergistic effects of corosolic acid and sorafenib on HCC cells 42
13. Corosolic acid interacts with the ATP-binding site of VEGFR2 kinase domain by molecular docking 43
14. Corosolic acid does not exhibit significant inhibitory effects on Huh7 cell 43

Discussion

Part I

Role of L-FABP in hepatocellular carcinoma 45

Part II

Effects of corosolic acid on hepatocellular carcinoma 50

Summary 53

Figures and Figure legend

Part I

Figure 1. Correlation between the expression levels of L-FABP and VEGF-A 54
Figure 2. L-FABP expression is associated with VEGF-A expression of HCC cells 55
Figure 3. Expression level of VEGF-A is up-regulated in L-FABP stably expressed Hus cells 56
Figure 4. L-FABP promotes in vitro and in vivo angiogenic activity of Hus cells 57
Figure 5. Sequence aliment of L-FABP interacting domains 58
Figure 6. Co- immunoprecipitation of L-FABP and VEGFR2 in Hus/L-FABP cells 59
Figure 7. L-FABP associates with VEGFR2 in apical membrane of Hus/L-FABP cells 60
Figure 8. Localization of L-FABP and signaling molecules in lipid rafts 61
Figure 9. L-FABP increases the phosphorylation level of VEGFR2 in Hus cells 62
Figure 10. L-FABP increases the phosphorylation level of Src and FAK kinases in Hus cells 63
Figure 11. L-FABP promotes cdc42 activity of Hus cells 64
Figure 12. Analysis of migration activity of L-FABP stably expressed Hus cells 65
Figure 13. L-FABP up-regulates migration activity through VEGFR2/ Src pathway 66
Figure 14. L-FABP activates Akt/ mTOR/ P70S6K/ 4EBP1 signaling 67
Figure 15. HIF-1α significantly enriched in the nucleus of L-FABP overexpressed cells 68

Figure 16. Role of HIF-1α in VEGF-A transcriptional activity of L-FABP overexpressed cells 69
Figure 17. Post-transcriptional regulation of VEGF-A in L-FABP stably expressed Hus cells 70
Figure 18. L-FABP promotes tumor growth *in vivo* 71
Figure 19. L-FABP promotes *in vivo* metastasis by lung metastasis model 72
Figure 20. Effect of L-FABP mutants in VEGF-A expression 73
Figure 21. Effect of L-FABP mutants in migration activity 74
Figure 22. Cholesterol binding properties are essential for L-FABP induced cell migration and angiogenesis 75
Figure 23. Knockdown of L-FABP in Hus/L-FABP cells reversely decreased VEGF-A expression and migration activity 76
Figure 24. Knockdown of L-FABP in Huh7 cells down-regulates VEGF-A expression and migration activity 77
Figure 25. Reduction of L-FABP and VEGFR2 co-localization on membrane is observed in Huh7 L-FABP stably knockdown cells 79
Figure 26. Aberrant overexpression of L-FABP in HCC tissues (with cirrhosis) is associated with worse outcome 80

Part II

Figure 27. Cytotoxicity and migration inhibitory effect of *Actinidia chinensis* on Huh7 cells 81
Figure 28. HPLC analysis of *Actinidia chinensis* 82
Figure 29. Migration activity of Huh7 cells is inhibited by corosolic acid without cytotoxicity 83
Figure 30. Corosolic acid reduces phosphorylation level of VEGFR2 84
Figure 31. Corosolic acid reduces VEGFR2 kinase activity 85
Figure 32. CA-induced inhibition of migration activity in Huh7 cells is VEGFR2 dependent 86
Figure 33. Corosolic acid down-regulates VEGFR2 downstream signals 87
Figure 34. Corosolic acid inhibits cdc42 activity 88
Figure 35. Effect of corosolic acid on actin rearrangement 89
Figure 36. Corosolic acid exhibits significant anti-tumor effects on Huh7 cells *in vivo* 90
Figure 37. Combinatorial effects of corosolic acid and sorafenib on migration activity of Huh7 cells 92
Figure 38. Combinatorial effects of corosolic acid and sorafenib on signaling molecules of Huh7 cells 93
Figure 39. Combinatorial effects of corosolic acid and sorafenib on Huh7 cells by 94

in vivo xenograft model
Figure 40. Inhibitory effects of corosolic acid combined with sorafenib on Src and FAK kinases *in vivo* 95
Figure 41. Corosolic acid interacts with the ATP-binding site of VEGFR2 kinase domain by molecular docking analysis 96
Figure 42. Analysis of relative distance and surface charge distribution between corosolic acid and VEGFR2 ATP binding pocket 97
Figure 43. Corosolic acid inhibits growth of Huh7, HepG2, and Hep3B cells 98
Figure 44. Cytotoxicity and migration-inhibitory effects of corosolic acid on HepG2 cells 99
Figure 45. Cytotoxicity and migration-inhibitory effects of corosolic acid on Hep3B cells 100
Figure 46. Corosolic acid doesn't exhibit significant inhibitory effect on invasion activity of Huh7 cells 101
Figure 47. Corosolic acid shows no inhibitory effect on NFκB signaling 102

Tables

Table 1. Correlation between L-FABP and VEGF-A protein expression in tissue pairs from 90 HCC patients 103
Table 2. Clinical characteristics of the cases included in analyses of L-FABP protein expression evaluated by immunohistochemistry 103
Table 3. Association of L-FABP protein expression with clinical pathologic characteristics in patients with HCC 104

Supplementary data

Table 1 105
Figure 1. Knockdown of VEGFR2 in Hus/L-FABP cells decreased the activation of down-stream signaling molecules 107
Figure 2. Prediction of the interaction models of L-FABP and VEGFR2 kinase domain 108
Figure 3. Amino acid substitution of L-FABP in present studies 109

References

110

Publications

List of Abbreviation

L-FABP:	Liver fatty acid-binding protein
HCC:	Hepatocellular carcinoma
VEGF-A:	Vascular endothelial growth factor A
VEGFR2:	Vascular endothelial growth factor receptor 2
Akt:	Protein kinase B
mTOR:	Mammalian target of rapamycin
P70S6K:	70 kDa ribosomal protein S6 kinase 1
4EBP1:	Eukaryotic translation initiation factor 4E-binding protein 1
Src:	Proto-oncogene tyrosine-protein kinase Src
FAK:	Focal adhesion kinase 1
CDC42:	CDC42 small effector protein 1
HIF-1α:	Hypoxia-inducible factor 1-alpha
PI3K:	Phosphoinositide 3-kinase
P.H. medium:	Primary hepatocyte used medium
HEPES:	4-(2-hydroxyethyl)-1-piperazineethanesulfonic acid
DMEM:	Dulbecco's modified eagle medium
DMSO:	Dimethyl sulfoxide
G418:	Geneticin
HUVEC:	Human umbilical vein endothelial cells
NOD/SCID mice:	NOD.CB17-Prkdcscid/NcrCrl mice
siRNA:	Small interfering RNA
shRNA:	Short hairpin RNA
O/N:	Overnight
GTPase:	Hydrolase enzymes that can bind and hydrolyze guanosine

	triphosphate (GTP)
Rac1:	Ras-related C3 botulinum toxin substrate 1
RhoA:	Ras homolog gene family, member A
GST-PBD:	Fusion protein of GST tag with The Rac/Cdc42 (p21) binding domain
GST-RBD:	Fusion protein of GST tag with the Rho binding domain
TNM stage:	Tumor, lymph nodes, metastasis stage of cancer classification
CD31:	Platelet endothelial cell adhesion molecule
Sorafenib:	Nexavar
PP1:	Src inhibitor (CAS 172889-26-8)
MG132:	Inhibitor of proteasome (CAS 133407-82-6)
MβCD:	Methyl-beta-cyclodextrin
MTT:	3- (4, 5-cimethylthiazol-2-yl)-2, 5-diphenyl tetrazolium bromide
SRB:	Sulforhodamine B
F-actin:	Filamentous actin
G-actin:	Globular actin

中文摘要

國際上肝細胞癌在癌症發生率中排行第五，在癌症致死率中排行第三。肝細胞癌的生長及進展仰賴於新生血管的形成，而血管內皮生長因子(VEGF)在此過程中扮演非常重要的角色。

肝型脂肪酸結合蛋白（L-FABP）在肝細胞中大量表現，並已知可參與脂質代謝。L-FABP 過度表現已在許多癌症中被發現，但它在肝細胞癌中扮演的角色仍不清楚。本研究中，我們分析了 L-FABP 與 VEGF 在 90 個 HCC 患者中的關聯性。我們發現，L-FABP 在肝癌組織中與 VEGF-A 呈現正相關性。此外，L-FABP 在異種移植小鼠模式中可顯著促進腫瘤生長及轉移。我們亦討論 L-FABP 活性與腫瘤生成的關係：L-FABP 可與細胞膜上脂筏中的 VEGFR2 結合，接著活化下游的 Akt/mTOR/P70S6K/4EBP1 與 Src/FAK/CDC42 路徑，這也使得 VEGF-A 表現量增加，並促進血管新生與細胞移行之活性。我們的研究結果證實，L-FABP 可望成為治療肝癌的新目標。

在臨床上，抑制第二型血管內皮生長因子受體(VEGFR2)之活性已被建議作為治療 HCC 的重要策略。本研究中，我們發現獼猴桃根部之化合物，科羅索酸(CA)，對肝癌細胞表現出顯著的抗癌作用。研究指出， CA 可透過與 VEGFR2 上 ATP 結合口袋的交互作用，抑制 VEGFR2 之活性。 CA 在 Huh7 細胞實驗中可抑制性調控 VEGFR2/Src/FAK/CDC42 路徑，減少絲狀肌動蛋白（F-actin）之形成，並降低細胞移行能力。在動物實驗中，CA 對腫瘤生長的有效抑制劑量為每隻小鼠給予 5 毫克/公斤/天。我們也證實， CA 與蕾莎瓦(Sorafenib)在廣範圍濃度下具有協同效應。本研究闡明了 CA 抗肝癌的細胞分子機制，並建議 CA 可作為治療侵襲性肝癌之抗癌藥或佐劑。

關鍵詞：

肝細胞癌，血管新生作用，肝型脂肪酸結合蛋白，血管內皮生長因子，科羅索酸，細胞移行，第二型血管內皮生長因子受體

Abstract

Hepatocellular carcinoma (HCC) is the fifth most commonly occurring cancer and the third most common cause of cancer death worldwide. The progression of HCC relies on the formation of new blood vessels, and VEGF is critical in this process.

Liver fatty acid-binding protein (L-FABP) is abundant in hepatocytes and known to be involved in lipid metabolism. Overexpression of L-FABP has been reported in various cancers; however, its role in hepatocellular carcinoma (HCC) remains unclear. In this study, we investigated L-FABP and its association with vascular endothelial growth factors (VEGFs) in 90 HCC patients. We found that L-FABP was highly expressed in their HCC tissues, and its expression level was positively correlated with that of VEGF-A. Additionally, L-FABP significantly promoted tumor growth and metastasis in a xenograft mouse model. We also studied the mechanisms of L-FABP activity in tumorigenesis: L-FABP was found to be associated with VEGFR2 on membrane rafts and subsequently activate the Akt/mTOR/P70S6K/4EBP1 and Src/FAK/cdc42 pathways. This resulted in up-regulation of VEGF-A expression accompanied by an increase in both angiogenic potential and migration activity. Taken together, our results suggest that L-FABP may be a potential target for HCC chemotherapy.

Inhibition of VEGFR2 activity has been proposed as an important strategy for the

clinical treatment of hepatocellular carcinoma (HCC). In this study, we identified corosolic acid (CA), which exists in the root of *Actinidia chinensis* (藤梨), as having a significant anti-cancer effect on HCC cells. We found that CA inhibits VEGFR2 kinase activity by directly interacting with the ATP binding pocket. CA down-regulates the VEGFR2/Src/FAK/cdc42 axis, subsequently decreasing F-actin formation and migratory activity of Huh7 cells *in vitro*. In an *in vivo* model, CA exhibites an effective dose (5 mg/kg/day) on tumor growth, and we further demonstrate that CA has a synergistic effect with sorafenib within a wide range of concentrations. In conclusion, we elucidate the effects and molecular mechanism for CA on HCC cells and suggest that CA could serve as a therapeutic or adjuvant target for patients with aggressive HCC.

Keywords:

Hepatocellular carcinoma, angiogenesis, liver fatty acid-binding protein, vascular endothelial growth factor, corosolic acid, migration, vascular endothelial growth factor receptor-2 (VEGFR2)

Introduction

Hepatocellular carcinoma

Hepatocellular carcinoma (HCC), the most common type of liver cancer, is notoriously resistant to systematic therapies, and often accompanied by high recurrence. Because of its poor prognosis, HCC causes more than 700,000 deaths annually and becomes the third leading cause of cancer-related death worldwide [1, 2]. Previous studies have implicated several emerging pathways in HCC, such as HGF/MET, Wnt/β-catenin, and VEGF/VEGFR, can serve as novel molecular targets for developing anti-HCC therapies [3-5].

Vascular endothelial growth factor and HCC

Angiogenesis is known to play an important role in progression and metastasis of HCC. Vascular endothelial growth factor (VEGF) is a critical driver to stimulate new blood vessel formation to supply sufficient nutrients and oxygen for sustained tumor growth [1]. VEGF can bind to three similar receptor tyrosine kinases, including VEGFR1 (FLT1), VEGFR2 (KDR) and VEGFR3 (FLT4) by different affinities, yet VEGFR2 is the major receptor for VEGF-induced signaling, and serves as the main therapeutic target [6]. Previous studies also suggested a strong correlation of VEGFR2 expression with HCC malignance and liver cirrhosis [7, 8]. However, since HCC

patients are often diagnosed at an advanced stage accompanied with tumor angiogenesis and metastasis, VEGF-targeted therapies were seemed to have apparent therapeutic benefits [2, 9].

Liver fatty acid-binding protein (L-FABP)

Liver fatty acid-binding proteins (L-FABP) is a member of the FABP family, which expresses abundantly in cytoplasm and is capable of binding hydrophobic lipid ligands with a high specificity. The FABP family proteins (~15 kDa) show moderate amino acid sequence homology, but highly similar tertiary structures, which are formed in a β-barrel shape. L-FABP can uniquely bind two ligand molecules (long chain fatty acids), or a various hydrophobic molecules, such as cholesterol and bile acids [10]. Furthermore, L-FABP can interact with plasma membrane to enhance cholesterol transfer or participate in membrane microdomains alteration [11], but its detailed mechanisms are less known.

Overexpression of L-FABP was observed in various cancer types, including liver [12], lung [13], gastric [14], pancreatic [15] and breast cancers [16, 17]. Although some studies have yielded contradictory findings that L-FABP expression is decreased in HCC [18], several reports showed that L-FABP expression was correlated with VEGF expression in HCC [12] and breast cancer [19], and the precise mechanisms remain to

be studied.

Lipid rafts, receptor tyrosine kinases (RTKs) and non-receptor tyrosine kinases

Lipid rafts are ordered structures of membrane microdomains, characterized by high concentration of cholesterol and glycosphingolipids, and are involved in fundamental cellular functions such as endocytosis, protein trafficking, and signal transduction [20]. A prominent feature of lipid rafts is their insolubility in neutral detergents such as Triton X-100, a reason for which they are often referred to as detergent-insoluble membranes (DIMs). The ability of lipid rafts to enhance receptor signaling has led to the concept of a signalosome– a region where proteins are localized together to facilitate receptor signaling. For example, rafts may contain incomplete signaling pathways that are activated when a receptor and/or other required molecules are recruited into the raft [21].

Receptor tyrosine kinases are a prominent example of the proteins involved in cell signaling that are enriched in lipid rafts. The EGF receptor, the insulin receptor, the PDGF receptor, the VEGF receptor and the NGF receptor among others have been shown to be localized to low density, cholesterol-rich membrane domains [22]. In all cases, signaling by these receptors is modulated by changes in cellular cholesterol content. Thus, raft localization appears to be of functional importance to the receptors.

Non-receptor tyrosine kinases in lipid rafts

Lipid rafts are also thought to play a central role in facilitating signal transduction from non-receptor tyrosine kinases. Signaling molecules such as Src family protein tyrosine kinases and small GTP-binding proteins of the Ras superfamily can localize to rafts by virtue of lipid modification [23]. Other signaling enzymes such as PI3K also localize to rafts, but the mechanism of their recruitment to these microdomains is unclear. Disruption of lipid rafts by cholesterol depletion agent: methyl-beta-cyclodextrin (MβCD), could inhibit multiple downstream signals of RTKs, including Src, FAK and Akt [24]. Mutation of the myristate or palmitate modification sites in Src kinases inhibits their partitioning into lipid rafts and blocks downstream signaling [25].

Chinese herbal medicines and *Actinidia chinensis*

Chinese herbal medicines (CHMs) have been used as potential therapies for a variety of human diseases, including hypertension, inflammation, and cancer [26]. Recent studies suggest that CHMs can be used to improve the efficiency of conventional cancer therapies and relieve the side effects of chemotherapies [27].

Anti-cancer effects of *A. chinensis* on cell proliferation, apoptosis, and angiogenesis have been noted in previous studies [28, 29]. In our study, *A. chinensis*

was found to exhibit a significant anti-migratory effect to Huh7 cells, and the IC_{50} migration of *A. chinensis* was identified as 0.2 mg/ ml. The cytotoxic effect of *A. chinensis* to Huh7 cells was between 0.5–4 mg/ml (Figure 27, A and B).

Corosolic acid (CA)

Corosolic acid (CA) is an ursane-type triterpenoid, and is known to be a STAT3 inhibitor in macrophages, myeloid cells, and ovarian cancer cells [30-32]. CA also has a significant inhibitory effect on endothelial angiogenic tube formation [29], and tumor growth in lung and ovarian cancer cells [31, 33]. In the above mentioned study, we observed that *A. chinensis* water extracts had an anti-migration effect in Huh7 cells. Therefore, we performed HPLC analysis and identified the active component of *A. chinensis*; corosolic acid (CA), which comprised about 8.4% of the dry weight of *A. chinensis* (Figure 28), was suggested to be a novel anti-HCC compound in our studies.

Materials and methods

§Part I

Antibodies used for western blot analysis and chemical inhibitors

Antibodies specific to L-FABP, VEGF-A, Flotillin-2, Lamin A/C, α-tubulin and β-actin were purchased from Santa Cruz Biotechnology, USA. Antibodies specific to VEGFR2, phospho-VEGFR2, Src, phospho-Src, FAK, phospho-FAK, PI3K (p85), Akt, phospho-Akt, mTOR, phospho-mTOR, phospho-4EBP1, 4EBP1 and HIF-1α were obtained from Cell Signaling Technology, USA. The chemical inhibitor Src inhibitor I was from Calbiochem, and Sorafenib was obtained from Selleckchem, USA.

Tissue microarray construction and immunohistochemistry

The tumor and adjacent normal tissues array (HLiv-HCC180Sur-02) were purchased from US Biomax, Inc. The microarray sections were immunestained with specific antibodies against L-FABP (1:100) and VEGF-A (1:100), respectively. The staining results were interpreted by pathologists of GenDiscovery Biotechnology, Taiwan. The staining results were emerged for intensity and percentage of staining area, respectively, and calculated by Quick-score analysis which scored by multiplying the percentage of positive cells (P) by the intensity (I). Formula: $Q = P \times I$; Maximum = 300. The results were then graded according to the following criteria: 1 for score 0-99, weak

staining; 2 for score 100-199, moderate staining; 3 for score 200-299, strong staining; 4 for score 300, very strong staining.

Cell culture

Huh7 cells were obtained from Japanese Collection of Research Bioresources (National Institute of Health Sciences; Japan, JCRB), and maintained in Dulbecco's modified Eagle's medium (DMEM) with 10% FBS. The immortalized cell line derived from human primary hepatocytes, Hus-E/2 (Hus), was cultured in P.H. medium (DMEM which contains 20 mM HEPES, 15 μg/ml L-proline, 0.25 μg/ml insulin, 50 nM dexamethasone, 44 mM sodium bicarbonate, 10 mM nicotinamide, 5 ng/ml EGF, 0.1 mM ascorbic acid). All of these cell lines were incubated in 5% CO_2 atmosphere at 37°C.

Creation and culture of L-FABP overexpressed stable clones

The pcDNA3.1/L-FABP was constructed by inserting full-length L-FABP cDNA fragment (1-121 aa) in the pcDNA3.1 Vector via TOPO PCR cloning system (Life technologies, USA), which was cloned by cDNA of Huh7 cells, and the construct was checked by nucleotide sequencing. Hus cells were transfected with pcDNA3.1/L-FABP using the Lipofectamine 2000 (Invitrogen, USA). Stable clones were selected by

medium containing 1 mg/ml G418 (Sigma-Aldrich, USA) for 2-4 weeks. Each of the clones was checked for L-FABP expression twice per month by western blot analysis.

Western blot analysis and immunoprecipitation

Purified proteins (50 μg) were resolved by 10% sodium dodecyl sulfate (SDS)-polyacrylamide gel electrophoresis and transferred to polyvinylidene fluoride (PVDF) membranes (Millipore, Bedford, MA, USA). The membrane was incubated with primary antibodies followed by horseradish peroxidase-conjugated secondary antibodies (Chemicon International, USA). Signals were visualized using enhanced chemiluminescence detection reagent from Millipore, and the images were obtained using a Luminescence/Fluorescence Imaging System (LAS-4000, Fuji).

For immunoprecipitation, cell lysates (500 μg protein) were pre-cleared by protein A/G Sepharose beads (Millipore), and then incubated with anti-L-FABP or anti-VEGFR2 antibody overnight at 4°C. The immunoprecipitated complexes were washed three times by ice-cold PBS, and captured by protein A/G Sepharose beads, and then the immunoprecipitated proteins were subjected to western blot analysis.

Cell migration assay

Transwell Boyden chambers (Millipore) were applied to cell migration and invasion assays. For migration assay, cells were maintained in serum-free medium for

24 h and then seeded into the chambers, and followed by incubation in complete medium with 10% fetal bovine serum at 37°C for 16 h. The cells on the bottom side of the membrane were fixed with 1% formaldehyde/phosphate buffered saline for 15 min, stained with 0.1% crystal violet for 40 min and counted using an inverted contrast light microscope.

Angiogenesis activity assay

1. Cell culture

Primary HUVEC (Sciencell, California, USA) were grown in M199 medium containing with Endothelial Cell Growth Supplement (ECGS) (100 μg/ml), 10 ng/ml heparin, and 5% fetal bovine serum (FBS) and cultured in 5% CO_2 atmosphere at 37°C.

2. *In vitro* tube formation assay

A 24-well plate was coated with 100 μl of Matrigel (1 mg/ml; BD Biosciences), which was allowed to solidify at 37°C for 1 h. HUVEC (1×10^4 cells per well) were seeded on Matrigel and incubated with the conditioned medium collected from the indicated cultured cells (L-FABP overexpressed Hus cells or L-FABP stable knockdown Huh7 cells) for 8~12 h, whereas the VEGF group was used to check the angiogenic activity of HUVEC cells. Photographs from random fields were taken using a microscope (Olympus, DP-50, Tokyo, Japan), and the quantification of each images was

followed by the following formula [34],

Angiogenic score= [(No. of sprouting cells) ×1 + (No. of connected cells) ×2 + (No. of polygons) ×3)] / Total number of cells + [0, 1 or 2]

The definition of cell types and parameters 0, 1 or 2 can be found in the above mentioned studies.

3. *In vivo* Matrigel plug assay and CD31 IHC staining

Matrigels (phenol red-free, BD Biosciences) were mixed with L-FABP overexpressed or L-FABP-knockdown stable clones (2×10^6 cells/ matrigel/ mouse). The Matrigel plugs were subcutaneously injected into 4-week-old male NOD/SCID mice, and then recovered on day 10 for following analysis. We performed CD31 IHC staining to determine the angiogenic activity of these tissues, since CD31 is used to serve as a superior marker for angiogenesis [35]. For detail, samples were fixed in 10% paraformaldehyde, embedded in paraffin, sectioned, and then subjected to immunohistochemical staining with the Novolink Polymer Detection System (Leica Biosystems). The sections were stained for CD31 (Santa Cruz Biotechnology), and the nuclei were counterstained with hematoxylin.

Short interference RNA (siRNA) and Short hairpin RNA (shRNA)

The modified oligonucleotides used as siRNA for L-FABP and the control siRNA

were obtained from Invitrogen. The shRNA clones were purchased from National RNAi Core Facility Platform, Taiwan. For transfection, 1 $\times 10^5$ of Hus/L-FABP or Huh7 cells were plated in a six-well plate for 24 h, and siRNA or shRNA transfection was performed using the Lipofectamine 2000 (Invireogen) to knockdown mRNA expression [36].

Lipid rafts isolation

Raft microdomains were purified by method described previously [37]. Briefly, cells were washed and applied to 700 μl 1% Triton X-100 lysis buffer, and the cell membrane was disrupted by using a Teflon-coated dounce homogenizer (20-30 strokes). The lysate (4 mg) was then incubated at 4°C for 30 min, and mixed with the same volume of 80% sucrose solution to yield a mixture at a final of 40% sucrose gradient and then transferred into a 12 ml polyallomer ultracentrifuge tube (for an SW41 roter, Beckman Instruments). Then, 6.5 ml of 30% and 3.5 ml of 5% sucrose cushion was overlaid on the top of sample and applied to ultracentrifugation at 187,813 g, 20 h, 4°C using SW41 rotor. The floating opaque band corresponding to the detergent-resistant lipid rafts was collected and used for western blot analysis.

Confocal microscopy analysis

L-FABP stable expressed Hus cells were seeded on the 22 × 22 cover slide, washed, fixed, and permeabilized with 0.25% Triton X-100 for 10 min. For double staining, the slides were first incubated with L-FABP and VEGFR2 primary antibody O/N, and then stained with Alexa488 (anti-mouse) and Alexa568 (anti-rabbit) (20 mU/mL) for 1 h in darkness, followed by counter-staining for nuclei with DAPI (10 ng/mL) for 10 min. By using Leica TCS SP5 Spectral Confocal System, the images were captured and analyzed.

Small GTPase binding assay

The small GTPase binding assay was referred to previous study [38]. For detail, 1×10^7 cells were seeded and collected in 0.4 ml of ice-cold lysis buffer (50 mM Tris-HCl, pH 7.5, 10 mM MgCl2, 500 mM NaCl, 1% Triton X-100, and protease inhibitor cocktail). After lysis for 20 min on ice, cell debris was removed by centrifugation at 300 g for 10 min at 4°C. Half of each lysate (100 μg protein) was mixed with 15 μl of GST-PBD or GST-RBD beads (50 μg of protein) and incubated for 1 h at 4°C with rotation. Samples were then centrifuged (5,000 rpm for 1 min at 4°C) and washed twice in ice-cold wash buffer (25 mM Tris-HCl, pH 7.5, 30 mM MgCl2, and 40 mM NaCl), finally resuspended in 30 μl SDS sample buffer and heated at 100°C

for 5 min, and then processed for western blot analysis.

Construction of human VEGF-A promoter

The VEGF-A promoter (full-length, bp -1127 to +73, total 1190 bps) was synthesized by ShineGene Molecular Biotech Inc, and constructed into puc57 vector. By cutting with SacI and HindIII restriction enzymes, the full length promoter was cloned into pGL4.22 luciferase reporter vector. The 5' serial deletion constructs of VEGF-A promoter were generated and named as follows: D1: bp -901 to +73; D2: bp -782 to +73; D3: bp -199 to +73. The primers used in the above cloning were listed in supplementary data, Table 1, and all constructs were checked by nucleotide sequencing.

Luciferase reporter assay

Luciferase activities were determined using Dual-Luciferase Reporter Assay System (Promega, USA). L-FABP overexpressed Hus cells were transfected with constructed pGL4.22/ VEGF-A promoter plasmids and pGL4-Renilla luciferase control reporter plasmid as an internal control. For 24 h incubation after transfection with lipofectamine 2000, the cells were lysed and the luciferase activities were examined by using the above assay system following the technical manual (Promega) and measured by SpectraMax L luminometer.

Animals

All animal experiments were carried out according to regulations approved by the Institutional Animal Care and Use Committee of College of Medicine, National Taiwan University. Male NOD-SCID mice (4 weeks old) were obtained from the LASCO Taiwan Co., Ltd. For xenograft experiments, Hus/L-FABP or Hus/Vector cell lines (2×10^6 cells each) were suspended in 200 μl of OPTI-MEM (Invitrogen) and inoculated into the right hind limb of each mice (n=6 for each group). Tumor size was measured twice per week with calipers, and the tumor volume was estimated using the formula: $(\text{width})^2 \times \text{length}/ 2$. After 8 weeks, the mice were anesthetized by Zoletil 50 (Virbac Animal Health) and sacrificed by CO_2 euthanasia, and the tumors were removed, measured, and processed for immunohistochemistry.

For metastasis assay, we used lung metastasis model according to previous studies [39]. For detail, Hus/L-FABP or Hus/Vector cell lines (4×10^6 cells each) were suspended in 100 μl of OPTI-MEM, and inoculated i.v. into the tail vein of male NOD/SCID mice (n=6 for each group). The experimental mice were anesthetized by Zoletil 50 (Virbac Animal Health) and sacrificed by CO_2 euthanasia after 10 weeks; the metastatic colonies in lungs of each mice were counted and photographed, and all the lungs were removed, fixed, and embedded in paraffin for immunohistochemical analysis.

Cloning of L-FABP mutants

The amino acid substitution of wild-type L-FABP protein was carried out as follows: L-FABP point-mutation clones were generated by QuickChange Site-Directed mutagenesis kit (Stratagene), including Phe3 to Trp (F3W), Lys31 to Glu (K31E), and Thr94 to Ala (T94A). The primers for PCR reaction and subsequent treatment with DpnI to eliminate the template DNA were listed in supplementary data, Table 1, and all constructs were checked by nucleotide sequencing.

Statistical analysis

Relationships between protein expression and categorical variables (sex, grade, invasion depth, lymph node metastasis and TNM stage) were compared using Chi-square tests. For multivariate analysis, independent prognostic factors were determined using Cox's proportional hazard model. Survival curves were calculated by the Kaplan-Meier method and compared by log-rank tests. The *in vitro* and *in vivo* experiments were analyzed by GraphPad Prism 5, with the data presented as the mean ± standard error of the mean (SEM). Statistical significance was defined as a p value < 0.05.

§Part II

Plant extracts

Water extracts from *A. chinensis* were supplied by the Sun Ten Pharmaceutical Company (Taipei, Taiwan). The plant materials were boiled in water and concentrated to 1 g/ml with an evaporator, and the stock solutions were stored at −20°C until use.

HPLC analysis

We analyzed the constituent distribution and content in the water extracts of *A. chinensis* by high-performance liquid chromatography-diode array (HPLC-DAD)/evaporative light scattering detector (ELSD) chromatography under the following conditions: a linear gradient of ddH2O to methanol for 60 minutes, and 100% methanol for another 10 minutes at a flow rate of 1mL/minute with DAD/ELSD.

Reagents

Corosolic acid (CA), ursolic acid, 3-(4,5-Dimethylthiazol-2-yl)-2,5-dipheny ltetrazoliumbromide (MTT), and sulphorhodamine (SRB) were obtained from Sigma-Aldrich. Sorafenib was purchased from Santa Cruz Biotechnology. Lipofectamine 2000, VEGFR2 (KDR) siRNA, phalloidin, and Alexa Flour Dyes were obtained from Invitrogen Life Technologies. The primary antibodies against VEGFR2,

p-VEGFR2 (Tyr1054), p-VEGFR2 (Tyr951), Src, p-Src (Tyr416), FAK and p-FAK (Tyr397) were purchased from Cell Signaling Technology. The Matrigel Matrix was obtained from BD Biosciences.

Cell culture

The HCC cell lines: Huh7, HepG2 and Hep3B were obtained from Japanese Collection of Research Bioresources (National Institute of Health Sciences; Japan, JCRB) and maintained in Dulbecco's Modified Eagle Medium-High Glucose (Invitrogen) medium with 10% fetal bovine serum (FBS), 2mM L-glutamine (Invitrogen), and 100 μg/mL penicillin-streptomycin (Invitrogen). Cells were cultured in a humidified atmosphere in 5% CO_2 at 37°C.

Cytotoxicity assay

To study the cytotoxicity of CA, the MTT assay was performed as described previously [40]. Huh7 cells were seeded at 5×10^3 cells/well in 96-well plates and treated with 0.1% DMSO (control) or various concentrations of CA for 24 h. The number of viable cells was estimated by measuring the conversion of tetrazolium salt MTT to formazan crystals. After incubation with MTT for 6 h, the formazan crystals were solubilized with an SDS solution (10% SDS and 0.01M HCl) and quantified by

measuring the absorbance at 590 nm with a reference wavelength of 650 nm.

Migration assay

In the upper chamber, Huh7 cells (5×10^4 cells) were starved overnight, and resuspended in 300 μL serum-free DMEM medium with 0.1% DMSO (control) or various concentrations of CA, and seeded into Transwell inserts (8 μm pore; BD Biosciences). The complete DMEM medium was added to the lower chamber, and then incubated for 16 h; the migrated cells were fixed, stained with crystal violet, and quantified in 3 random fields (40x magnification) per insert [40].

Immunoprecipitation

For immunoprecipitation, Huh7 cells were treated with 0.1% DMSO (control) or CA for 15 min and lysed in RIPA buffer. The lysates were then sonicated and centrifuged, and the supernatant was incubated with anti-VEGFR1, R2, and R3 antibody (Santa Cruz Biotechnology, Inc.) overnight at 4°C. The immune-complexes were then incubated with PureProteome magnetic beads (Millipore) for 1 h at 4°C, washed and eluted with protein sample buffer, and analyzed by western blotting.

Western blot analysis

Cells were collected at the indicated time points and protein was extracted with RIPA buffer. Proteins samples were analyzed by SDS-PAGE, transferred to PVDF membrane, and blocked with 5% milk in TBST. Membranes were then incubated with the following primary antibodies against VEGFR2, p-VEGFR2 (Tyr1054), p-VEGFR2 (Tyr951), Src, p-Src (Tyr416), FAK and p-FAK (Tyr397). After incubation with an HRP-conjugated secondary antibody (Santa Cruz Biotechnology), membranes were developed with ECL reagent (Millipore). Signals were captured with an LAS-3000 image capture system (Fuji) and quantified with ImageJ software [41].

Kinase activity assay

The experiment was performed with the ADP-Glo kinase assay kit (Promega, WI, USA). Briefly, CA was first diluted with kinase reaction buffer at a 1:2 dilution ratio in different tubes (starting from 1 mM). Three nanograms of KDR (#V2681, Promega) were added to each tube and incubated for 10 min. Then, 0.1 μg/μL substrate and 10 μM ATP were added to each tube and incubated for 1h at room temperature. Next, 25 μL ADP-Glo reagent was added to the mixture and incubated at room temperature for 40 min. Finally, 50 μL kinase detection reagent was added to introduce luciferase and samples were measured with a SpectraMax L Microplate reader (Molecular Device, CA,

USA).

Rho GTPase activity assay

Huh7 cells were treated with 0.1% DMSO (control) or CA for 6 h and collected in RIPA buffer. Whole cell lysates (500 μg) were combined with purified GST fusion protein conjugated with Rac1, RhoA, or cdc42 binding domain (PAK-PBD for Rac1 and cdc42, Raf-RBD for RhoA) and incubated with head-to-head rotation at 4°C overnight [42]. MagneGST beads (Promega, WI, USA) were then added to the mixture to pull down the immune-complex. Samples were centrifuged at 14,000 rpm for 30 min, washed with RIPA buffer 5 times, boiled with SDS sample buffer, and analyzed by western blot analysis.

G-actin/F-actin activity assay

The assay was performed as previously described [43]. To summarize, Huh7 cells were treated with 0.1% DMSO (control) or CA for 6 h and incubated in stabilizing buffer (1% Triton X-100, 1 μg phalloidin, and protease inhibitor cocktail) at room temperature for 5 min. Cell lysates were collected, followed by centrifugation at 100,000 g for 1 h at 37°C. The supernatant was removed and saved as the G-actin fraction. The pellets were washed twice with PBS and dissolved in 200 μL dissolving

buffer (1% Triton X-100, 2% SDS, and protease inhibitor cocktail) by sonication twice, put on ice for 1 h, and saved as the F-actin fraction. Both fractions were then analyzed by western blotting.

Confocal microscopy analysis

Huh7 cells were seeded on a 22 × 22 cover slide and treated with 0.1% DMSO (control) or CA for 6 h. At the indicated time, the cells were washed, fixed, and permeabilized with 0.25% Triton X-100 for 10 min. For double staining, the slides were first incubated with p-FAK (Tyr397) primary antibody overnight, and then stained with Alexa488 (anti-rabbit) and Alexa568-phallodin (20 mU/mL) for 1 h in darkness [44]. Finally, the samples were counter-stained for nuclei with DAPI (10 ng/mL) for 10 min. The images were captured and analyzed using the Leica TCS SP5 Spectral Confocal System. The actin filament intensity was measured by ImageJ (NIH) and calculated by the following formula [45]:

Corrected total cell fluorescence (CTCF) = Integrated Density – (Area of selected cell × Mean fluorescence of background readings)

Animal model

All animal experiments were conducted according to the guidelines approved by

the Institutional Animal Care and Use Committee of the College of Medicine, National Taiwan University, and the study were approved by the Animal Care and Use Committee at National Taiwan University. The male NOD/SCID mice (4–6 weeks old) were obtained from BioLASCO Taiwan Co., Ltd, and kept in Laboratory Animal Center of the College of Medicine, National Taiwan University. The experimental mice were housed into individually-ventilated cages (IVC), and free accessed to food and drinking water. For studying the anti-tumor effect of CA alone, Huh7 cells (2×10^6 cells) were suspended in 200 μL of Opti-MEM (Invitrogen) and injected subcutaneously into the flanks of each mouse. After one week, the mice were treated with 50 μL DMSO (control) or CA (5 mg/kg/day) by intraperitoneal injection (n = 5 for each group) for 21 days. To study the combinatorial effect of CA and sorafenib, Huh7 cells (5×10^6 cells) were suspended in 100 μL of Opti-MEM with matrigel-matrix (1:1 mix ratio), and injected subcutaneously into the flanks of each mouse. After one week, the mice were treated with 50 μL DMSO (control) and compounds by intraperitoneal injection (n = 5 for each group) for 20 days. The tumor volume was calculated by the following formula: tumor volume [mm^3] = (length [mm]) × (width [mm] ^{2}) × 0.5. At the end of the experiment, the mice were anesthetized by Zoletil 50 (Virbac Animal Health) and sacrificed by CO_2 euthanasia. The tumors were excised, weighed, and fixed for further studies.

Immunohistochemistry

Samples for these experiments were obtained from the xenograft experiment and fixed in 10% paraformaldehyde, embedded in paraffin, and sectioned. The tissue sections were then subjected to immunohistochemical staining with the Novolink Polymer Detection System (Leica Biosystems). The sections were stained for p-VEGFR2 (Tyr951, Cell Signaling Technology), Ki-67 and p-FAK (Tyr397) (Santa Cruz Biotechnology), and the nuclei were counterstained with hematoxylin.

Synergistic analysis

The synergistic analysis was analyzed by the Compusyn software, which was developed by Chou and Martin [46]. The software was used to estimate the combination index (CI) and fa (fraction affected by drugs) to study the combined effect of drugs. A CI < 1, CI = 1, and CI > 1 indicates synergistic, additive, and antagonistic effects, respectively.

Molecular docking

The interaction of CA and the ATP-binding site in VEGFR2 was studied by Discovery Studio Modeling 4.0 and displayed by PyMOL (ver. 1.6.0b1). The structure of CA was obtained from ZINC (code: 08829484), and the crystal structure of VEGFR2

was obtained from Protein Data Bank (PDB id: 1YWN).

SRB cell growth assay

Huh7, HepG2, and Hep3B cells were seeded into 96-well plates (5×10^3 cells/well) and treated with 0.1% DMSO (control) or various concentrations of CA and sorafenib. After 24 hours, cells were fixed with 10% TCA and stained with SRB at 0.4% (w/v) in 1% acetic acid. The cells were then washed by 1% acetic acid, solubilized with 10 mM Tris base solution, and measured the absorbance by ELISA reader (515 nm wavelength).

Statistical analysis

Data were presented as means with standard errors (SE) and analyzed with Prism 6 (GraphPad Software, Inc.) and Sigmaplot version 10 (Systat Software Inc.). One-way ANOVA was used to compare results with more than one treatment, and the Student's t-test was performed to compare differences between two groups. $P < 0.05$ was considered statistically significant.

Results

§Part I

1. Up-regulation of L-FABP expression in HCC tissues is correlated with VEGF-A overexpression

First, we performed IHC staining for the tissues from total 90 patients, including 12 females and 78 males, with average age 53.5 ± 10.0 years (Table 2). The expression level of L-FABP in 90 pairs of HCC tumor (T)/ normal adjacent tissue (NAT) were classified into different expression levels including weak, moderate and strong, and the related photographs were represented in Figure 1A. L-FABP showed a significantly higher expression level in tumor part compared with that of NAT part among all tissue types of HCC tissues (NAT, HCC with cirrhosis, HCC without cirrhosis) (Table 1, $p=0.012$). In addition, the level of VEGF-A revealed a strongly positive correlation to the level of L-FABP ($r=0.737$, $p<0.01$, $n=90$) (Figure 1B). Taken together, these clinical results indicate that L-FABP up-regulation is associated with VEGF-A expression in HCC.

2. L-FABP induces VEGF-A expression and angiogenic potential in immortalized Hus and Huh7 cells

The functional role of L-FABP in HCC was studied by analyzing the expression

level of L-FABP in various cell lines, including immortalized normal hepatocyte (Hus) and HCC (HepG2, Hep3B, Huh7 and PLC/PRF/5) cells. As shown in Figure 2A, L-FABP was highly expressed in HepG2 and Huh7 cells, and VEGF was also highly expressed in these cells; angiogenic potential was higher in these cells than in those with lower L-FABP expression level (Hus, Hep3B and PLC/PRF/5) (Figure 2B). Accordingly, to examine the effects of L-FABP on VEGF-A expression, we generated Hus cells that stably express L-FABP, as well as Huh7 cells that L-FABP was knockdown by shRNA. Figure 3 showing that Hus/L-FABP cells exhibited a higher VEGF-A expression level including mRNA, cytosolic protein, and protein secreted to cultured medium than that of control cells (Figure 3), whereas the expression levels of VEGF-A were decreased in Huh7/L-FABP shRNA cells (Figure 24). The Hus/L-FABP cells also exhibited higher angiogenesis activity than the control cells (Figure 4A), whereas angiogenic activity was down-regulated in Huh7/L-FABP shRNA cells (Figure 24B). To further examine whether L-FABP promotes angiogenesis *in vivo*, we performed matrigel plug-in assay in NOD/SCID mice by using Hus/L-FABP (Figure 4, B and C) or Huh7/L-FABP shRNA cells (Figure 24C), and the results showed that L-FABP over-expressed cells promoted angiogenesis activity by inducing neovascular formation in matrigel as shown by anti-CD31 IHC staining.

3. Association of L-FABP with VEGFR2 in membrane rafts

Previous studies reported that some FABPs, such H-FABP or B-FABP, could interacts with membrane associated receptors, including integrin or dopamine D2 receptor [47-49]. It also suggested that L-FABP possibly associated with cell membrane or membrane proteins [10, 50]. Thus, we proposed that L-FABP could be also associated with membrane receptors, and by the alignment of FABP interacted amino acid sequence in previous studies, we found that the consensus sequence-WKIGFXKRLXXVXXXI (Figure 5) of membrane receptors is most likely as interaction site with L-FABP. By comparing the consensus sequence to other membrane receptors, we observed that the kinase domain of VEGFR2 showed a possibility of interacting to L-FABP. Thus, we performed co-immunoprecipitation by using primary antibodies against VEGFR2 or L-FABP, followed by western blotting with L-FABP, or VEGFR2. Both experiments showed that L-FABP could interact with VEGFR2 (Figure 6). Furthermore, we used confocal microscopy analysis revealed that L-FABP located in both membrane and cytosol, whereas VEGFR2 was located mainly on membrane. Notably, the co-localization of L-FABP and VEGFR2 in apical membrane was demonstrated in Hus/L-FABP cells (Figure 7, indicated by arrows). Furthermore, isolation of membrane by sucrose gradient ultra-centrifugation also showed co-localization of L-FABP and VEGFR2 in membrane. As shown in Figure 8, fractions

with lipid rafts of Hus/L-FABP cells were identified by lipid raft marker, flotillin-2; interestingly, not only L-FABP and VEGFR2, membrane associated signal transduction proteins including PI3K (p85), p-Akt/Akt, p-Src/Src, p-FAK/FAK were also detected the increasing distribution levels in membrane rafts. Taken together, these results indicated that overexpressed L-FABP not only associated with membrane VEGFR2, but may also activate its downstream signal transduction signals including PI3K/Akt and Src/FAK.

4. L-FABP increases VEGFR2/ Src phosphorylation and cell migration by FAK/cdc42 pathway

Previous reports indicated that VEGFR2/Src pathway is associated with cancer cell migration by activating FAK and Rho-GTPase [51-53]. In Hus/L-FABP cells, the phosphorylation of VEGFR2, Src and FAK was increased significantly (Figure 9 and 10), and by small GTPase binding assay, the activity of cdc42 was significantly up-regulated in Hus/L-FABP cells (Figure 11). By performing wound-healing assay for studying 2D migration activity (Figure 12A), and Boyden chamber based migration assay for studying 3D migration activity (Figure 12B), Hus/L-FABP cells had higher migration activity than that the control cells. Furthermore, L-FABP knockdown resulted in a significant decrease in 3D migration activity in Huh7 cells. (Figure 24D).

Additionally, by treating Hus/L-FABP cells with Sorafenib (VEGFR2 inhibitor) or PP1 (Src inhibitor), significant inhibitory effects on migration activity were found (Figure 13). Moreover, knockdown of L-FABP in Hus/L-FABP cells reversely down-regulated its 3D migration activity (Figure 23C). These results suggest that VEGFR2/ Src/FAK/cdc42 signaling is participated in L-FABP induced migration activity.

5. L-FABP induced VEGF-A expression by Akt/mTOR/P70S6K/4EBP1 in translation level

According to our above-mentioned results in Figure 8, we proposed that the signal transduction of L-FABP mediated VEGF-A expression was activated through Akt pathway. Since Akt signaling has been reported to be the major pathway to increase VEGF-A expression level in previous reports [54, 55]. Therefore, we performed western blot analysis, and the results showed that the L-FABP activated Akt/mTOR/ P70S6K/4EBP1 pathway in Hus/L-FABP cells (Figure 14). Previous results have suggested that VEGF-A mRNA expression level could be regulated by HIF-1α dependent or independent manner [54, 56]. In our studies, we found that the mRNA expression level of VEGF-A was significantly up-regulated in L-FABP overexpressed cells as showed in Figure 3, and HIF-1α, which serves as the major transcription factor to regulate VEGF-A expression, was also shown an increased level in the nucleus

fraction of Hus/L-FABP cells (Figure 15). To further confirm this observation, the full-length construct and a serial of successive 5' deletions (D1-D3 constructs) of VEGF-A gene promoter were cloned into pGL4.22 luciferase reporter vector, and the luciferase reporter assay was performed to measure the transcriptional activity of VEGF-A promoter and its deletion mutants in L-FABP overexpressed Hus cells. The results revealed that the VEGF-A transcriptional activity was elevated ~16.5-fold as compared with that of control cells, whereas the deletion of HIF-1α binding site (D1-D3) clearly abolished its activity to ~2.5 fold of control group (Figure. 16).

To further discuss the regulation of VEGF-A expression in post-transcription level, Hus/L-FABP cells were treated with Rapamycin (mTOR inhibitor) or Cyclohexamide (translation inhibitor), and a dose-dependent decreased of VEGF-A expression level or its angiogenic potential was found (Figure 17, A and C). The effects of proteasome inhibitor, MG132, on Hus/Vector cells were investigated, and the results indicated that L-FABP induced VEGF-A expression was not via the inhibition of protein degradation (Figure 17B). Taken together, these data suggested that the induction of VEGF-A expression by L-FABP was regulated both in transcription and translation levels.

6. L-FABP promotes tumor growth and metastasis *in vivo*

The role of L-FABP in tumorigenesis was examined in immune-deficient

NOD/SCID mice, and the results indicated that tumor weight was significantly enhanced in the group injected with Hus/L-FABP cells as measured on day-50. (Figure 18A). The levels of VEGF-A in mice serum were also up-regulated 2.8-fold in Hus/L-FABP group than that of control group (Figure 18B), and the immunohistochemistry staining of CD31 also indicated that L-FABP induced angiogenesis *in vivo* (Figure 18C). We further investigated the role of L-FABP in tumor metastasis *in vivo*, and the Hus/L-FABP cells or control cells were injected i.v. into the tail vein of NOD/SCID mice. After 60 days, the number of metastatic nodules formed in lung was 3.9-fold higher in Hus/L-FABP group than that of control group (Figure 19A), the increase of angiogenic vessel formation in these nodules was also demonstrated (Figure 19B). These *in vivo* experiments further supported the correlation of L-FABP and VEGF-A expression in present clinical tissue analysis.

7. Cholesterol associating and membrane interacting activities are essential for L-FABP induced cell migration and angiogenesis

Previous studies suggested that L-FABP mutations result in the ablation of fatty acid or cholesterol uptake, even the membrane structure [57-61]. Thus, to examine how L-FABP interacts with membrane in overexpressed cells, we used site-directed mutagenesis to generate L-FABP mutant stable clones with the substitution of different

functional amino acids expressed in Hus cells. As showed in Figure 20A, three mutants including F3W, K31E, and T94A showed a reduced VEGF-A expression level and a significantly decreased angiogenic activity than that of wild type group (Figure 20B). However, the migration level down-regulated significantly only in K31E and T94A mutants, but not in F3W mutant which exhibited minor effect (Figure 21). T94A is the most common mutation occurred in Europeans and has been found to affect fatty acid and cholesterol uptake as a loss-of-function mutation [61]. Thus, to verify this result, we reduced membrane cholesterol content with MβCD (cholesterol depletion reagent) in Hus/L-FABP cells, and the result suggested that the VEGF expression, migration activity, and their related signals in Hus/L-FABP cells were all down-regulated significantly (Figure 22, A and B). Taken together, the oncogenic activity of L-FABP showed a certain degree of correlation to its membrane-binding property.

§Part II

8. Corosolic acid significantly decreases the migration activity of Huh7 cells

To study anti-migration effects of corosolic acid (CA) on Huh7 cells *in vitro*, we first treated Huh7 cells with various concentrations of CA for 24 h. Cell viability was then measured with an MTT assay, and as shown in Figure 29A, CA decreased the survival rate of Huh7 cells; the IC_{50} of cytotoxicity was determined to be 50 μM. Then,

we performed a transwell assay with Huh7 cells, CA inhibited Huh7 cell migration in a dose-dependent manner, and the IC_{50} for migration was found to be 2.5 μM (Figure 29B). The results indicate that CA has a relatively higher inhibitory effect on Huh7 cell migration than cell viability. (IC_{50} cytotoxicity/IC_{50} migration = 20).

9. Corosolic acid inhibits VEGFR2 kinase activity

Previous studies suggest that VEGF/VEGFR signaling can facilitate cancer cell metastasis [62], and inhibition of VEGFR can reduce HCC cell migration [63]. Thus, to investigate whether CA inhibits VEGFR activation, we performed immunoprecipitation to pull down three key VEGFRs in Huh7 cells, including VEGFR1, R2, and R3, followed by blotting with phospho-tyrosine antibody. The results suggest that CA significantly reduced phosphorylation of VEGFR2 by 70% without affecting total VEGFR2 expression, while CA exhibited weaker effect to VEGFR1 & R3 (Figure 30). With a VEGFR2 kinase activity assay, 0.95 μM CA was also found to inhibit VEGFR2 kinase activity by 50% (Figure 31). To examine whether the anti-migration effect of CA is mediated by VEGFR2, we attenuated endogenous VEGFR2 of Huh7 cells by siRNA. The knockdown cells lost sensitivity to CA-induced inhibition of migration (Figure 32). Taken together, these results suggest that CA inhibits Huh7 cell migration by inhibiting VEGFR2 activation.

10. Corosolic acid decreases cell motility by inhibiting VEGFR2/Src/FAK/cdc42 activity and actin rearrangement

To further elucidate the mechanism underlying the anti-migration effect of CA, we performed western blot analysis. Treatment with CA decreased the phosphorylation level of VEGFR2 (Tyr1058), and the phosphorylation level of non-receptor tyrosine kinase, Src (Tyr416), and focal adhesion kinase, FAK (Tyr397), were also down-regulated by CA (Figure 33). It was reported previously that focal adhesion kinase (FAK) is activated by membrane receptors such as RTKs or integrins, then the Src/FAK complex modulates cell migration and actin rearrangement via Rho-GTPase pathways. Therefore, using a Rho-GTPase activity assay, we found that active cdc42, but not active Rac1, or active RhoA, is significantly down-regulated by CA treatment (Figure 34). Recent studies have revealed that cdc42 may play an important role in the dynamic change of actin and the formation of filopodia during cell migration. To study whether CA disrupts actin rearrangement in Huh7 cells, we performed a G-actin/F-actin assay. The results demonstrated that CA treatment reduces the ratio of F-actin/G-actin (polymer/monomer) by about 50% compared to that of control group (Figure 35A). By confocal microscopy analysis, we also found that CA decreases the co-localization of phospho-FAK (Tyr397) and F-actin on the filopodium (leading edge) in Huh7 cells

(Figure 35B). Taken together, these results indicate that CA inhibits Huh7 cell migration by suppressing the VEGFR2/Src/FAK/cdc42 pathway and actin rearrangement.

11. Corosolic acid exhibits anti-tumor effects *in vivo*

The effects of CA on tumor growth were investigated *in vivo* using a xenograft model. Mice were given daily i.p. injection of CA (5 mg/kg/day). CA had significant inhibitory effects on tumor growth in NOD/SCID mice injected with Huh7 cells (2×10^6 cells/mice) (Figure 36A). After 21 days of treatment, the mice were sacrificed and the volume of tumors in CA-treated group (63 ±19 mm3) were much smaller than that of control group (669 ±67 mm3). In addition, the CA-treated group (5 mg/kg/day) showed 85% reduction in tumor mass compared to that of the control group (Figure 36B). Body weight of mice treated with CA were similar to that of control group (Figure 36C), suggesting that the dosage of CA administered had no significant toxic effects to the mice. The levels of Ki-67, phospho-VEGFR2 and phospho-FAK in tumor lesions were examined by immunohistochemistry; CA reduced the expression level of Ki-67, and the phosphorylation of both VEGFR2 and FAK significantly in HCC xenograft mice (Figure 36D).

12. Synergistic effects of corosolic acid and sorafenib on HCC cells

Sorafenib (Nexavar), a multi-kinase inhibitor including VEGFR2/3, PDGFRβ, and Flt-3, has been used to treat HCC patients and has a significant migration-inhibitory effect on HCC cells [64]. We performed a transwell assay with both CA and sorafenib treatment; CA exhibited a migration inhibitory activity comparable with that of sorafenib (Figure 37A). Ursolic acid (3β-hydroxyurs-12-ursen-28-ic acid) (UA) shares a similar chemical structure with CA and has been implicated in cancer prevention [65]. However, in the transwell assay, UA exhibited no significant anti-migration activity on Huh7 cells compared to that of CA. We demonstrated that CA has an inhibitory effect on migration comparable to sorafenib in HCC.

Then, to explore the effects of CA when used in combination with chemotherapeutic agents for HCC, we studied the combinatorial effects of CA and sorafenib on migration activity of Huh7 cells. The results of transwell assay demonstrated that CA has a synergistic effect with sorafenib on cell migration at a wide range of doses (Figure 37B). Moreover, to verify this, we performed a western blot analysis, and found that CA enhances sorafenib-mediated inhibition of phosphorylation of VEGFR2, Src, and FAK (Figure 38). Finally, the xenograft model indicated that combined treatment with CA and sorafenib showed a synergistic effect on tumor growth (CA 2.5 mg/kg/day with sorafenib 10 or 20 mg/kg/day) (Figure 39). These results

demonstrate a synergistic interaction between CA and sorafenib in the treatment of HCC cells.

13. Corosolic acid interacts with the ATP-binding site of VEGFR2 kinase domain by molecular docking

To further study whether CA decreases phosphorylation of VEGFR2, we used molecular docking software to analyze the interaction between CA and the kinase domain of VEGFR2. This analysis suggests that CA may bind to the ATP-binding cavity of the VEGFR2 kinase domain (Figure 41A). Previous studies suggested that Gln883, Cys917, and Asp1044 of VEGFR2 are involved in ligand binding through H-bond interactions [66]. As shown in Figure 41B, CA potentially interacts with Gln883 at a distance of 2.67Å. It also interacts with Val846, Lys866, Val897, Val914, and Cys1043. These interactions between CA and the VEGFR2 kinase domain could result in inhibition of VEGFR2 and subsequent downstream intracellular signaling.

14. Corosolic acid does not exhibit significant inhibitory effects on Huh7 cell invasion

The matrix metalloproteinases (MMPs) are very important factors on cancer migration or metastasis [67]. To examine whether corosolic acid (CA) could inhibit

invasion activity of Huh7 cells, studies on the effects of CA for MMPs and NF- kappa B pathway, which is an important event to regulate the MMPs activity were evaluated. However, in our model, corosolic acid (CA) had no significant inhibitory effect on Huh7 cell invasion (Figure 46A). The expression level of MMP2 and MMP9 and the activity of MMP1, MMP2, and MMP9 were not affected by CA treatment (Figure 46B). The level of phosphorylated IκB, IκB, and NFκB was maintained at a stable level (Figure 47) which suggested that NFκB pathway may not participate in CA effect.

Discussion

§Part I

Role of L-FABP in hepatocellular carcinoma

HCC is characterized by the high aggressive and angiogenic capacities, and the angiogenic factor, VEGF, has been considered as one of investigated targets for cancer therapy in HCC [1, 6]. We reported here for the first time that L-FABP overexpression plays an important role in VEGF-A expression and cell migration in HCC, and demonstrates that L-FABP associates with VEGFR2 in cell membrane, following by the activation of VEGFR2 related signaling, including Src/ FAK/cdc42 and Akt/mTOR/HIF-1α. T94A mutation of L-FABP, which was related to the cholesterol binding activity, significantly decreased the angiogenic potential and migration activity of L-FABP overexpressed cells.

It has been suggested that L-FABP promotes growth of hepatocyte and protects cells from ROS by its anti-oxidative activity, which was related to the methionine and cysteine [68, 69]. Other studies also found the several lines of evidences in correlation of L-FABP and VEGF [12, 19]. However, the link of L-FABP and tumor malignance still remains unclear. In the present study, we found a significant increase of L-FABP expression in tumor part versus their NAT part in 90 HCC patients (p=0.012) by IHC staining. The well correlation between the expression level of L-FABP and VEGF-A in

90 clinical tissue pairs of HCC patients was also demonstrated ($r=0.737$, $p<0.01$). By screening of liver cell lines of, we also found that L-FABP expressed higher in malignant HCC cell lines, HepG2 and Huh7, but lower expressed in immortalized normal hepatocyte, Hus cells, and the tendency was consistent with that of VEGF-A expression level. Thus, it strongly suggests that L-FABP may regulate VEGF expression in HCC. Furthermore, it was suggested that we generated stable clones of Hus/L-FABP cells, and that the up-regulated VEGF-A expression level and angiogenic potential of Hus/L-FABP cells were observed by *in vitro* and *in vivo* studies. These observations were also further proofed by L-FABP knockdown in Huh7 cells and Hus/L-FABP cells (Figure, 24C and 23B). Previous study has suggested that VEGF is essential for HCC cell migration [63], therefore, we have observed that the migration activity of Hus/L-FABP cells increased significantly than that of control cells. Knockdown of L-FABP in Huh7 cells or L-FABP stably expressed Hus cells also showed a decreased migration activity compared with that of control group (Figure, 24D and 23C). Taken together, these results suggested that L-FABP overexpression plays a critical roles in the angiogenic potential and migration activity of HCC cells, which could be reversely regulated by RNA knockdown technology.

In previous study, L-FABP has been suggested to be interacted with cell membrane

[11], however, most studies focused on its biological function in transport fatty acids and the regulation to lipid metabolism [70]. However, in this study, we found that L-FABP co-localized with VEGFR2 on membrane rafts of L-FABP overexpressed cells. Previous study has reported that L-FABP co-expressed with VEGF in cell membrane [19]. Other studies also suggested that lipid rafts seemed to be capable of acting in signaling platform [71-73]. Comply with this, our confocal microscopy analysis suggested the co-localization of L-FABP and VEGFR2 on apical membrane of Hus/L-FABP and Huh7 cells (Figure 7 and Figure 25). The downstream signal proteins including Src/ FAK and PI3K/Akt showed an increased level in membrane fraction. Knockdown of VEGFR2 in Hus/L-FABP cells decreased the phosphorylation level of these downstream signal molecules (Supplementary, Figure 1). Moreover, by protein docking software, we predicted two possible interacting model of L-FABP and VEGFR2 kinase domain (Supplementary, Figure 2). As a result, our observation provides a possible mechanism of how L-FABP activates VEGFR2 signaling.

The regulation of VEGF in HCC has been highlighted since its related pathway plays an important role in cancer progression [2]. In fact, only the anti-VEGFR2 therapy revealed a significant benefit on clinical HCC patients, and was approved by FDA [9]. In our experiment, we found that the increased VEGF-A expression was via translation

regulation of PI3K/Akt and its downstream mTOR/P70S6K/4EBP1 pathway. Since VEGF-A could be regulated by HIF-1α in transcription level of cancer cells, in our model, both mRNA level and transcriptional activity of VEGF-A showed a significant up-regulation by L-FABP overexpression. Interestingly, previous study also showed that L-FABP revealed a positive correlation with VEGF-A in mRNA level [12]. Taken together, these data suggested the possible mechanism which regulates VEGF-A expression in HCC cells.

L-FABP is the only member of mammalian FABP family to transfer fatty acids to membranes by aqueous diffusion [74], furthermore, direct interaction of L-FABP and PPARα has also been reported for ligand trafficking to nucleus [75]. Therefore, the studies on ablation or mutation of L-FABP protein in normal hepatocyte has been studied for a long time. In L-FABP knockout mice, it showed decreased lipid metabolism and exacerbated obese phenotype with high-fat diet [70, 76]. For the mutation studies, L-FABP (F3W) and (K31E) mutants showed a significance decreased binding ability to phospholipid [57, 58]. Moreover, L-FABP (T94A) mutant altered structure and stability of L-FABP and caused a loss-of-function [59-61]. In present studies, we have mutated four amino acids which located in different domains of L-FABP protein (Supplementary, Figure 3): F3 to W (β sheet A, N-terminal), K20 to E

(α-helix I), K30 to E (α-helix II), T94 to A (β sheet G, C-terminal) to examine the functional amino acids of L-FABP in L-FABP induced angiogenesis and migration. The results demonstrated that a decreased level of VEGF in L-FABP K31E and T94A mutants, and a significant down-regulation in migration activity. The treatment of MβCD, a membrane cholesterol depletion agent [77] with Hus/L-FABP cells also support the above-mentioned observation, and it suggests that the cholesterol-binding activity of L-FABP is indispensable to its function. Taken together, the function of L-FABP in cell membrane not only for metabolism, but also for its oncogenic role in HCC tumorigenesis.

Previous studies reported that L-FABP promoted diet induced fatty liver disease and hepatic steatosis [78]. It also suggested that VEGF level was correlated with HCC malignance and poor prognosis [79]. In the present study of clinical sample data, we found that L-FABP up-regulated significantly in HCC patients, with and without cirrhosis. Moreover, in the cirrhosis patients, high L-FABP expression indicated high risk and poor survival time (Figure 26). Previous study suggested that it needs "angiogenic switch" to become a solid HCC tumor [80], and VEGF showed an autocrine feed-forward loop to trigger angiogenesis [55, 81], Since the correlation of L-FABP expression and HCC progression remains unclear, and there was no appropriate

prognosis marker in HCC with cirrhosis [82], L-FABP may serve as a potential research target for further studies.

§Part II

Effects of corosolic acid on hepatocellular carcinoma

CA is an ursane-type triterpenoid, and is known to be a STAT3 inhibitor in macrophages, myeloid cells, and ovarian cancer cells [30-32]. CA also has a significant inhibitory effect on endothelial angiogenic tube formation [29], and tumor growth in lung and ovarian cancer cells [31, 33]. In this study, we found that CA significantly reduced the migration activity of HCC cells, including Huh7, HepG2 and Hep3B at a low-cytotoxicity dosage. When combined with sorafenib, CA showed synergistic effects on HCC cell growth and migration. An *in vivo* xenograft mouse model was used to verify the anti-HCC activity of CA, which showed significant inhibitory effects on Huh7 cells at 5 mg/kg/day.

VEGFR2 is the major receptor in the VEGF signaling pathway that regulates cell migration, proliferation, and angiogenesis. This study revealed that CA reduces the tyrosine phosphorylation level of VEGFR2, with an IC_{50} of kinase activity of 0.95 μM. Further studies also found that CA suppressed the activation of Src, FAK, and cdc42.

These results provide a potential mechanism for the anti-migration effects of CA on Huh7 cells in HCC.

The inhibition of VEGFR2 has been proposed as a novel therapeutic strategy for HCC patients. Various VEGFR2 kinase inhibitors such as sorafenib, sunitinib, and linifanib were developed and used in clinical trials. Recently, anti-HCC therapy with sorafenib has been approved by FDA [9, 64]. To further investigate how CA inhibits VEGFR2, a structure-based interaction model between CA and VEGFR2 was developed by molecular docking analysis. The results suggest that the ATP binding pocket in the VEGFR2 catalytic domain binds CA with lower binding energy than ATP (-15.2 kcal/mol versus -12.3 kcal/mol). Moreover, the surface charge distribution of VEGFR2 demonstrated that the OH groups of CA showed stable interactions with the ATP binding pocket. It also revealed that most uncharged areas of CA could generate hydrophobic forces with valine and cysteine resulting in stabilizing the binding affinity. This strongly suggests that the binding of CA to the ATP-binding pocket of VEGFR2 mediates the down-regulation of VEGFR2 phosphorylation and subsequent signals. Furthermore, the combination of CA and sorafenib had significant synergistic effects on Huh7 cell migration and VEGFR2 phosphorylation. The *in vivo* combinatorial experiment further verified that CA combined with sorafenib shows potential for HCC

treatment without toxic effects to mice (data not shown). We also observed that CA down-regulated the phosphorylation level of Src and FAK kinases when combined with sorafenib, since sorafenib alone did not show any inhibitory effect to the activation of FAK kinase in the xenograft model. Collectively, these results indicate that CA shows potential as a novel VEGFR2 inhibitor or an adjuvant therapy to be used with existing anti-cancer drugs.

Previous studies have discussed the pharmacophore modeling of different VEGFR2 inhibitors [66]. These inhibitors could be divided in two types, sunitinib-like or sorafenib-like, depending on the interacting hydrogen bonds. The binding of type I inhibitor (sunitinib) formed hydrogen bonds with Asp1044, Cys917, and Asn921 near the protein surface. On the other hand, the type II inhibitor (sorafenib) could interact with Asp1044, Cys917, and Glu883. By docking analysis, we found that CA formed hydrogen bond and relatively closed to Glu883 than Asn921 (2.67 Å versus 9.2 Å, Figure 42). Although the interaction model of CA with VEGFR2 are likely to sorafenib, however, the chemical structure of CA varied widely with both two types of VEGFR2 inhibitor. Thus, it could be interesting to explore and design novel VEGFR2 inhibitors based on present findings.

Summary

We have been focusing on finding out novel oncogenic mechanisms and therapeutic agents of HCC, and the first study reveals for the first time that L-FABP potently induces the up-regulation of VEGF-A and increases angiogenic potential and migration activity in HCC cells. The results also suggest that the function of L-FABP in HCC could be influenced by mutations in its cholesterol interaction sites. When considered alongside previous studies, our findings indicate that L-FABP is a potential therapeutic target in HCC therapy. Next, we demonstrates that corosolic acid could be a potential anti-HCC agent. We provide evidence that CA's anti-cancer effects stem from its anti-migratory effect, by blocking the VEGFR2 ATP binding pocket and down-regulating the downstream Src/FAK/cdc42 signaling axis. This study further demonstrates that the combination of CA and sorafenib may have potential as a chemotherapy for HCC.

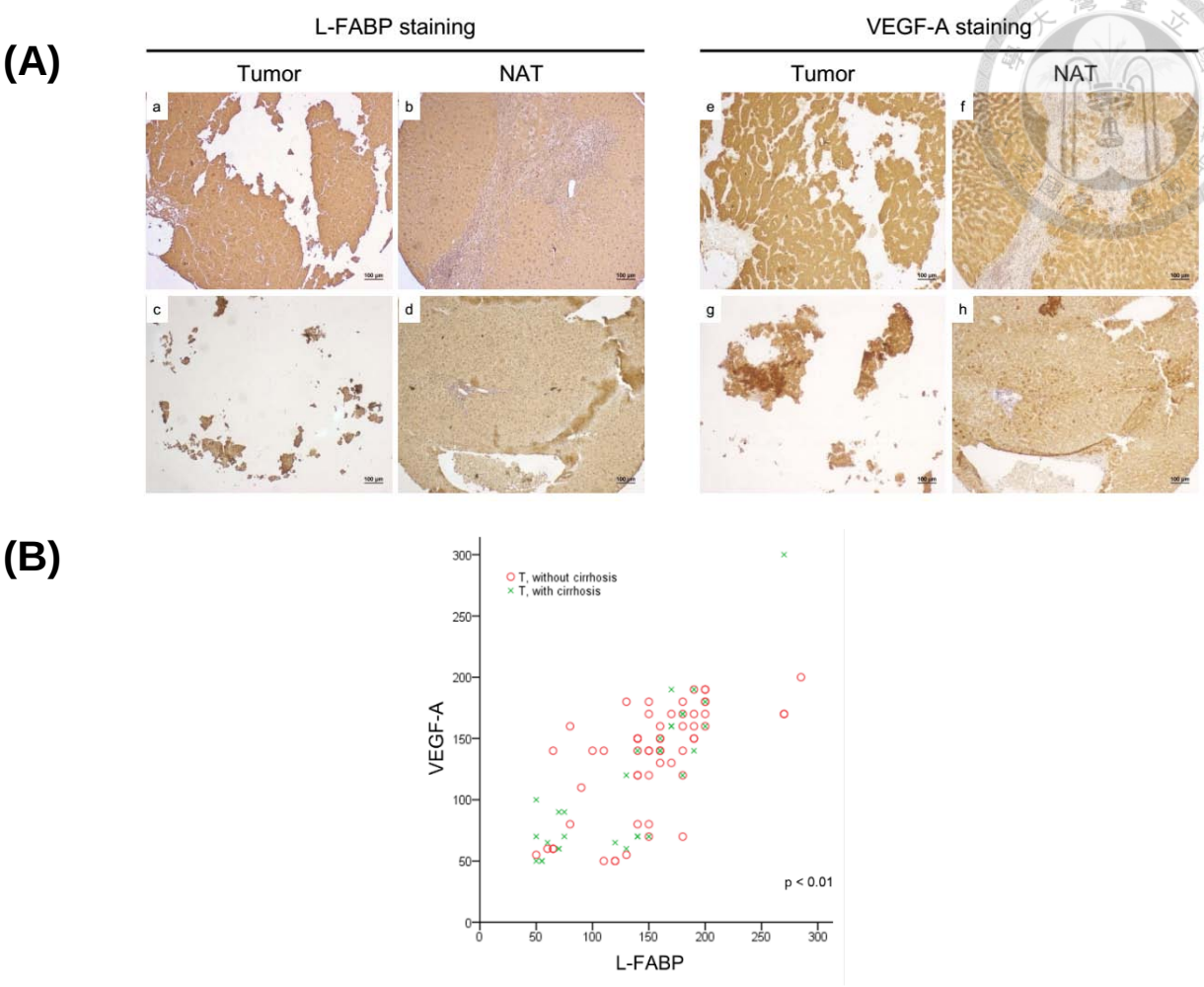

Figure 1. Correlation between the expression levels of L-FABP and VEGF-A

L-FABP and VEGF-A expression in 90 cases of HCC patients (normal and tumor paired tissue) was examined by IHC staining. (A) Representative images of different expression levels of HCC tissue pairs. a-d: Staining of L-FABP was observed in tumor parts (a and c) and their normal adjacent tissues (b and d). a: Strong staining; b and c: moderate staining; d: weak staining of L-FABP IHC results. e-h: Staining of VEGF-A was observed in tumor parts (e and g) and their normal adjacent tissues (f and h). e: Strong staining; f and g: moderate staining; h: weak staining of VEGF-A IHC results. (B) Correlation between L-FABP and VEGF-A expression in 90 HCC tissues (with and without cirrhosis). L-FABP exhibited a positive correlation with VEGF-A by the Pearson correlation coefficient ($r = 0.737$, $^{**}p < 0.01$).

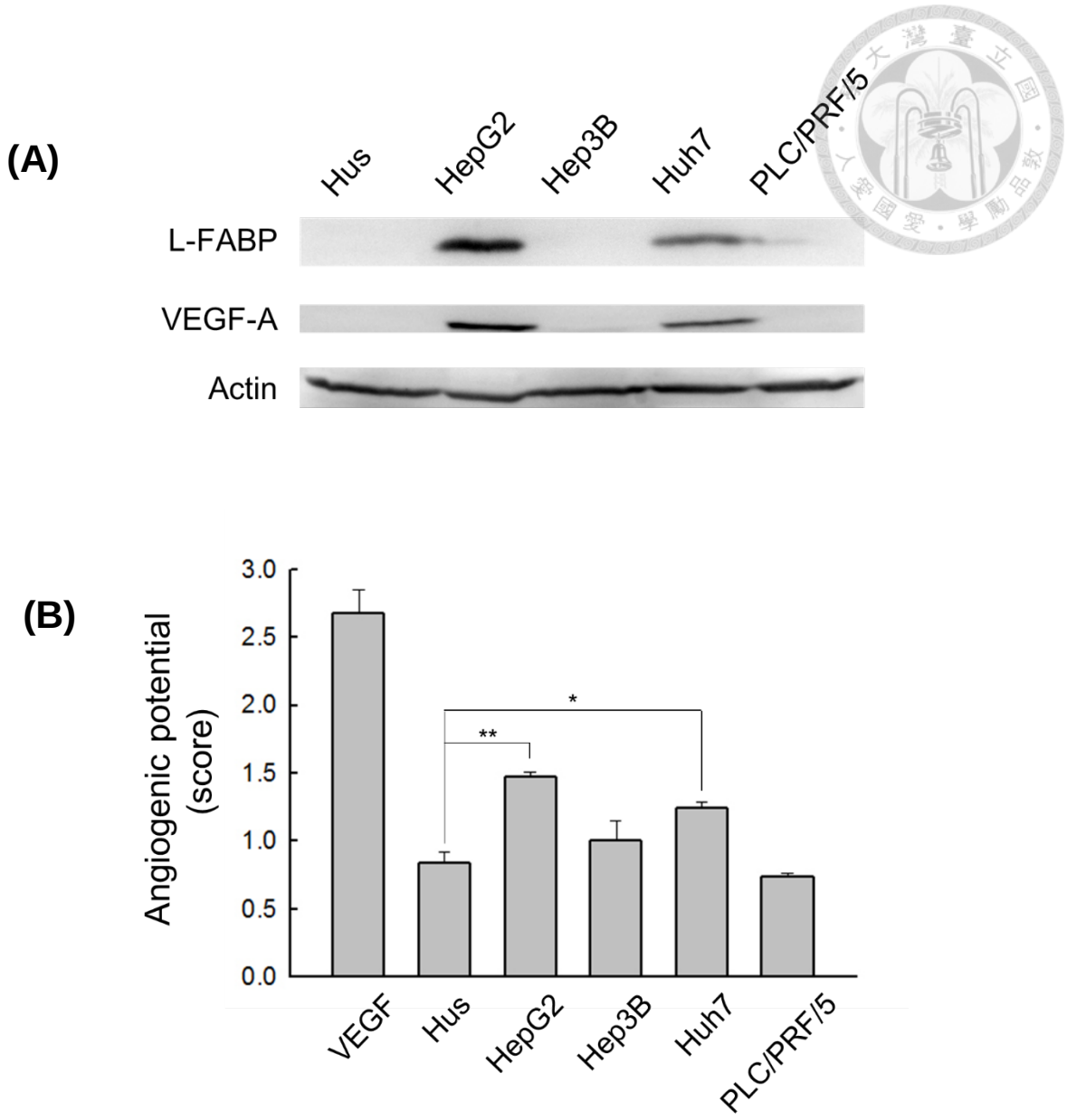

Figure 2. L-FABP expression is associated with VEGF-A expression of HCC cells. (A) Western blot analysis for L-FABP expression in normal immortalized hepatocyte (Hus) and hepatocellular carcinoma cell lines (HepG2, Hep3B, Huh7 and PLC/PRF/5). (B) Angiogeic potential of Hus, HepG2, Hep3B, Huh7 and PLC/PRF/5 cells was assessed by HUVEC endothelial cell tube formation assay. *$p < 0.05$, **$p < 0.01$ versus control group (Hus cells).

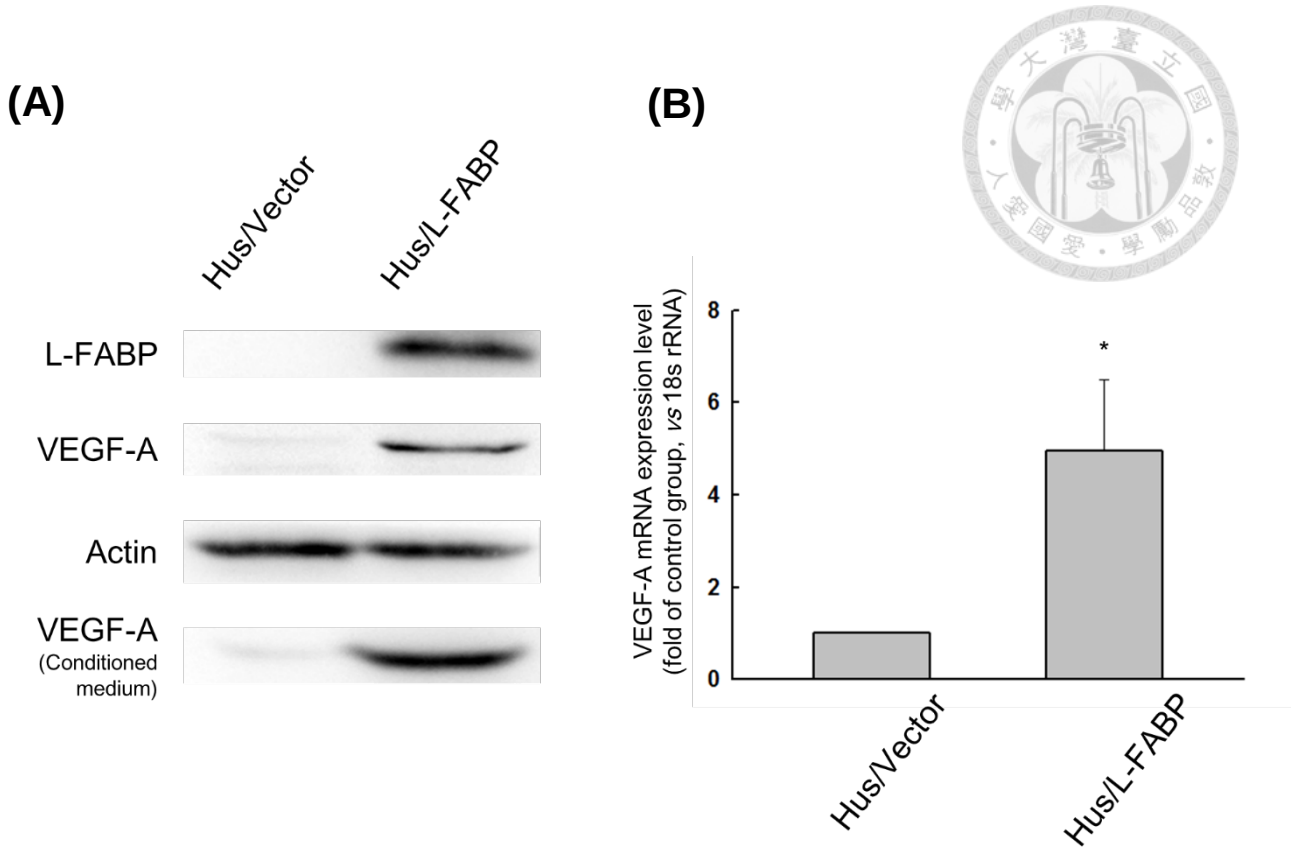

Figure 3. Expression level of VEGF-A is up-regulated Hus cells stably expressed L-FABP.

L-FABP was stably expressed in Hus cell using pcDNA3.1 expression system. The vector only cells were used as control group. (A)The protein expression level of L-FABP and VEGF-A was analyzed by western blotting. (B)The mRNA expression level of VEGF-A was determined by qRT-PCR. *$p < 0.05$, versus control group (Hus/Vector cells).

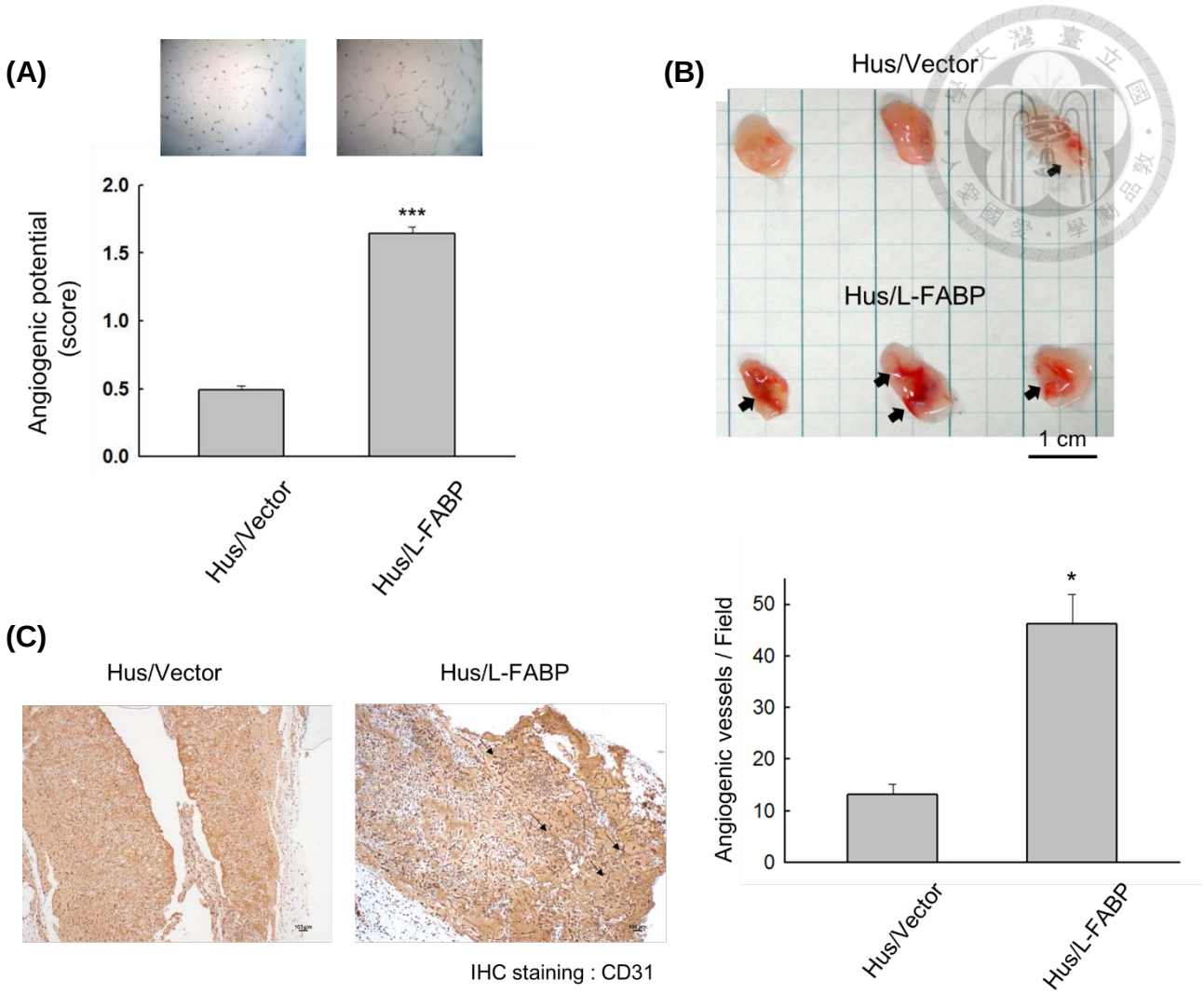

Figure 4. L-FABP promotes *in vitro* and *in vivo* angiogenic activity of Hus cells.

(A) The *in vitro* angiogenic activity was studied by tube formation assay which performed by HUVEC endothelial cells to determine angiogenesis activities of Hus/Vector and Hus/L-FABP cells. Angiogenic vascular tube was imaged at 8 h. The quantification of S.CORE tube formation was shown as panel bar. ***$p < 0.001$ versus control group (Hus/Vector cells). (B) The *in vivo* angiogenic activity was studied by matrigel plug in assay. Left: Macroscopic view of matrigel plugs recovered from mice injected with Hus/Vector and Hus/L-FABP cells, and the infiltration of blood vessels were indicated by arrows. (C) Immunohistochemical staining of CD31 (angiogenesis marker) in matrigel plugs were presented and quantified. n=3, *$p < 0.05$ versus control group (Hus/Vector cells).

```
                                                KDR : 795~830 (aa)
                                                1                                                  50
                  KDR kinase domian     (1) ILRTVKRANGGELKTGYLSIVMDPDELPLDEHCERLPYDASKWEFPRDRL
            CD36 TSP binding domains    (1) ------TYRVRFLAKENVTQDAEDNTVSFLQPNG-------------
                       DSLR domains     (1) -------GNCTHPEDMKLCTVIMKSNGSFPVNRRRV--------------
integrin alpha 1 cytoplasmic domains    (1) -------WKIGFFKRPLKKKMEK---------------------------
integrin alpha 2 cytoplasmic domains    (1) -------WKLGFFKRKYEKMTKNPDEIDETTELSS---------------
                          Consensus     (1)        WKIGF KR  L  V     I
```

Figure 5. Sequence aliment of L-FABP interacting domains

Amino acid sequence alignment of L-FABP interacting domains, including: CD36 TSP binding domain, DSLR cytoplasmic domain, integrin α1 cytoplasmic domain, and integrin α2 cytoplasmic domain. Strictly conserved residues are highlighted in blue; residues with similar property are highlighted in green, respectively.

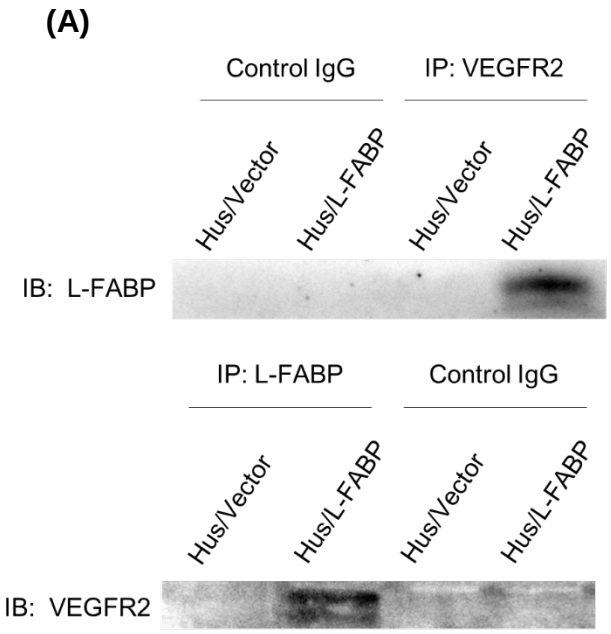

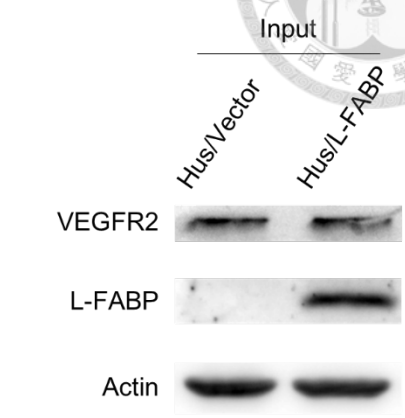

Figure 6. Co- immunoprecipitation of L-FABP and VEGFR2 in Hus/L-FABP cells

(A) The cell lysates of Hus/Vector and Hus/L-FABP cells were subjected to immunoprecipitation (IP) with VEGFR2 antibody, followed by blotting with L-FABP; or L-FABP antibody, followed by blotting with VEGFR2. (B) Cell lysates (50 μg) were immunoblotted as input control.

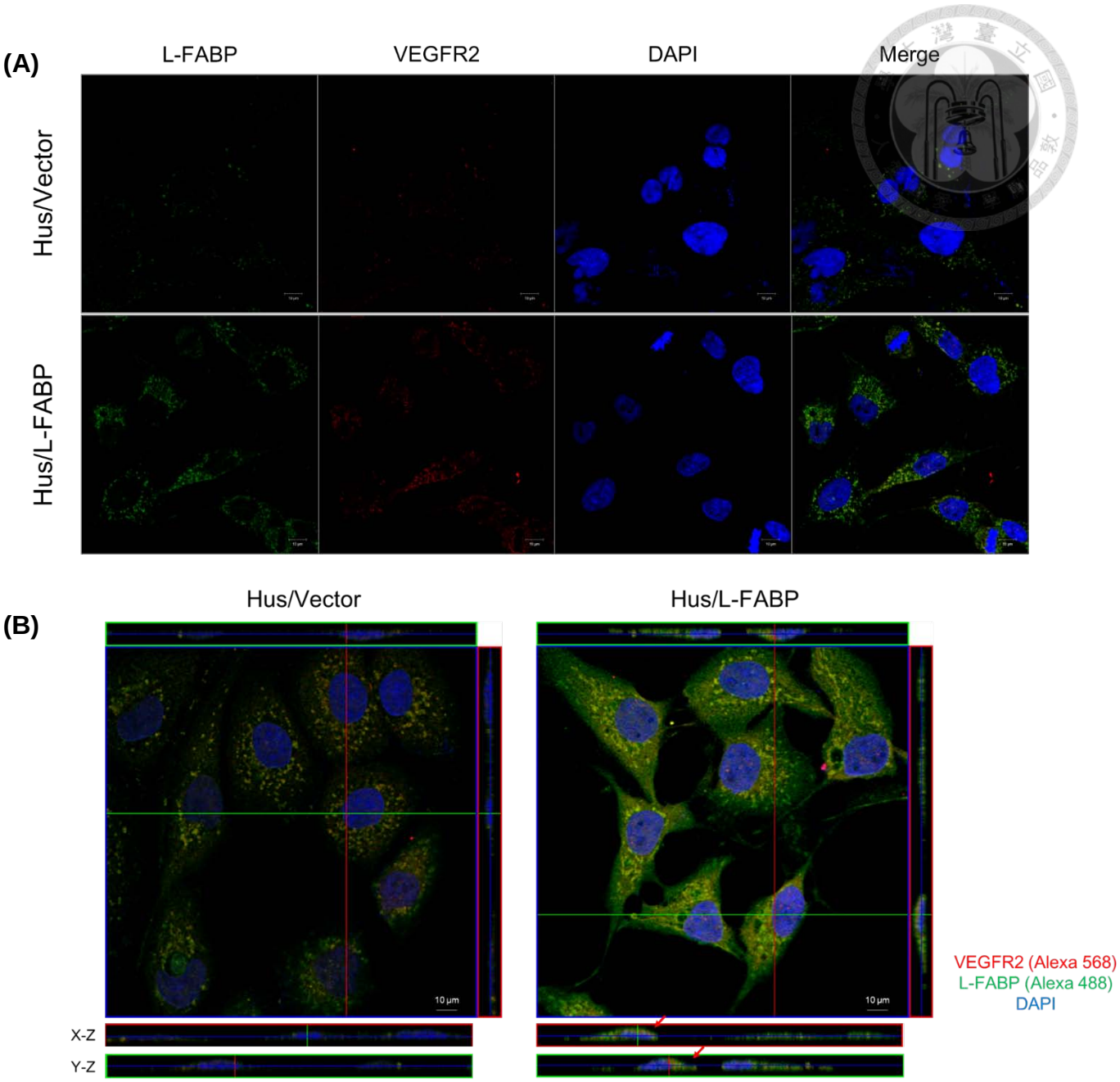

Figure 7. L-FABP associates with VEGFR2 in apical membrane of Hus/L-FABP cells

(A) Cells were fixed and stained with antibodies against to VEGFR2 and L-FABP. Three-color confocal images were acquired on a ZEISS, LSM 510 META Confocal Microscope (Magnification, 63 ×). (B) Red or green lines showed the X-Z or Y-Z optical section of Hus/Vector and Hus/L-FABP cells, respectively. The co-localization of VEGFR2 and L-FABP on the upside of cells was indicated by red arrows.

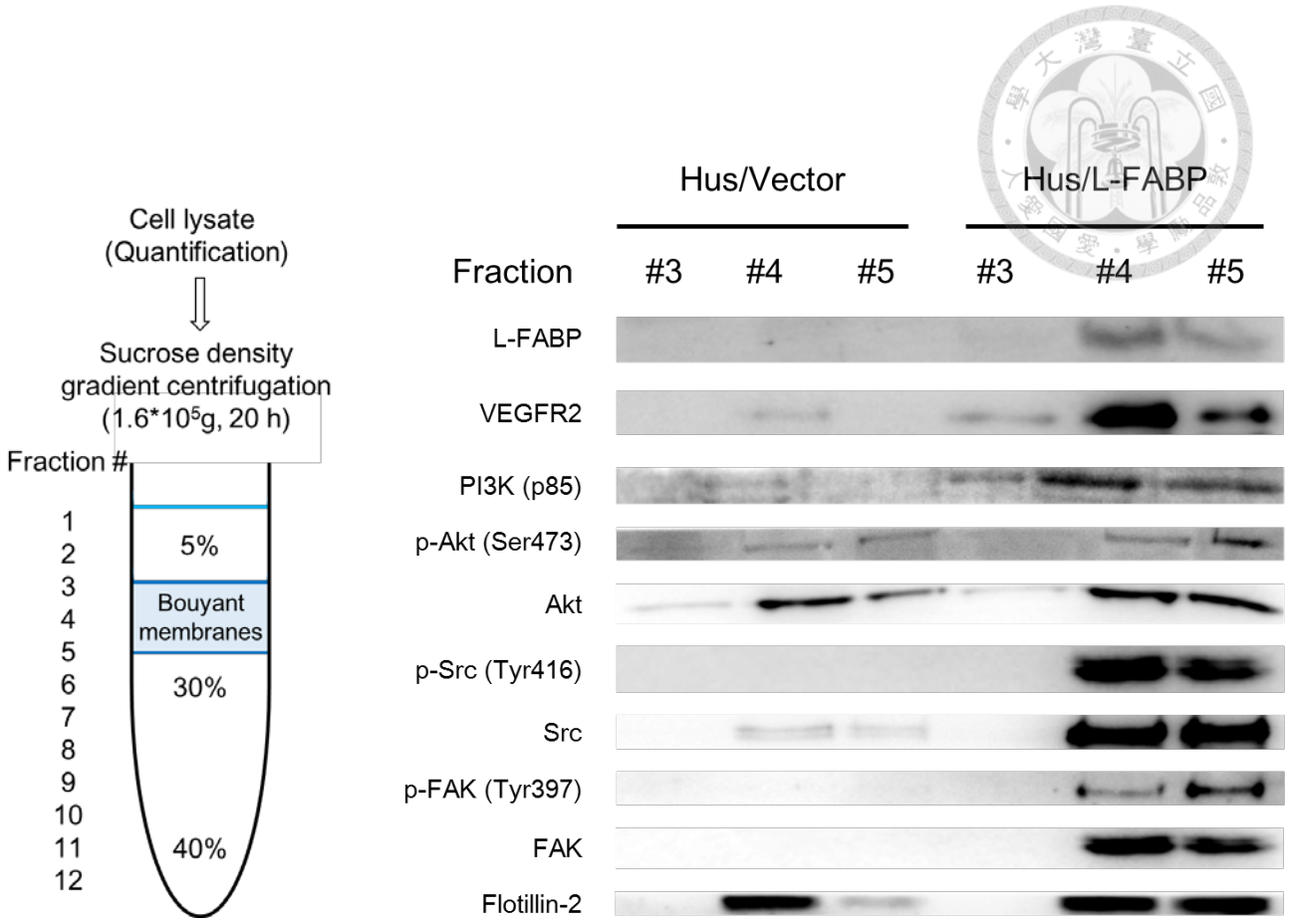

Figure 8. Localization of L-FABP and signaling molecules in lipid rafts

Membrane localization of L-FABP, VEGFR2, PI3K (p85), phospho-Akt (Ser473), Akt, phosho-Src (Tyr416), Src, FAK and phosho-FAK (Tyr397) in Hus/L-FABP or control cells. Membrane rafts were obtained by sucrose gradient based ultra-centrifugation and analyzed by western blot analysis (Fraction #3~#5).

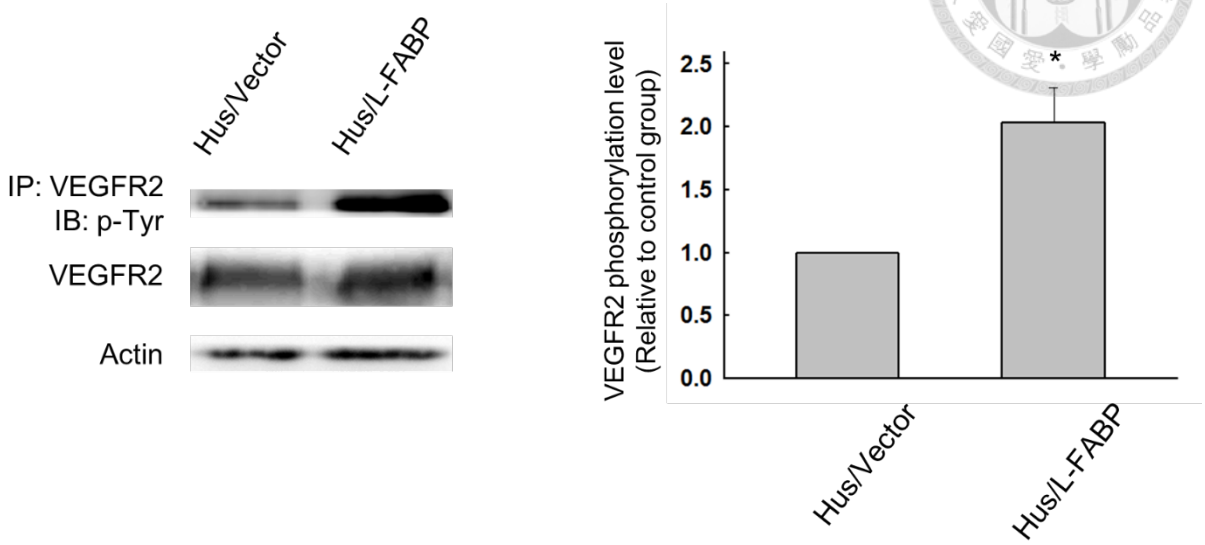

Figure 9. L-FABP increases the phosphorylation level of VEGFR2 in Hus cells

Phosphorylated levels of VEGFR2 in Hus/Vector and Hus/L-FABP cells were analyzed by immunoprecipitation (IP) of VEGFR2 antibody and blotted with phospho-tyrosine antibody. *$p < 0.05$ versus control group (Hus/Vector cells).

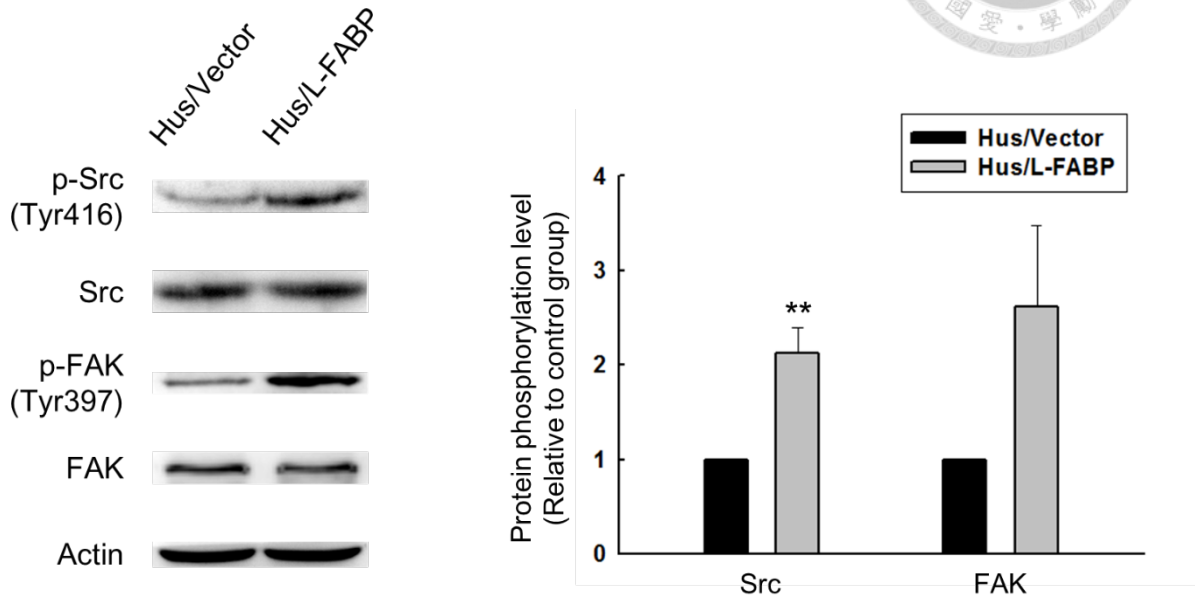

Figure 10. L-FABP increases the phosphorylation level of Src and FAK kinases in Hus cells

Phosphorylated level of Src (Tyr416) and FAK (Tyr397) in Hus/Vector and Hus/L-FABP cells were analyzed by western blot analysis. **$p < 0.01$ versus control group (Hus/Vector cells).

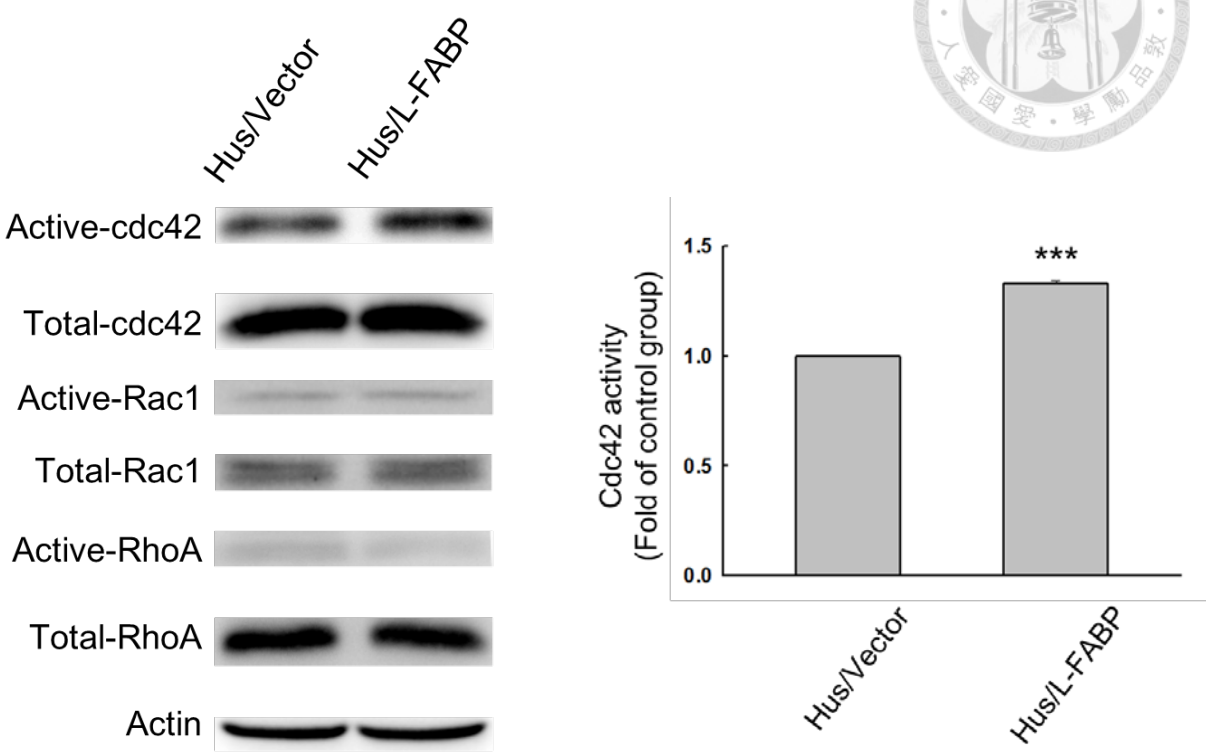

Figure 11. L-FABP promotes cdc42 activity of Hus cells

Small GTPase binding assay was carried out to Hus/L-FABP or control cells. Active cdc42 and Rac1 were detected by western blot analysis, however, active RhoA was not detectable in this study. For cdc42 activity, ***$p < 0.001$ versus control group (Hus/Vector cells).

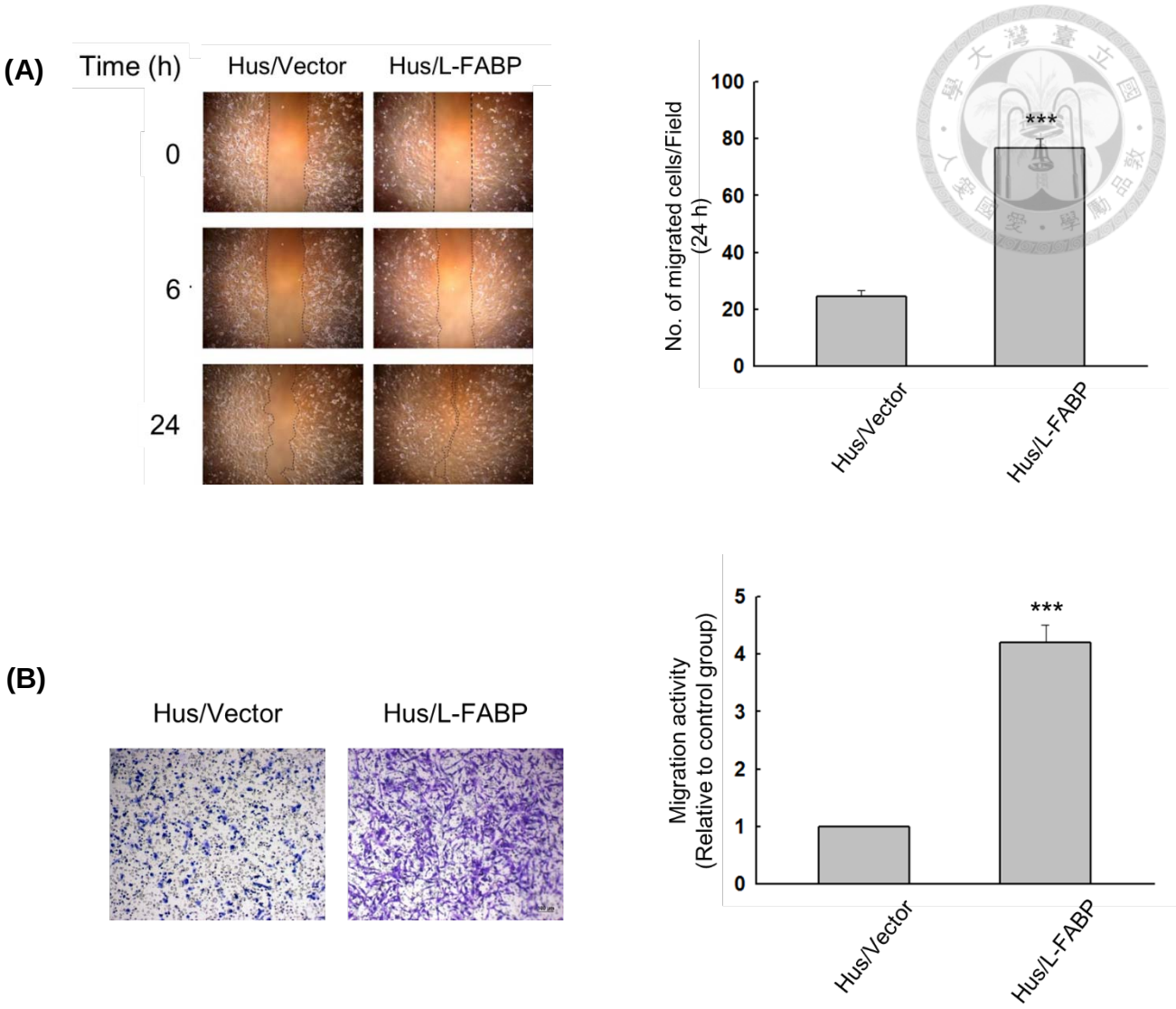

Figure 12. Analysis of migration activity of L-FABP stably expressed Hus cells

(A) Wound-healing migration assay of Hus/Vector and Hus/L-FABP were performed to examine two-dimensional migration activity and the migrated distance during the designated period was quantified. ***$p < 0.001$ versus control group (Hus/Vector cells). (B) For studying three-dimensional migration activity, Hus/Vector and Hus/L-FABP were seeded onto Boyden chambers and allowed to migrate toward 10% serum containing medium for 16 h. ***$p < 0.001$ versus control group (Hus/Vector cells).

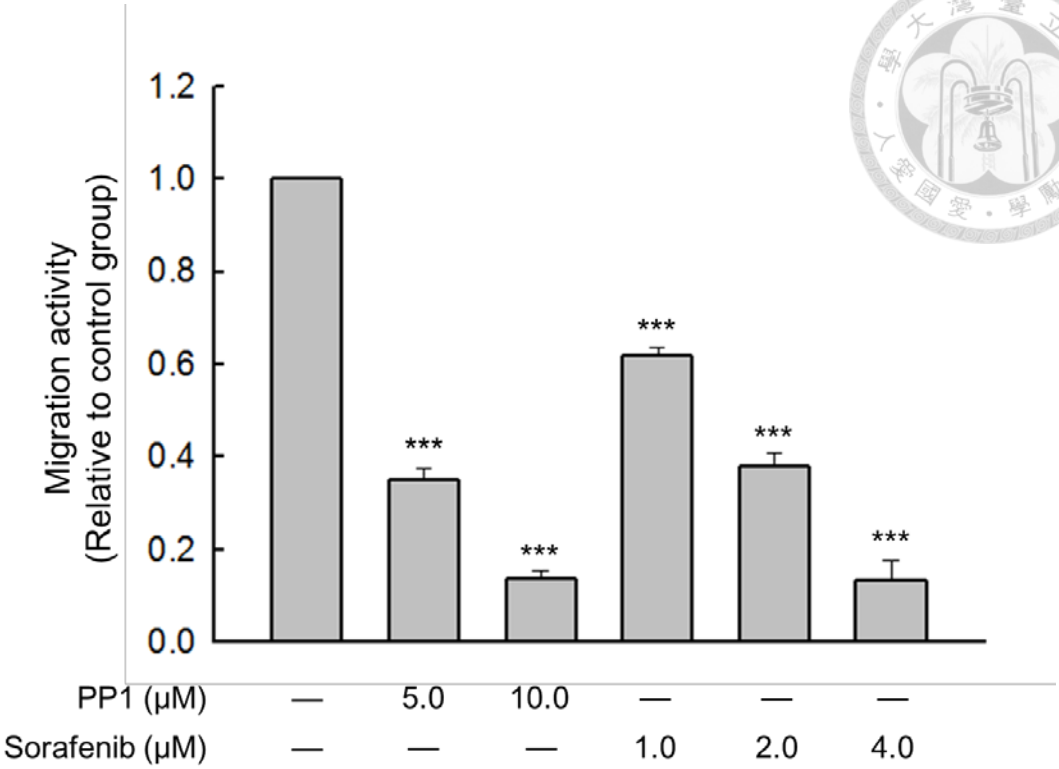

Figure 13. L-FABP up-regulates migration activity through VEGFR2/ Src pathway

Hus/L-FABP cells were treated with PP1 (Src inhibitor; 5, 10 μM, respectively) or Sorafenib (VEGFR2 inhibitor; 1, 2, 4 μM, respectively) for 16 h and analyzed by transwell assay. ***$p < 0.001$ versus control group (DMSO only treated cells).

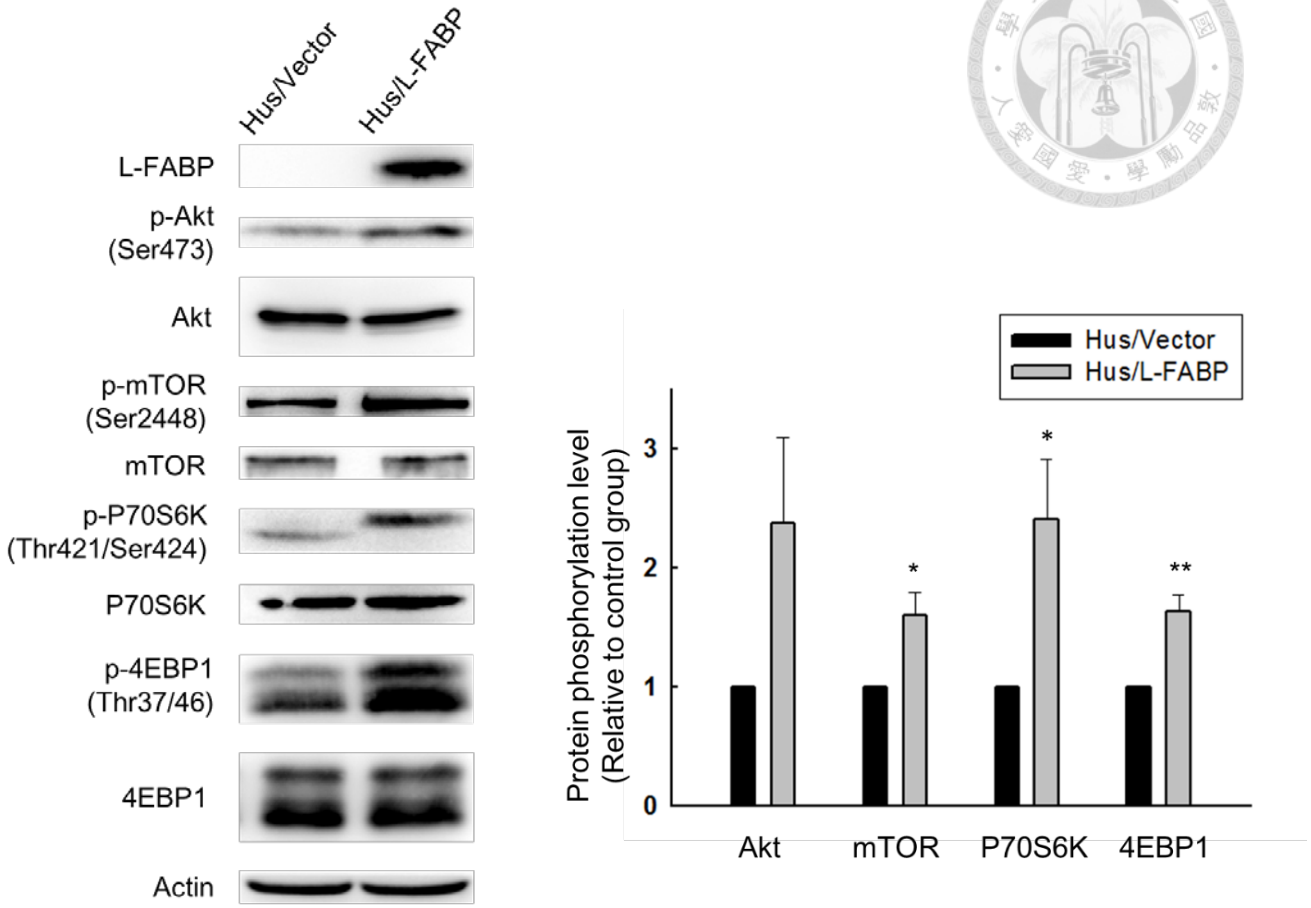

Figure 14. L-FABP activates Akt/ mTOR/ P70S6K/ 4EBP1 signaling

The phosphorylation level of Akt (Ser473), mTOR (Ser2448), P70S6K (Thr421/Ser424) and 4EBP1 (Thr37/46) in Hus/Vector and Hus/L-FABP cells were studied by western blot analysis. *$p < 0.05$, **$p < 0.01$ versus control group (Hus/Vector cells).

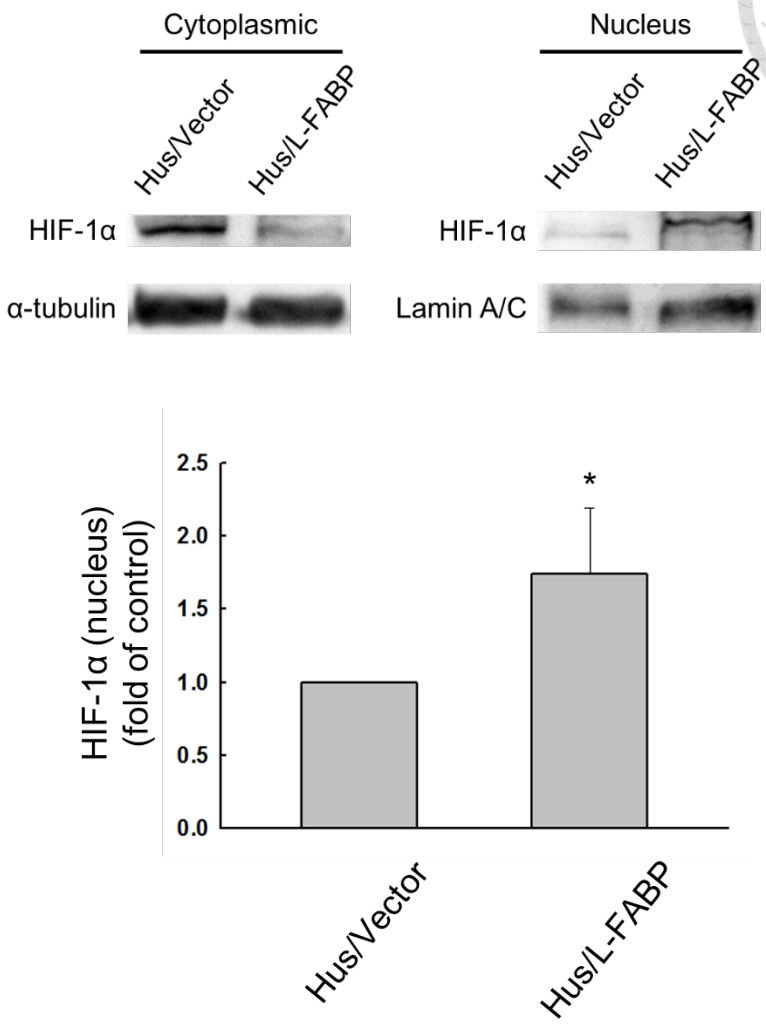

Figure 15. HIF-1α significantly increases in the nucleus of L-FABP overexpressed cells

Nucleus and cytoplasmic localization of HIF-1α in Hus/L-FABP cells was studied, and α-tubulin and lamin A/C were represented as loading controls for cytoplasmic and nucleus, respectively. Note that HIF-1α level was increased in Hus/L-FABP cells 1.7 fold higher than that of control group as the bar graph. *$p < 0.05$ versus control group (Hus/Vector cells).

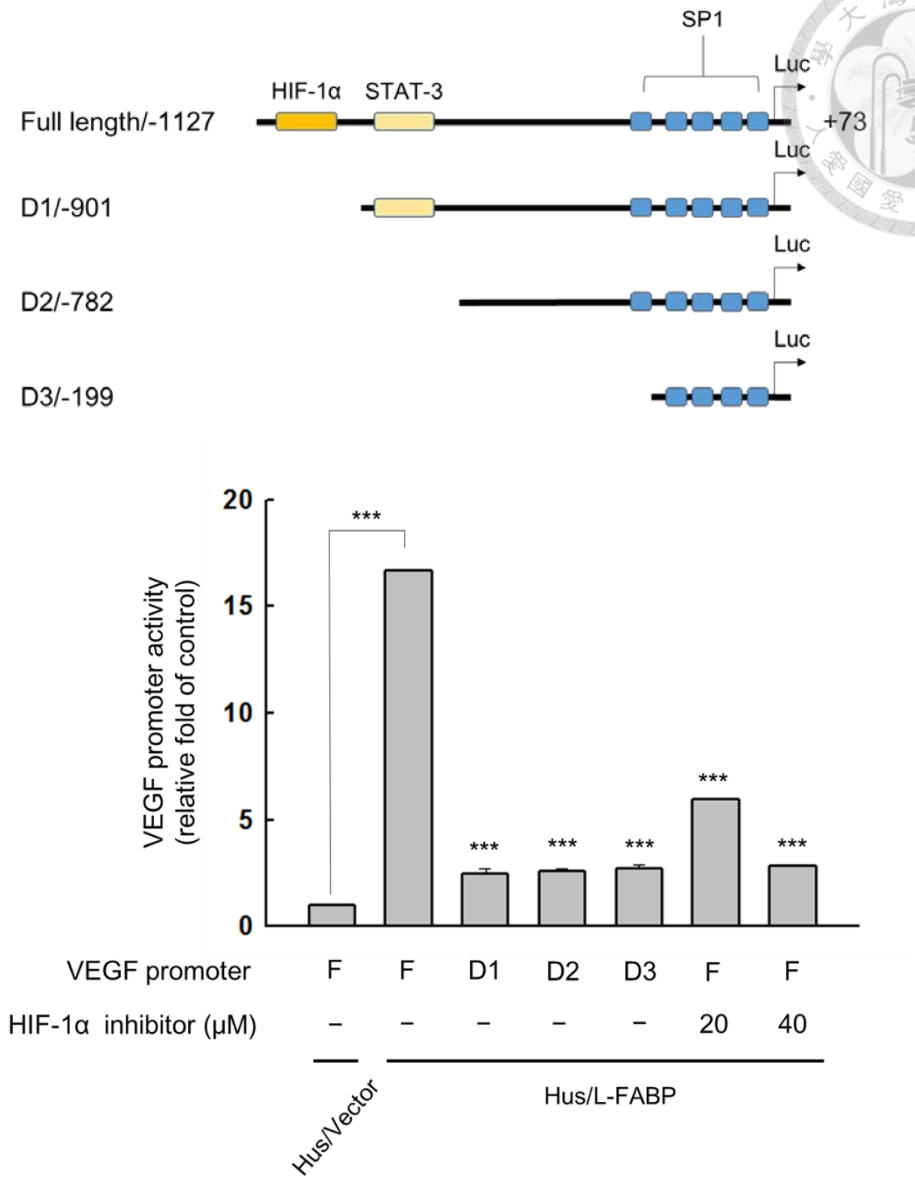

Figure 16. Role of HIF-1α in VEGF-A transcriptional activity of L-FABP overexpressed cells

The diagrams of the receptor constructs of full length and various deletion mutants of VEGF-A promoter (D1-D3) were showed as the graph. The luciferase activity of cell extracts was analyzed by luciferase reporter assay, and the data were presented as bar graph. For comparing full length activity, ***$p < 0.001$ versus control group (Hus/Vector cells); for deletion experiments, ***$p < 0.001$ versus control group (Hus/L-FABP cells); for adding HIF-1α inhibitor, ***$p < 0.001$ versus control group (Hus/L-FABP cells).

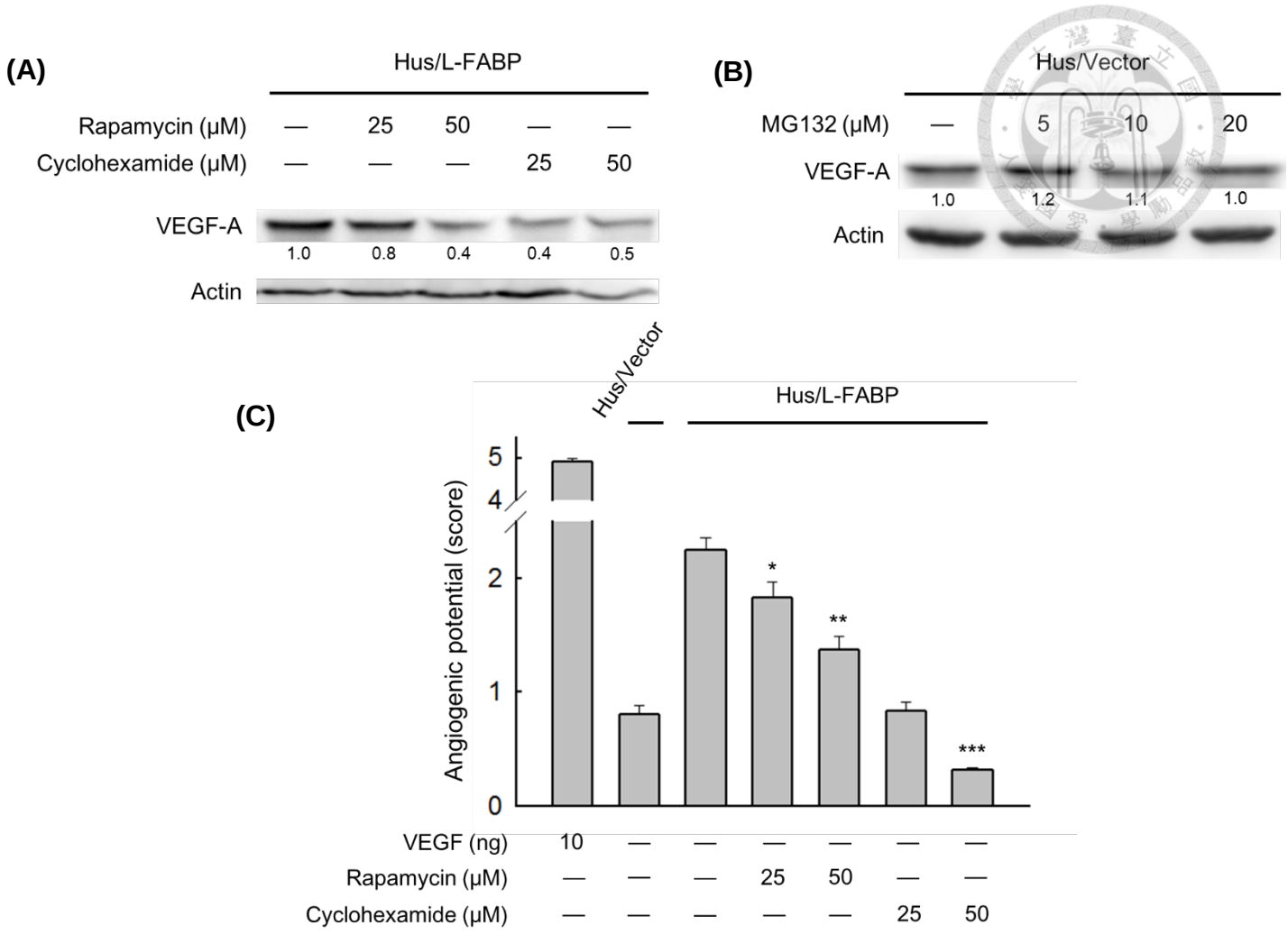

Figure 17. Post-transcriptional regulation of VEGF-A in L-FABP stably expressed Hus cells

(A) Hus/L-FABP cells were treated with Rapamycin (mTOR inhibitor) or cyclohexamide for 12 h and analyzed by western blot analysis. (B) On the other hand, Hus/Vector cells were treated with MG132 (proteasome inhibitor) for 24 h and analyzed by western blot analysis. (C) Cells were treated with Rapamycin or cyclohexamide for 12 h and the conditioned medium were subjected to tube formation assay to measure the in vitro angiogenic activity. Angiogenic vascular tube was imaged at 12 h and the quantification of S.CORE tube formation was shown as panel bar. ***$p < 0.001$ versus control group (DMSO only treated Hus/L-FABP cells).

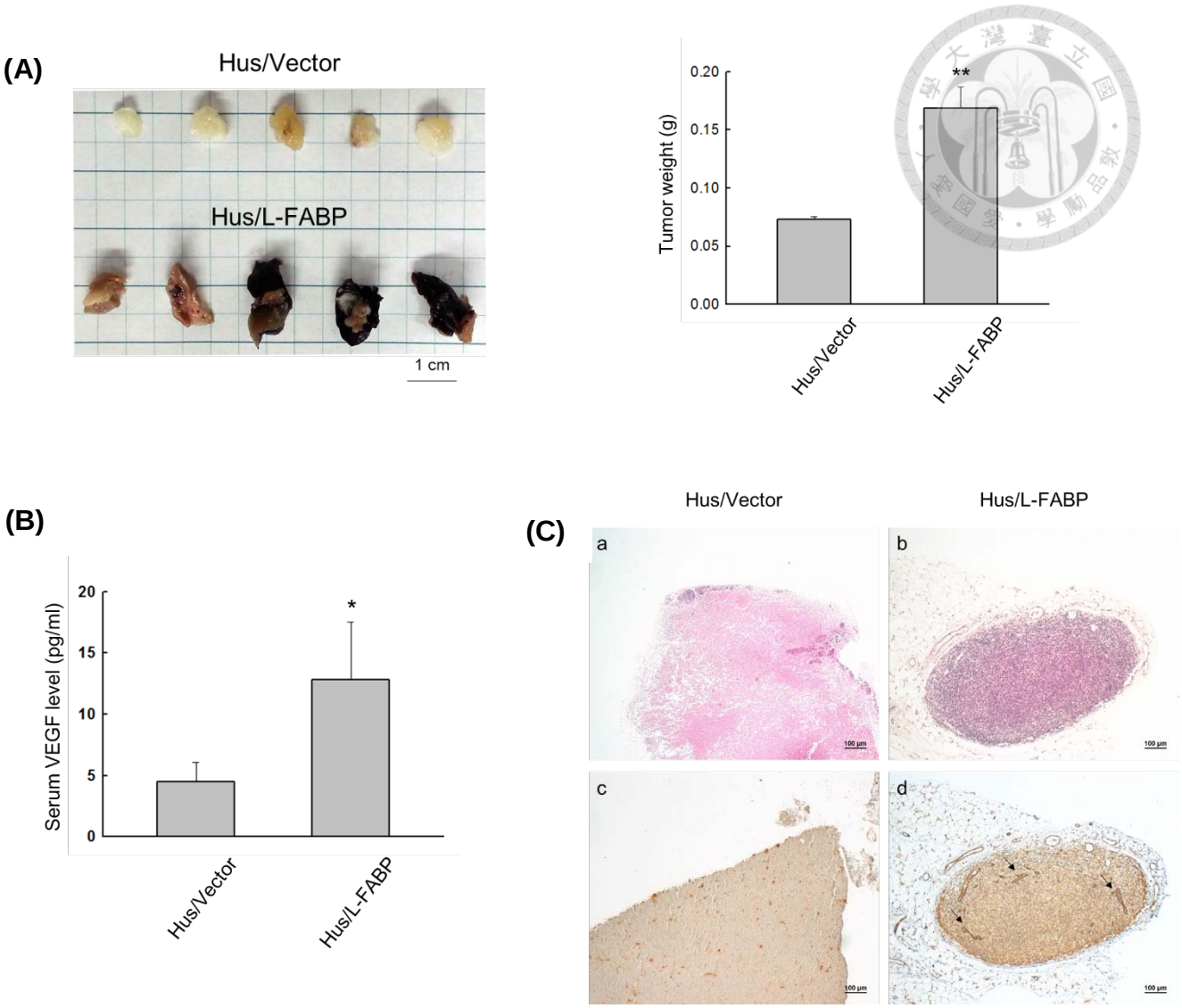

Figure 18. L-FABP promotes tumor growth *in vivo*

To study the effect of L-FABP on tumor growth, 2×10^6 of Hus/L-FABP or control cells were subcutaneously injected into the hind limb of NOD/SCID mice, and the resulting in situ tumors were removed 8 weeks later for analysis. (A) Representative photograph and average weight of tumors are presented. (n=5 per group). (B) VEGF-A contents in serum of the above mice were measured and presented in the bar graph. (C) The tumor sections analyzed by H&E staining (a & b) or anti-CD31 antibody IHC staining (c & d) indicated the strong angiogenesis activity in Hus/L-FABP mice group. Image a & c indicated Hus/Vector group; b & d indicated Hus/L-FABP group.

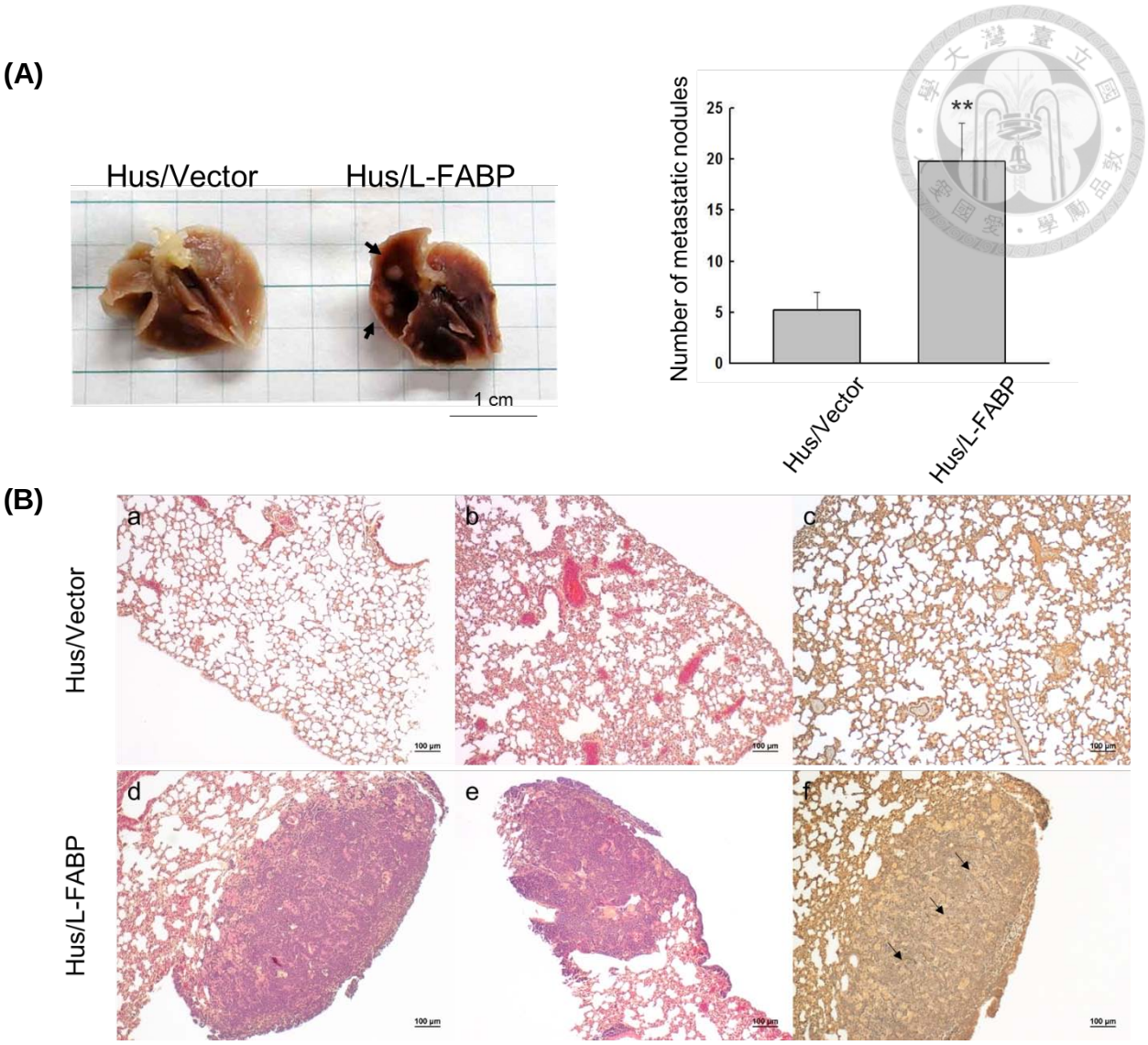

Figure 19. L-FABP promotes *in vivo* metastasis by lung metastasis model

The metastatic activity of Hus/L-FABP cells was carried out by lung metastasis model. 5 x 10^6 of Hus/L-FABP or control cells were intravenously injected into the lateral tail vein of NOD/SCID mice. After 10 weeks, the lungs were excised from each mice for analysis. (A) Metastatic nodules were presented and counted (n=5 per group). (B) The immunohistochemistry analysis by H&E staining (a, b, d and e) or anti-CD31 antibody IHC staining (c and f) were also studied. Image a – c indicated Hus/Vector group; d – f indicated Hus/L-FABP group. **P < 0.01 versus control group (mice injected with Hus/Vector cells).

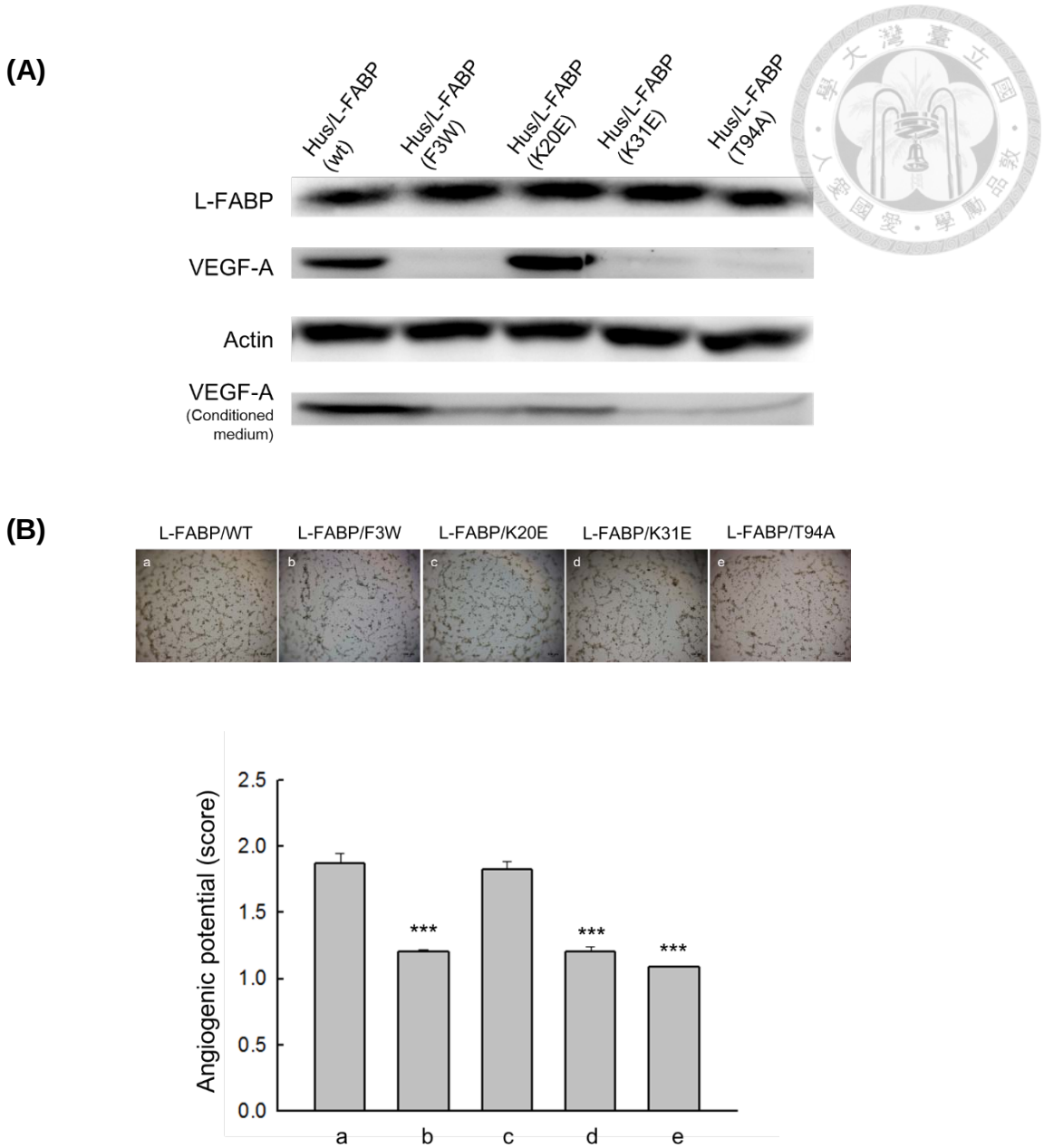

Figure 20. Effects of L-FABP mutants in VEGF-A expression

(A) Different mutant types of L-FABP stable expressed cells were generated by site directed mutagenesis, and the expression levels of L-FABP and VEGF-A (both intracellular level and extracellular level) were analyzed by western blotting. (B) The *in vitro* angiogenic activity of these mutants was studied by tube formation assay. ***P < 0.001 versus control group (L-FABP/WT cells). Amino acids substitution: a for L-FABP (wild type), b for L-FABP (F3 to W), c for L-FABP (K20 to E), d for L-FABP (K31 to E), and e for L-FABP (T94 to A)

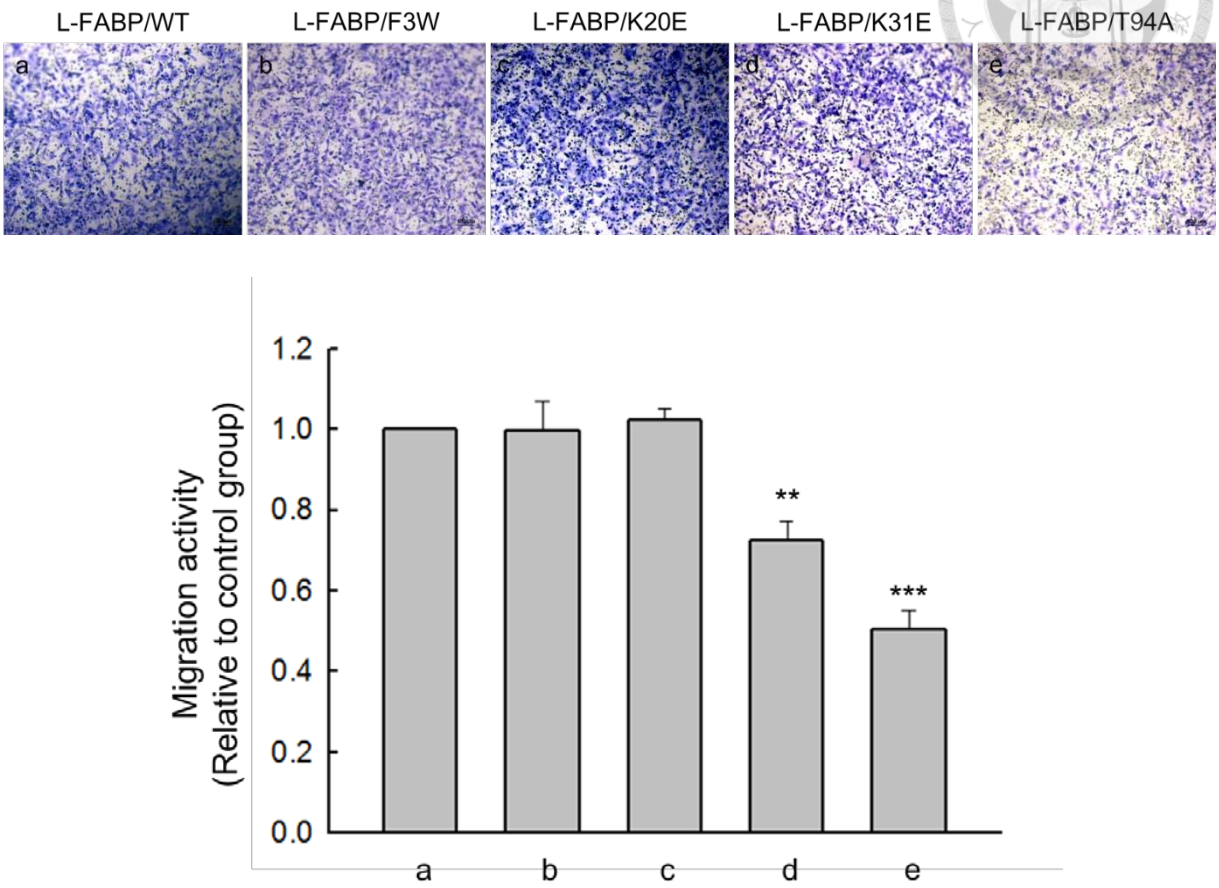

Figure 21. Effects of L-FABP mutants in migration activity

Migration activity of these mutants was carried out by transwell assay. **P < 0.01, ***P < 0.001 versus control group (L-FABP/WT cells). Amino acids substitution: a for L-FABP (wild type), b for L-FABP (F3 to W), c for L-FABP (K20 to E), d for L-FABP (K31 to E), and e for L-FABP (T94 to A)

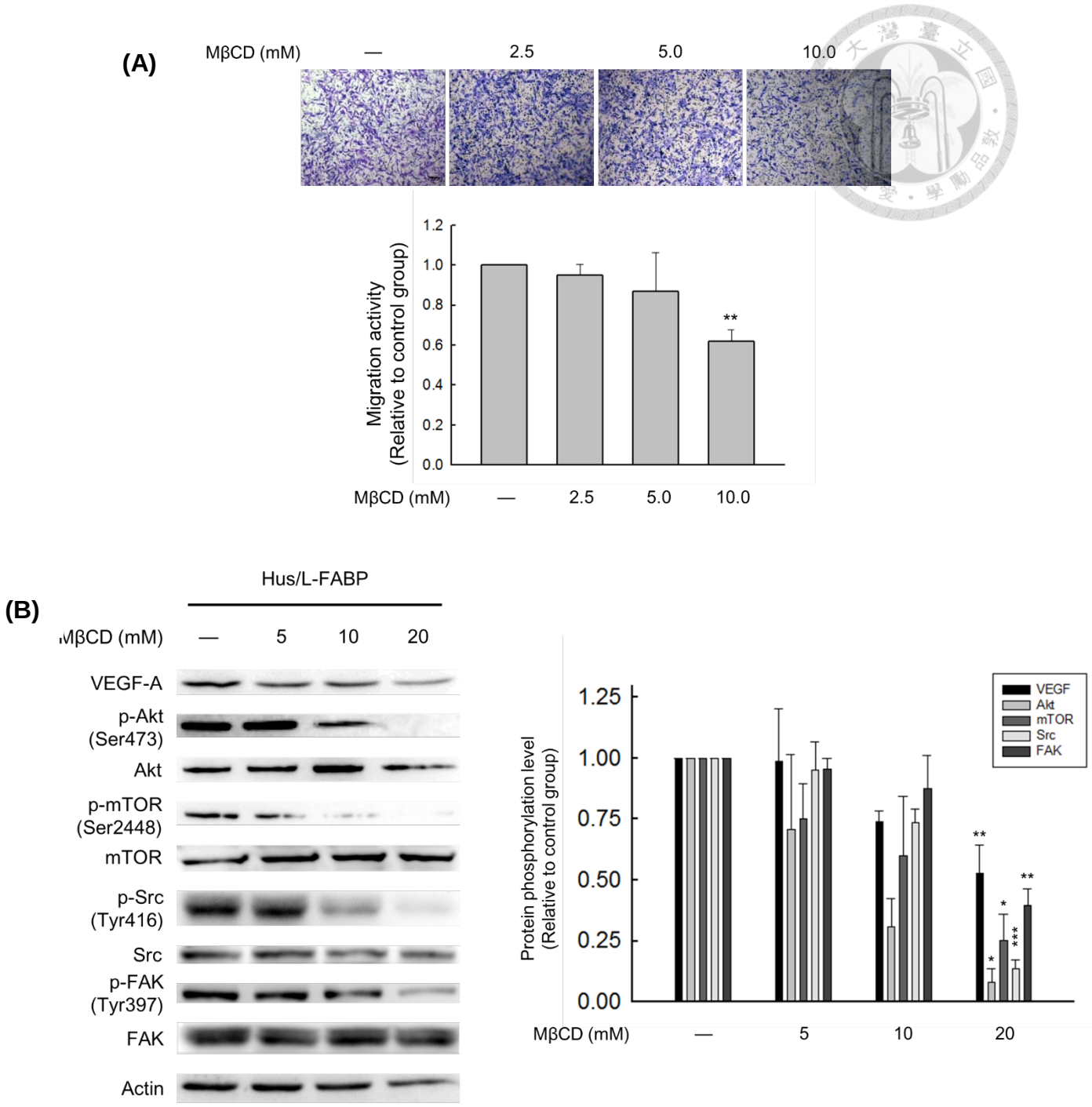

Figure 22. Cholesterol associating properties are essential for L-FABP induced cell migration and angiogenesis.

Hus/L-FABP cells were treated with MβCD (cholesterol depletion agent; 5, 10, 20 mM, respectively) for 12 h and analyzed by (A) transwell migration assay and (B) western blot analysis. *$p < 0.05$, **$p < 0.01$, ***$p < 0.001$ versus control group (DMSO only treated cells).

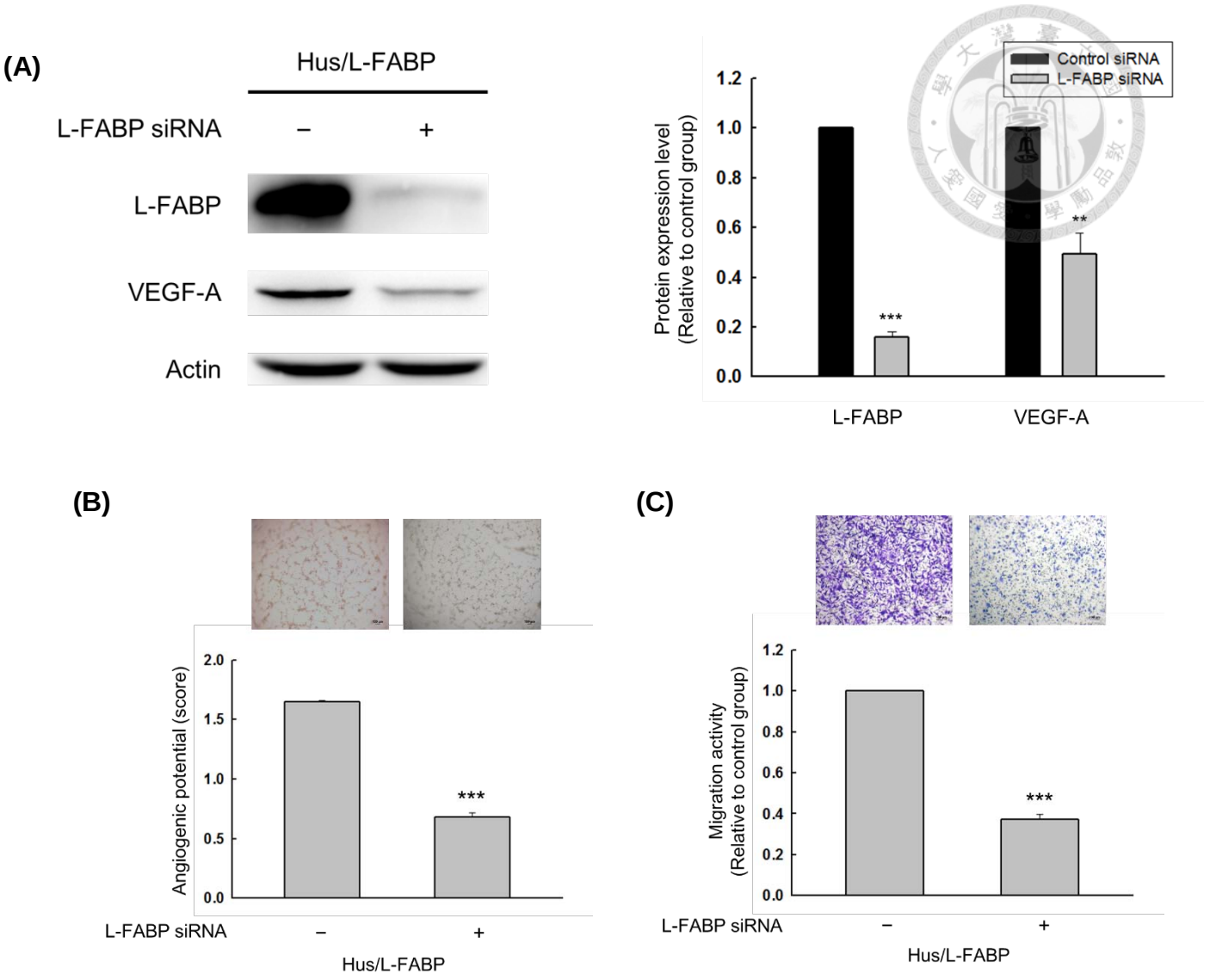

Figure 23. Knockdown of L-FABP in Hus/L-FABP cells reversely decreases VEGF-A expression and migration activity

(A) Hus/L-FABP cells were transfected with control or L-FABP targeting siRNA for 24 h, and the expression levels of L-FABP and VEGF-A were examined by western blot analysis. **$p < 0.01$, ***$p < 0.001$ versus control group. (B) The L-FABP siRNA treated cells were performed to tube formation assay to study in vitro angiogenic activity. Angiogenic vascular tube was imaged at 12 h. ***$p < 0.001$ versus control group. (C) The L-FABP siRNA treated cells were seeded onto Boyden chambers and allowed to migrate for 16 h. ***$p < 0.001$ versus control group.

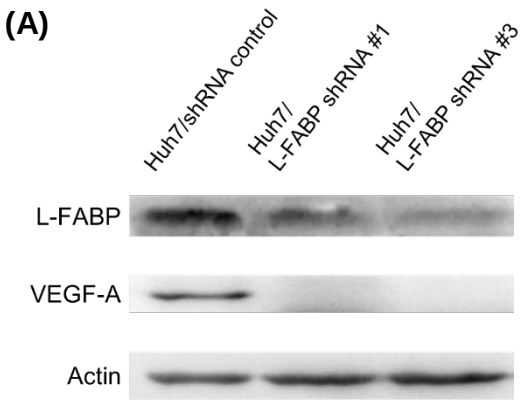
(A)
Huh7/shRNA control
Huh7/
L-FABP shRNA #1
Huh7/
L-FABP shRNA #3
L-FABP
VEGF-A
Actin

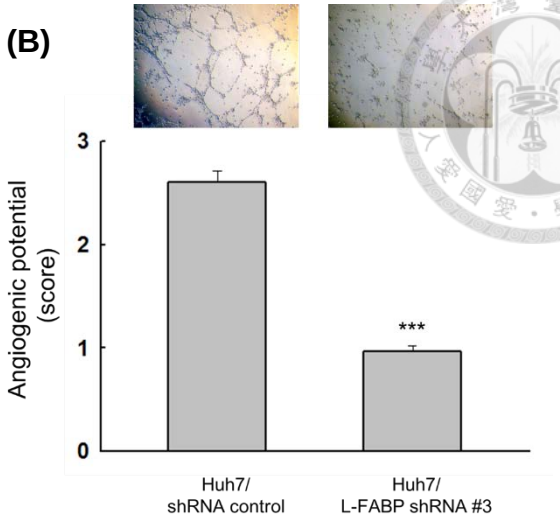
(B)
Angiogenic potential
(score)
3
2
1
0
***
Huh7/
shRNA control
Huh7/
L-FABP shRNA #3

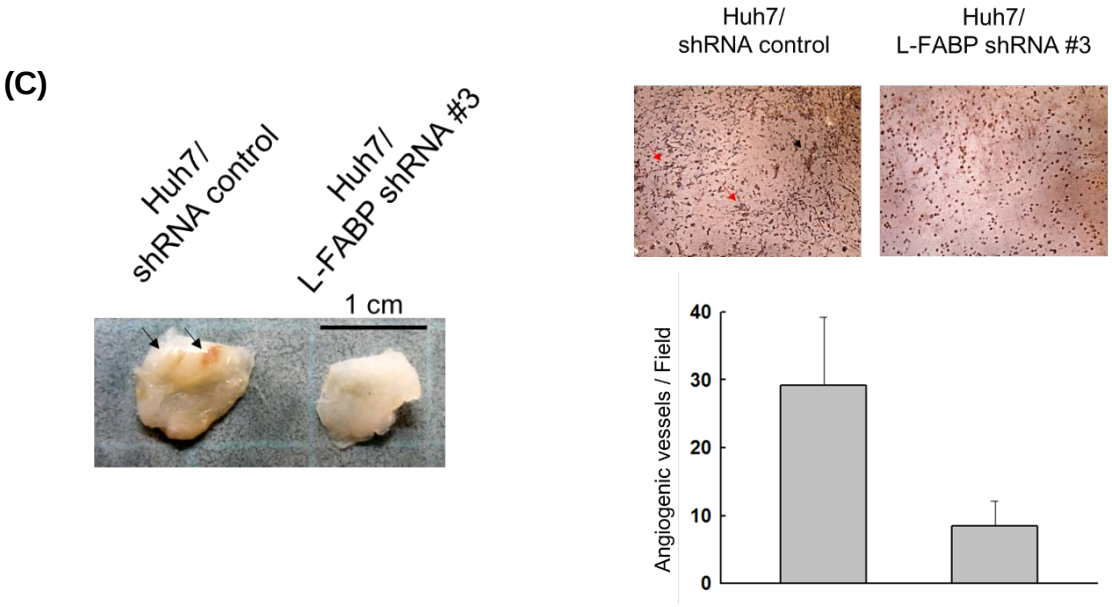
(C)
Huh7/
shRNA control
Huh7/
L-FABP shRNA #3
1 cm
Huh7/
shRNA control
Huh7/
L-FABP shRNA #3
Angiogenic vessels / Field
40
30
20
10
0

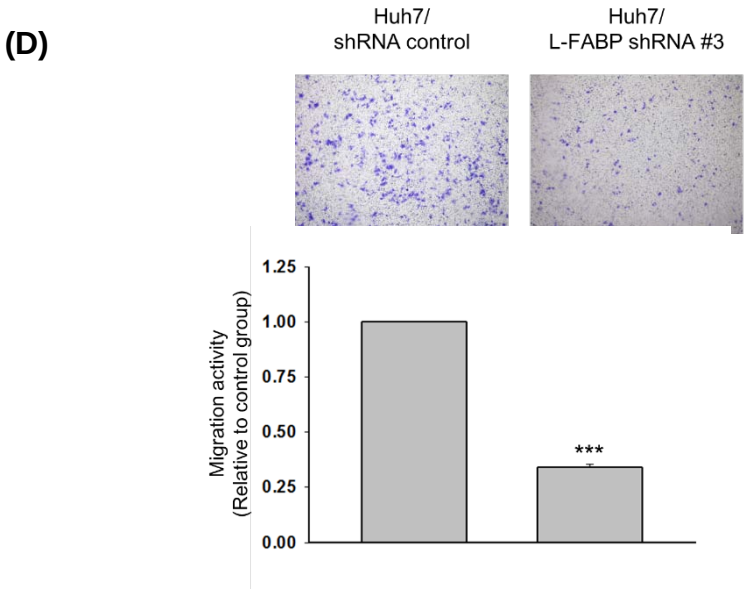
(D)
Huh7/
shRNA control
Huh7/
L-FABP shRNA #3
Migration activity
(Relative to control group)
1.25
1.00
0.75
0.50
0.25
0.00
***

Figure 24. Knockdown of L-FABP in Huh7 cells down-regulates VEGF-A expression and migration activity

(A) Huh7 cells were transfected with control or L-FABP targeting shRNA plasmid, and screened with puromycin for L-FABP stably knockdown clones. The expression levels of L-FABP and VEGF-A in selected two clones were examined by western blot analysis. (B) The *in vitro* angiogenic activity was studied by tube formation assay which performed by HUVEC endothelial cells to determine angiogenesis activities of L-FABP stably knockdown Huh7 cells. Angiogenic vascular tube was imaged at 8 h. The quantification of S.CORE tube formation was shown as panel bar. ***$p < 0.001$ versus control group. (C) The *in vivo* angiogenic activity was studied by matrigel plug in assay. Left: Macroscopic view of matrigel plugs recovered from mice injected with Huh7/shRNA control cells or Huh7/L-FABP shRNA cells, and the infiltration of blood vessels was indicated by arrows. Right: Immunohistochemical staining of CD31 (angiogenesis marker) in matrigel plugs were presented and quantified. n=3, p=0.067. (D) The Huh7/L-FABP shRNA stable clones were seeded onto Boyden chambers and allowed to migrate for 16 h to study 3D migration activity. ***$p < 0.001$ versus control group.

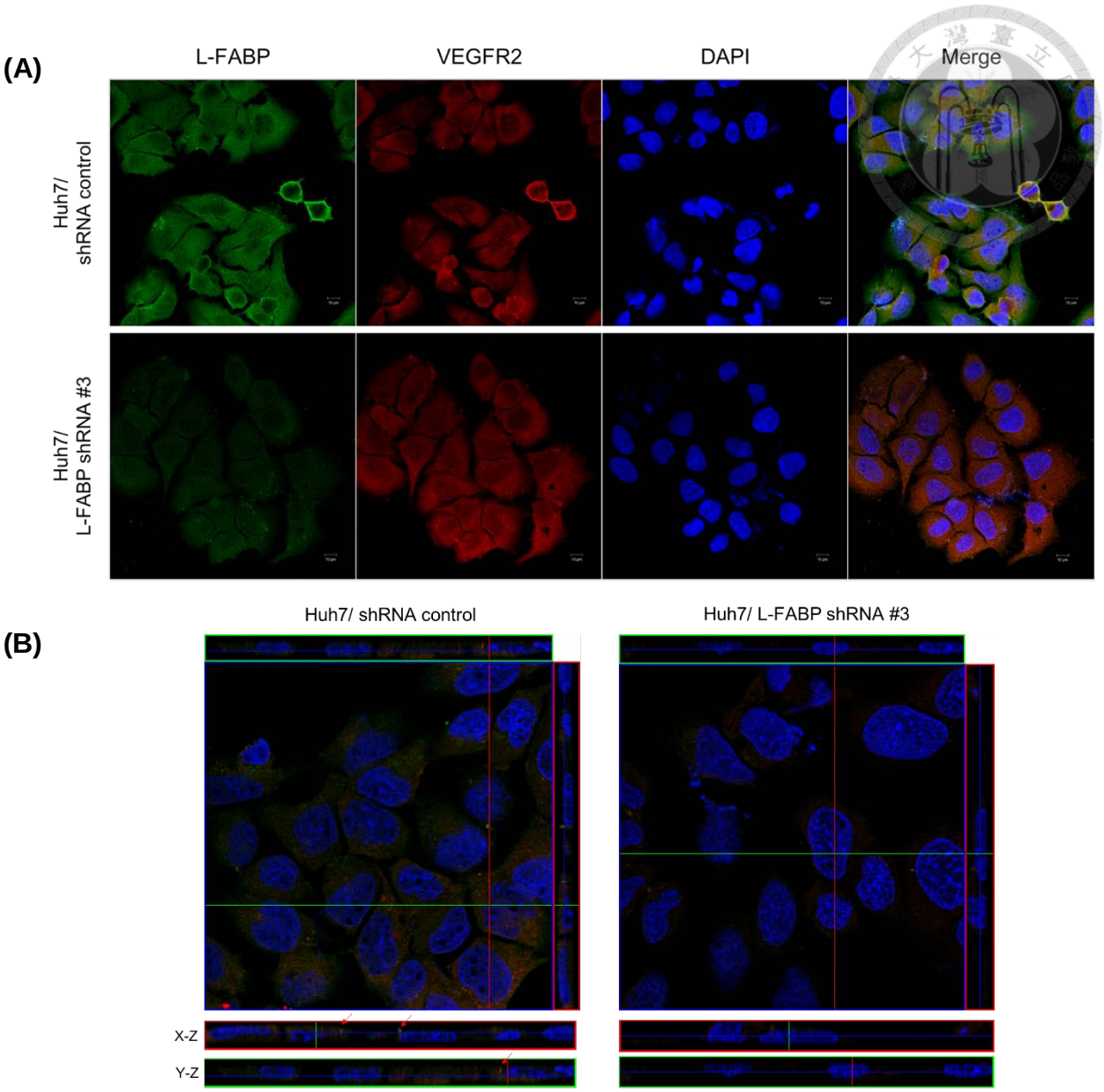

Figure 25. Reduction of L-FABP and VEGFR2 co-localization on membrane is observed in Huh7 L-FABP stably knockdown cells

(A) Huh7 L-FABP stably knockdown cells were fixed and stained with antibodies against to VEGFR2 and L-FABP. Three-color confocal images were acquired on a confocal microscope (Magnification, 63×). (B) Red or green lines showed the X-Z or Y-Z optical section of Huh7/shRNA control and Huh7/L-FABP shRNA cells, respectively. The co-localization of VEGFR2 and L-FABP on the upside of cells was indicated by arrows. The Signals of upper images were presented by different colors: L-FABP-Alexa 488 (green); VEGFR2-Alexa 568 (red); and DAPI (blue).

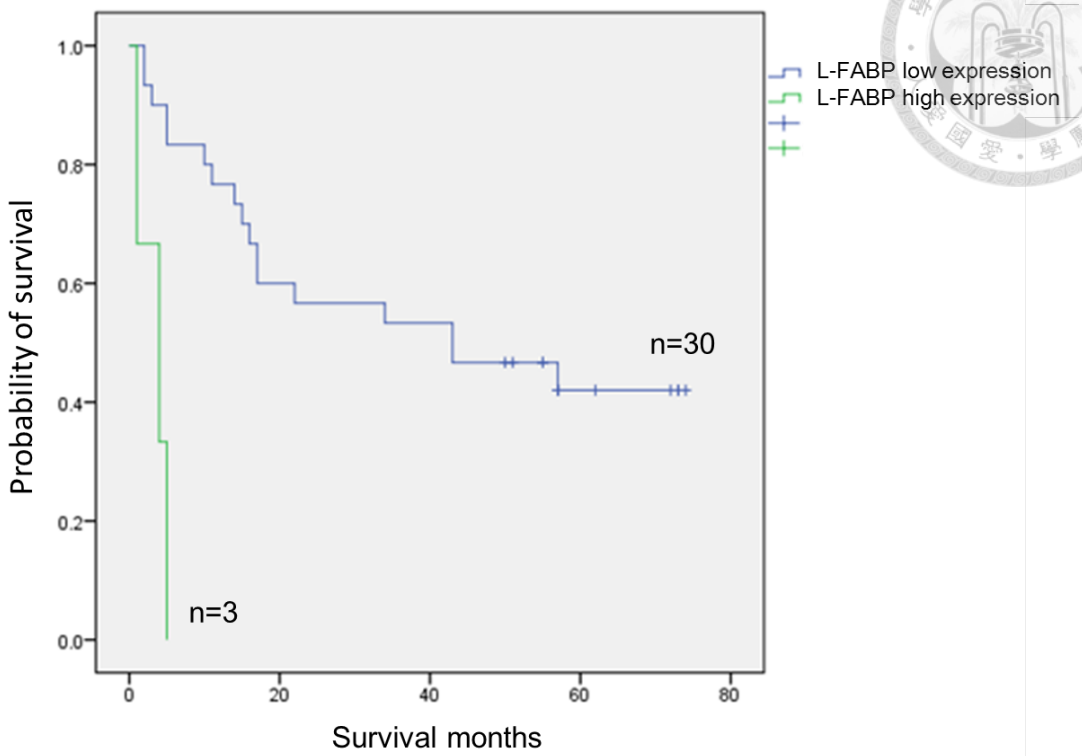

Figure 26. Aberrant overexpression of L-FABP in HCC tissues (with cirrhosis) is associated with worse outcome

Kaplan-Meier survival curves demonstrate that L-FABP high group (n=3) has a shortened survival time compared with that of the L-FABP low group (n=30). ***$p < 0.001$.

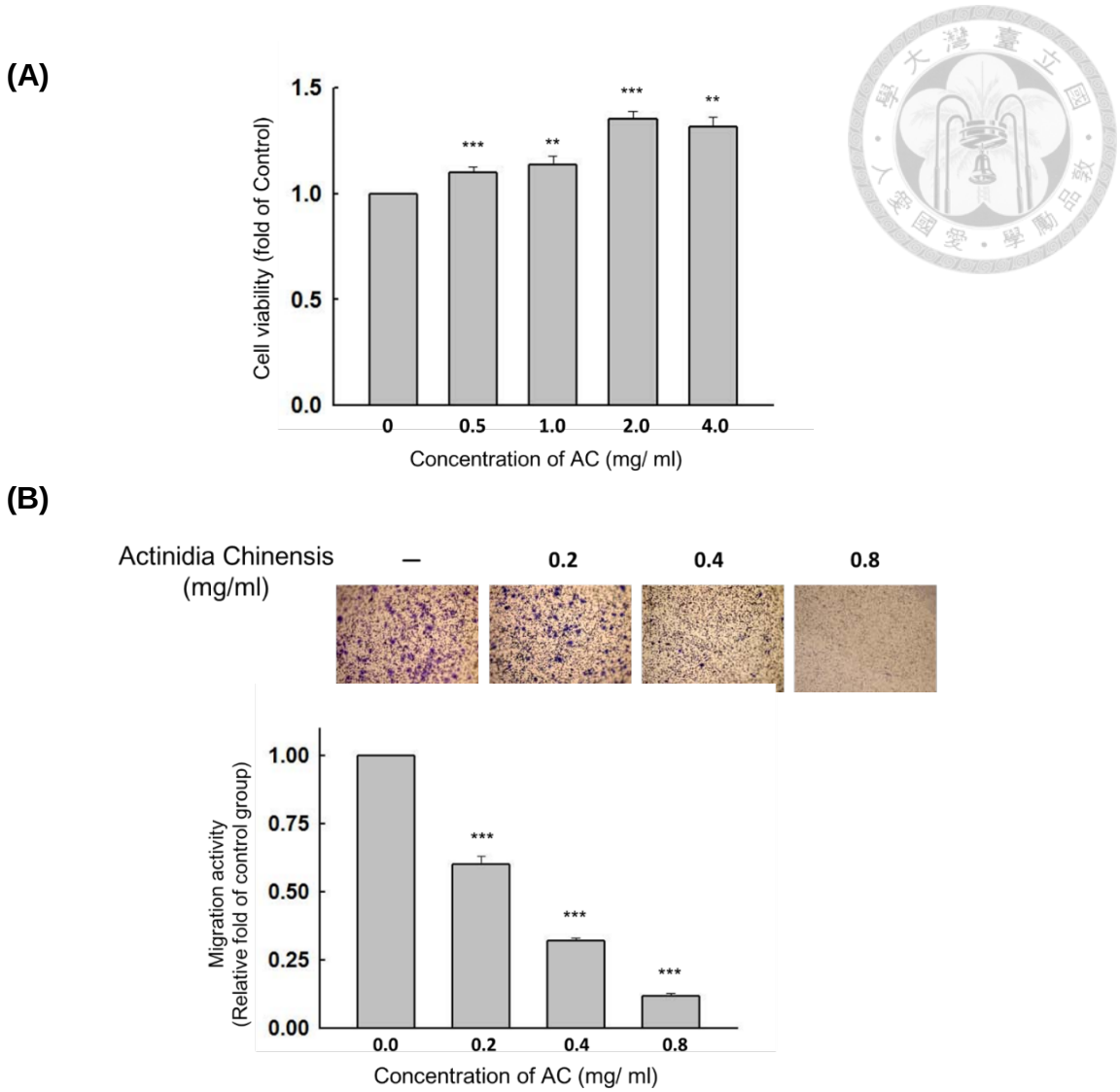

Figure 27. Cytotoxicity and migration inhibitory effect of *Actinidia chinensis* on Huh7 cells

(A) Huh7 cells were treated with 0.1% DMSO (control) or various concentrations of *A. chinensis* (AC) for 24 h and cell viability was determined with an MTT assay. Results are presented as mean value ± SE. (**P < 0.01, ***P < 0.001 compared with the DMSO treated group). (B) Migration activity of Huh7 cells was inhibited by *A. chinensis*. The control cells were treated with 100 μL ddH2O, and the migration activity of Huh7 cells was inhibited by *A. chinensis* in a dose-dependent manner. Results are presented as mean value ± SE. (***P < 0.001 compared with the water treated group)

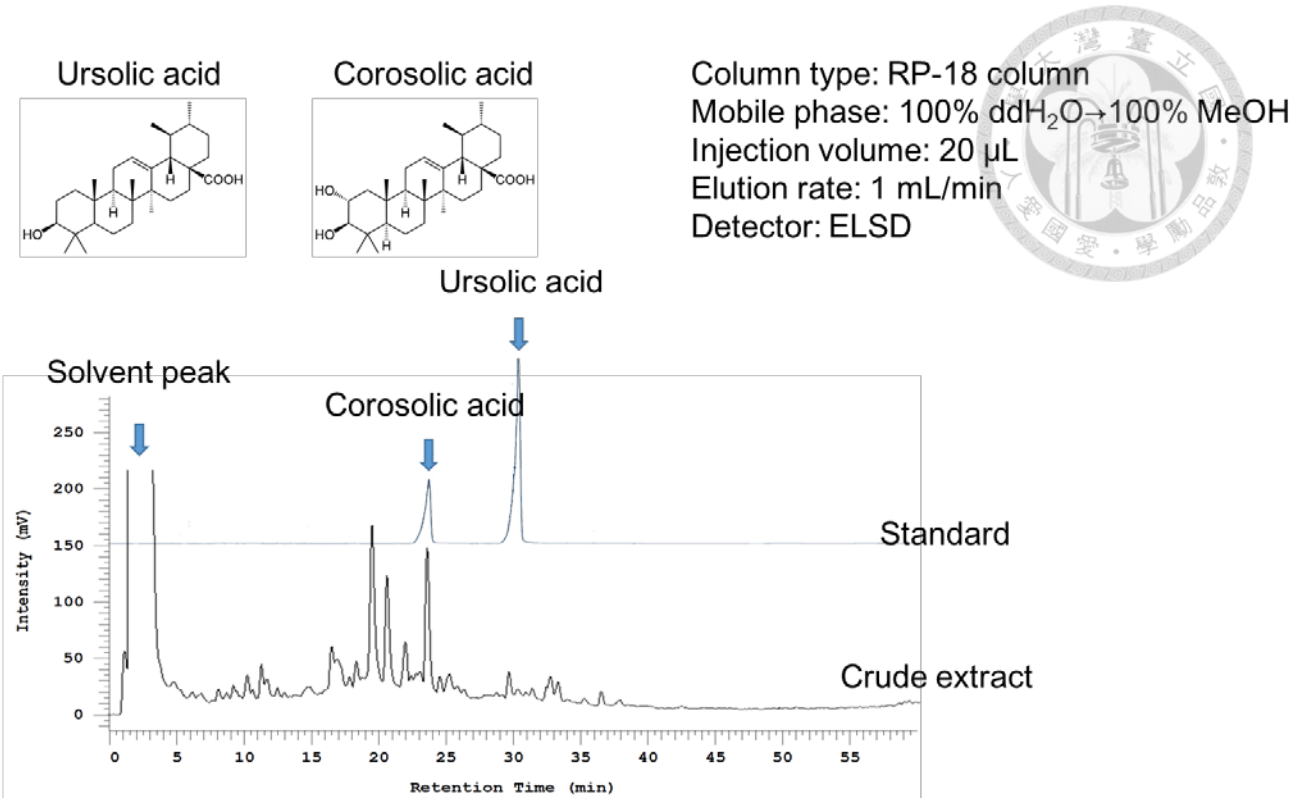

Figure 28. HPLC analysis of *Actinidia chinensis*

High-Performance liquid chromatographydiode array (HPLC-DAD)/ELSD chromatography was used to examine compounds in *A. chinensis*. The conditions for analysis are described in the methods section.

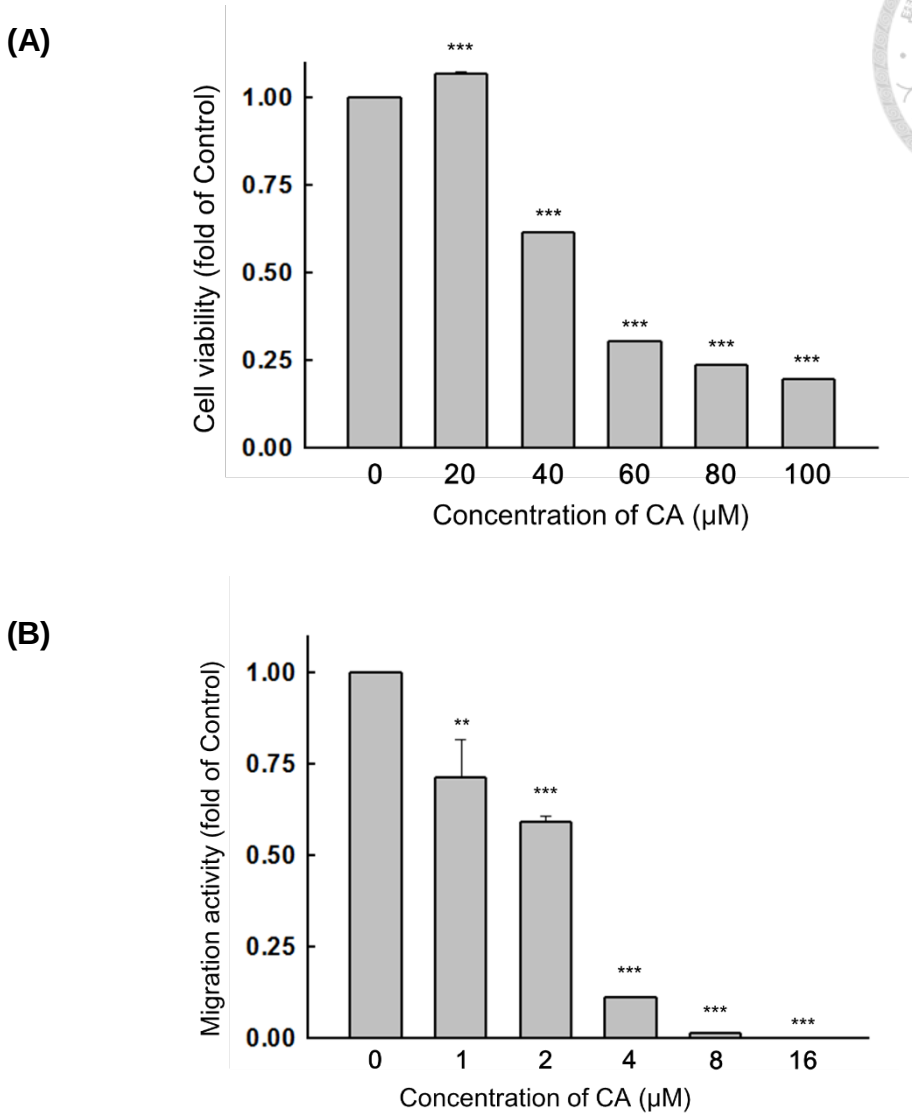

Figure 29. Migration activity of Huh7 cells is inhibited by corosolic acid without cytotoxicity

(A) Huh7 cells were treated with 0.1% DMSO (control) or various concentrations of corosolic acid for 24 h and cell viability was determined with an MTT assay. (B) The migration activity of Huh7 cells was inhibited by corosolic acid in a dose-dependent manner. (n = 3, **P < 0.01, ***P < 0.001 compared with the DMSO treated group)

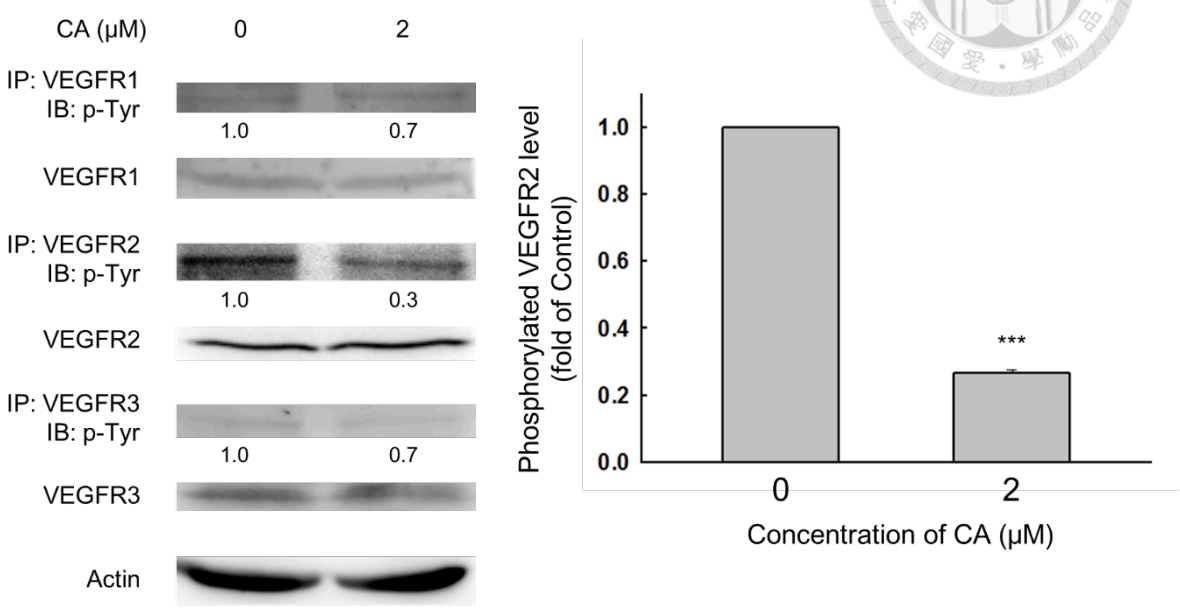

Figure 30. Corosolic acid reduces phosphorylation level of VEGFR2

Huh7 cells were treated with 0.1% DMSO (control) or corosolic acid for 15 min and lysates were immunoprecipitated with anti-VEGFR1, VEGFR2, and VEGFR3 Ab, followed by blotting with anti-phospho-tyrosine Ab. (For VEGFR2, n = 3, ***P < 0.001 compared with the DMSO treated group)

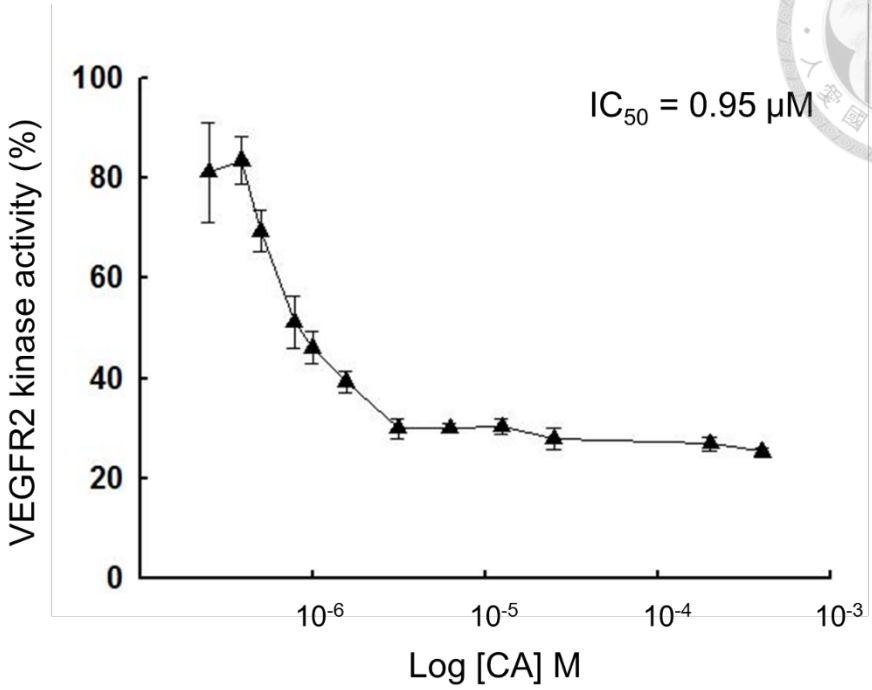

Figure 31. Corosolic acid reduces VEGFR2 kinase activity

ADP-Glo Kinase Assay (Promega, Madison, USA) was performed to assess the inhibitory effect of corosolic acid on VEGFR2 kinase activity. (n = 3, RLU data were normalized to the control group and shown as percentages)

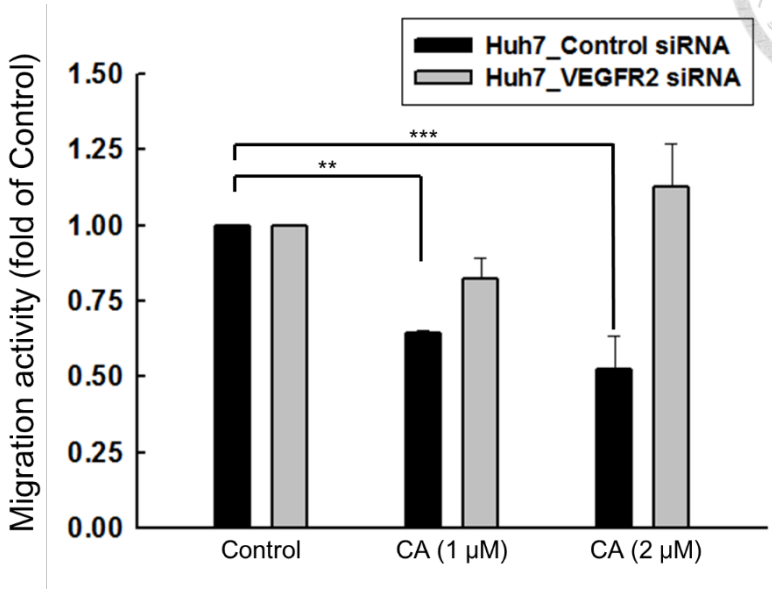

Figure 32. CA-induced inhibition of migration activity in Huh7 cells is VEGFR2 dependent

Huh7 cells were transfected with 100 nM KDR siRNA or control siRNA, recovered for 24 h, and treated with 0.1% DMSO (control) or CA. Migration activity was assessed with a transwell assay. (n = 3, **P < 0.01, ***P < 0.001 compared with the DMSO treated cells in Huh7 control siRNA group)

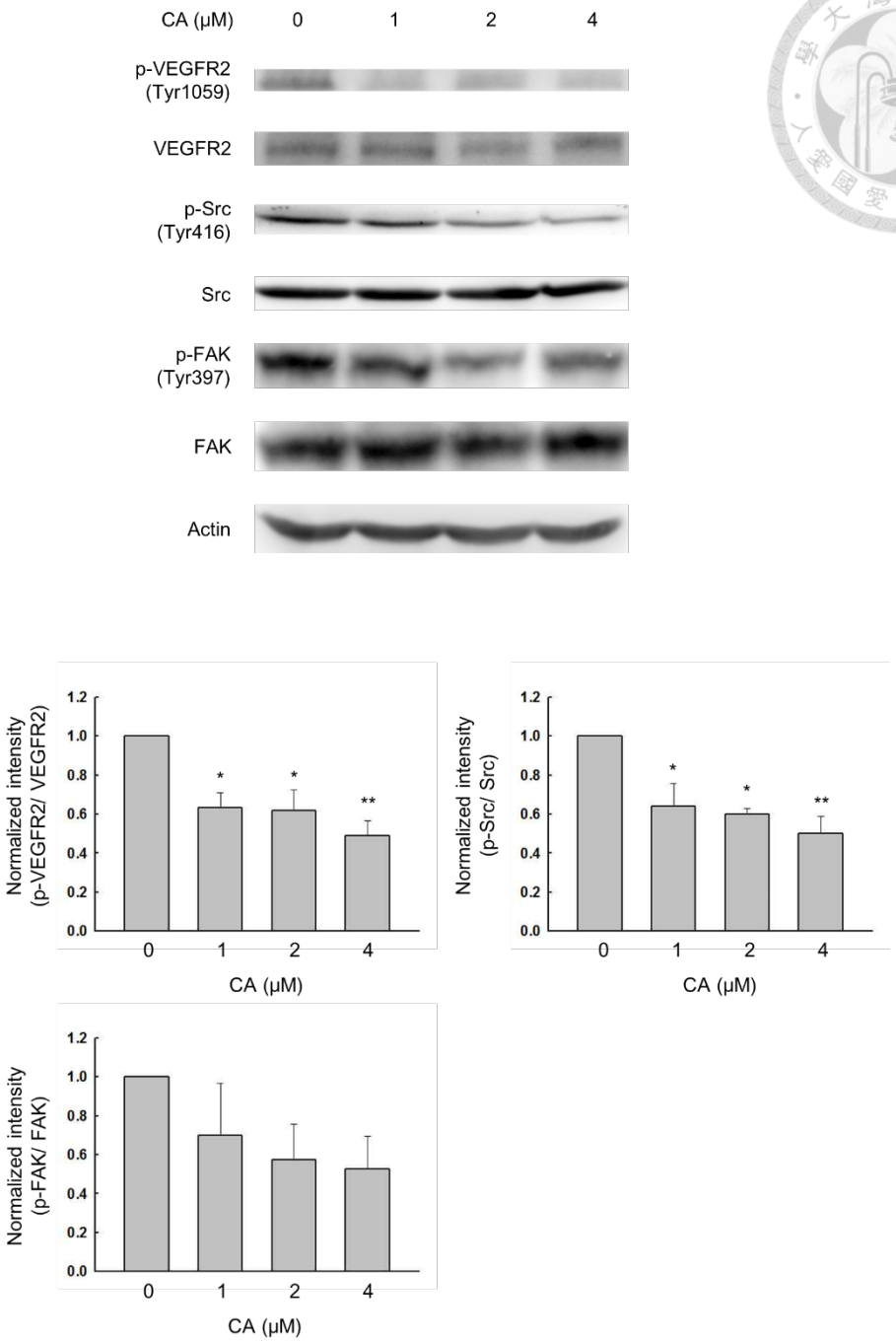

Figure 33. Corosolic acid down-regulates VEGFR2 downstream signals

Huh7 cells were treated with 0.1% DMSO (control) or corosolic acid for 30 min, and the phosphorylation level of VEGFR2 (Tyr1058), Src (Tyr416), and FAK (Tyr397) were analyzed by western blot. (n = 3, *P < 0.05, **P < 0.01 compared with the DMSO treated group)

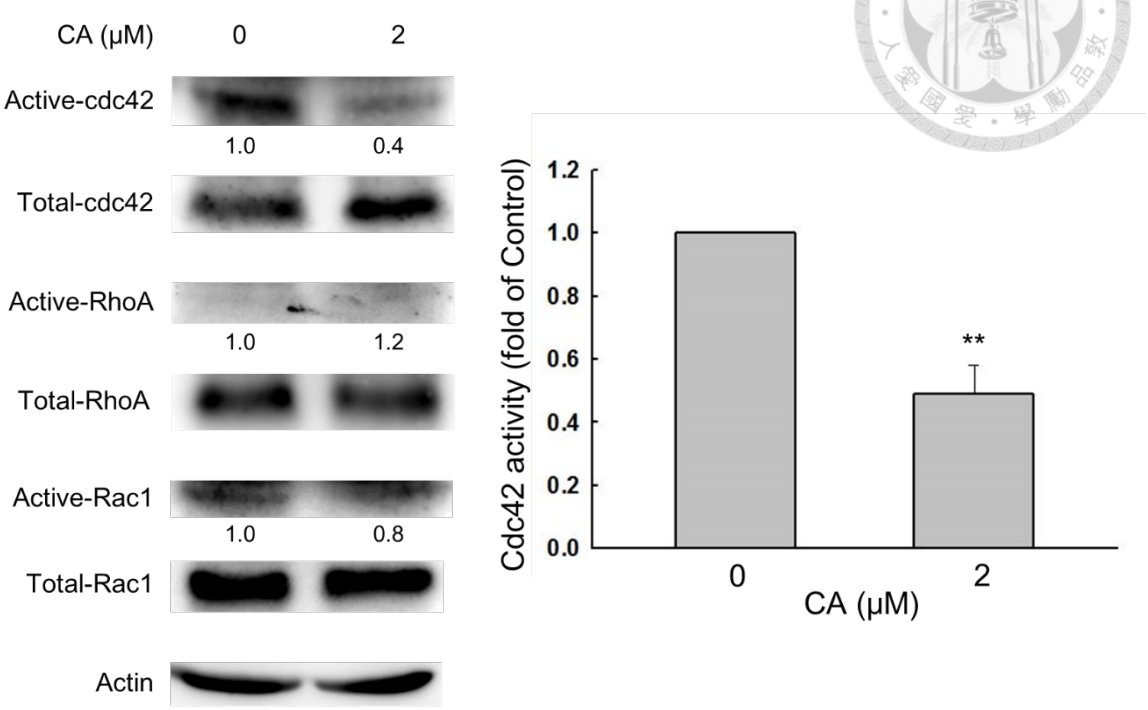

Figure 34. Corosolic acid inhibits cdc42 activity

Huh7 cells were treated with 0.1% DMSO (control) or corosolic acid for 6 h, and Rho-GTPase activity was examined with a GST pull-down assay and western blot analysis. (For cdc42, n = 3, **P < 0.01 compared with the DMSO treated group)

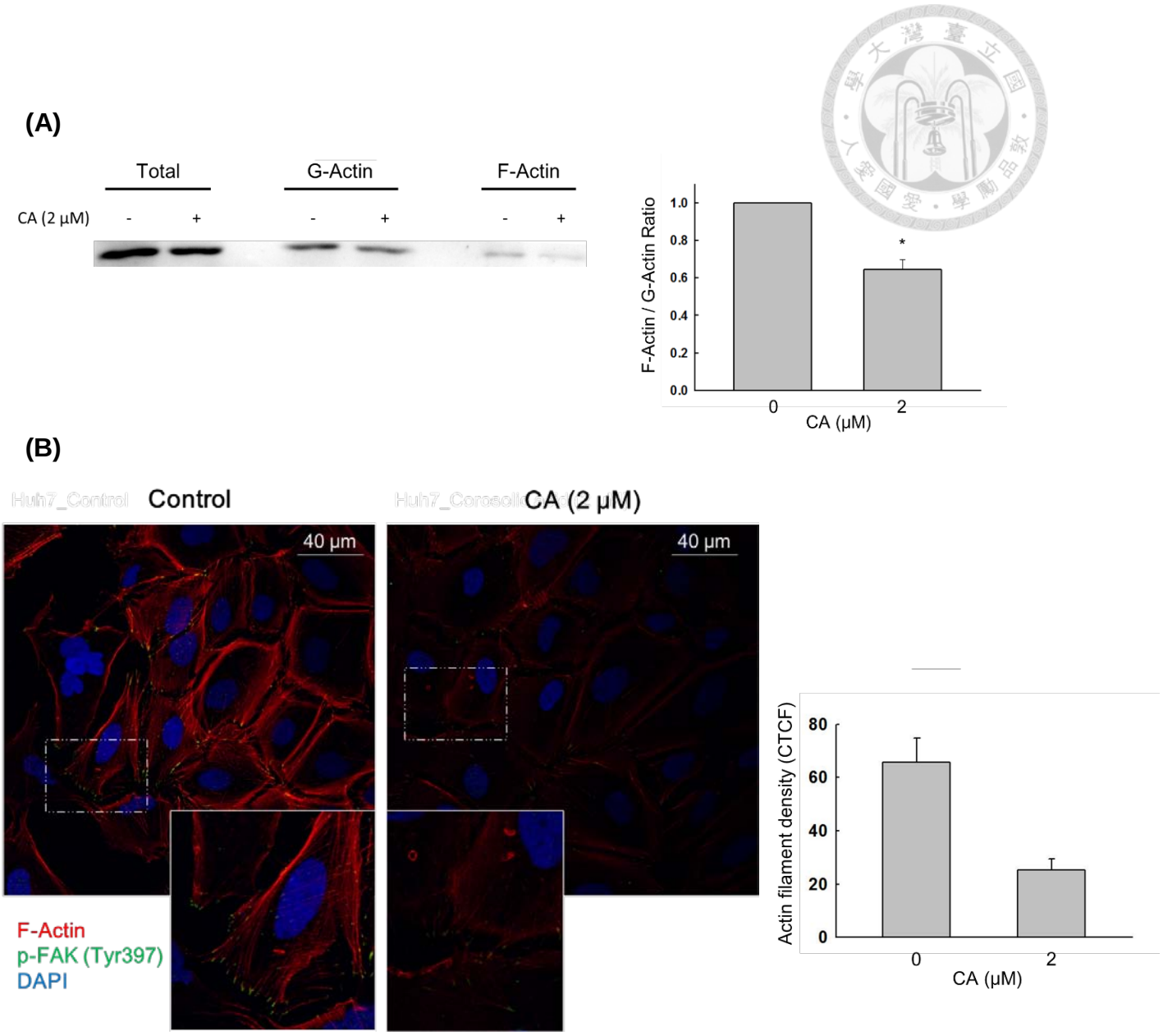

Figure 35. Effect of corosolic acid on actin rearrangement

(A) Huh7 cells were treated with 0.1% DMSO (control) or corosolic acid for 6 h, and fractions containing either F-actin or G-actin were separated by procedures outlined in materials and methods. The ratio of F-actin and G-actin were then calculated. (n = 3, ***P < 0.001 compared with the DMSO treated group) (B) Huh7 cells were treated with 0.1% DMSO (control) or corosolic acid for 6 h followed by immunocytochemistry staining. The phalloidin-stained Factin (red) and p-FAK (green) co-localized at the leading edge of control cells.

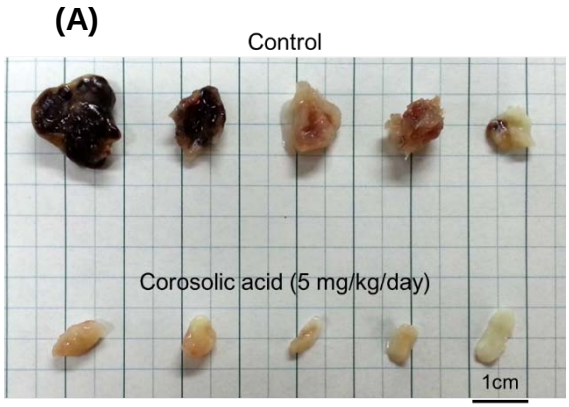
(A)
Control
Corosolic acid (5 mg/kg/day)
1cm

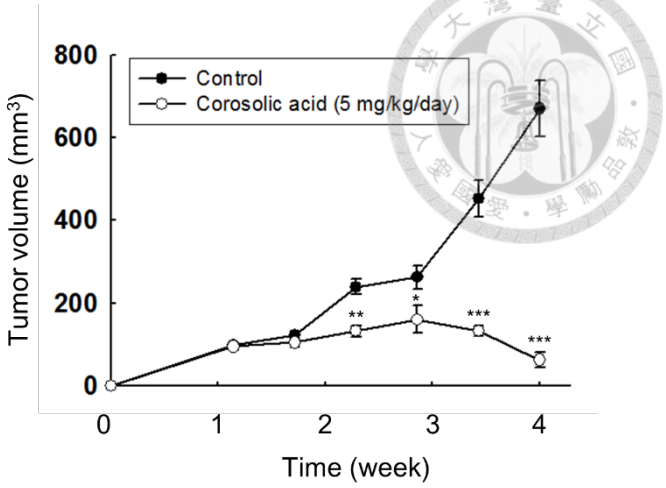
Control
Corosolic acid (5 mg/kg/day)
Tumor volume (mm³)
800
600
400
200
0
0
1
2
3
4
Time (week)
**
*
***
***

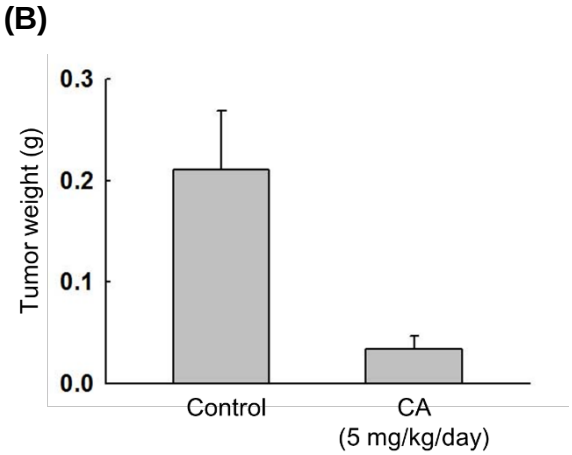
(B)
Tumor weight (g)
0.3
0.2
0.1
0.0
Control
CA
(5 mg/kg/day)

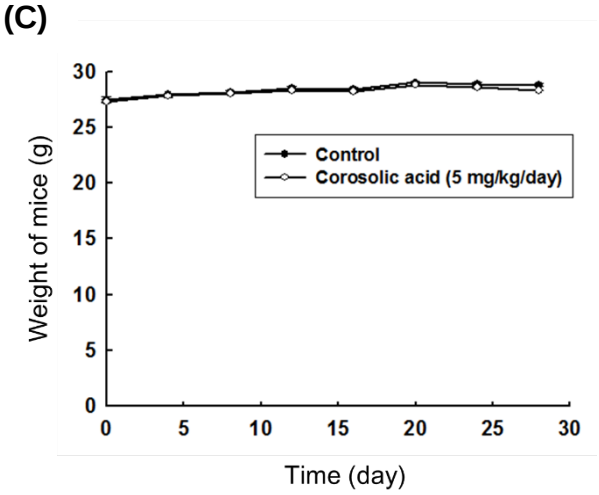
(C)
Control
Corosolic acid (5 mg/kg/day)
Weight of mice (g)
30
25
20
15
10
5
0
0
5
10
15
20
25
30
Time (day)

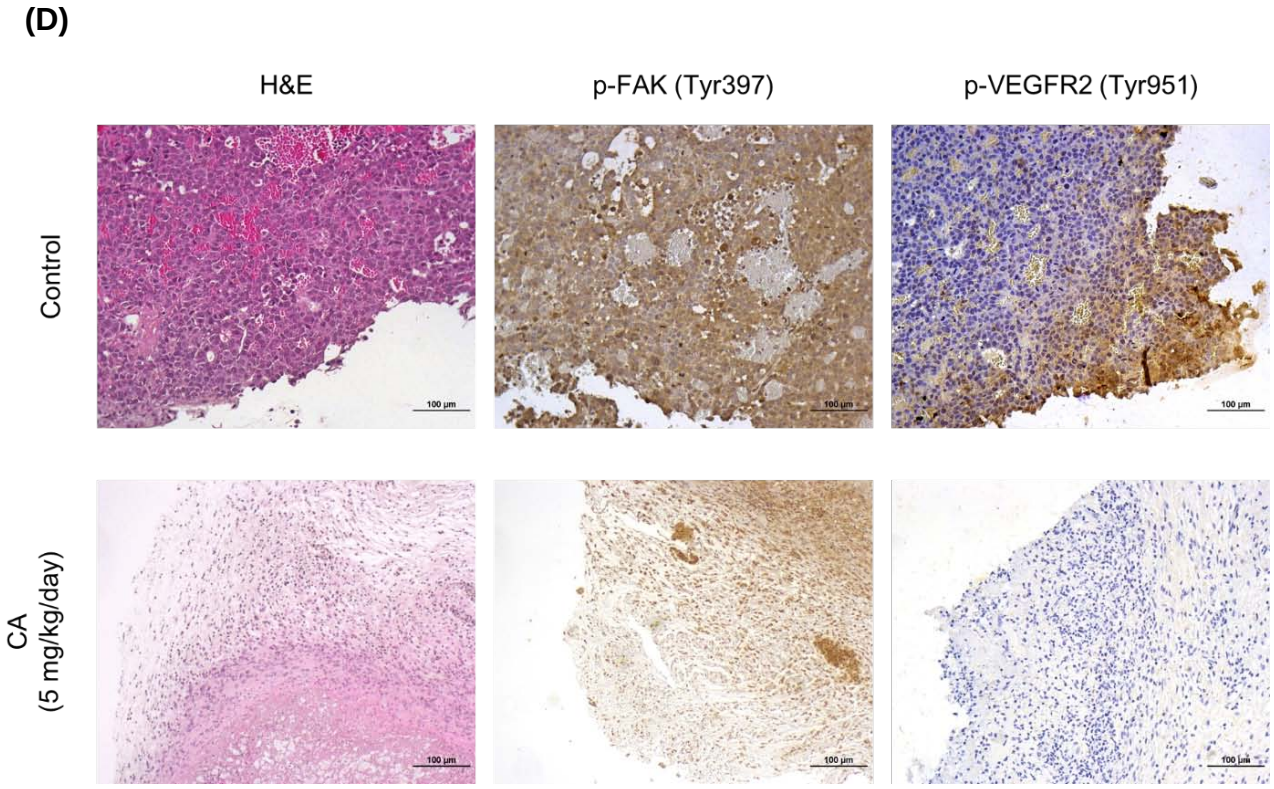
(D)
H&E
p-FAK (Tyr397)
p-VEGFR2 (Tyr951)
Control
CA
(5 mg/kg/day)

Figure 36. Corosolic acid exhibits significant anti-tumor effects on Huh7 cells *in vivo*

2×10^6 of Huh7 cells were subcutaneously injected into the hind limb of NOD/SCID mice (n = 5). Corosolic acid (5 mg/kg/day) was administered by intraperitoneal injection for 21 days. (A) Representative appearance of excised tumor, and tumor volume was measured every 5 days. (*P < 0.05, **P < 0.01, ***P < 0.001 compared with the DMSO treated control group) (B) Weight of tumor mass. (*P < 0.05, compared with the DMSO treated control group) (C) Body weight between mice treated with and without corosolic acid. (D) Immunostaining of Ki-67, pVEGFR2 (Tyr951) and p-FAK (Tyr397) in excised tumor in mice. Single staining was done on several sections.

(A)

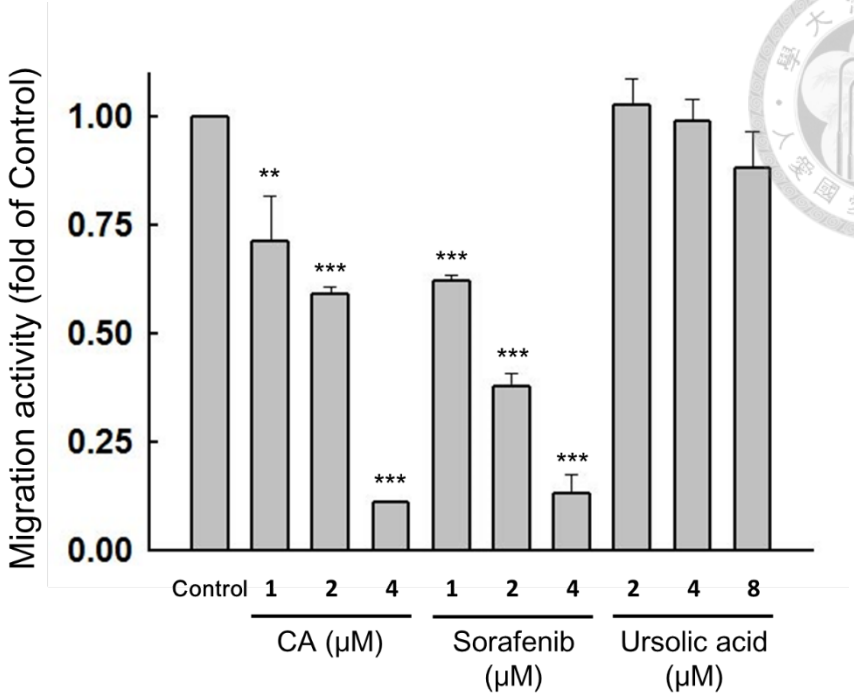

(B)

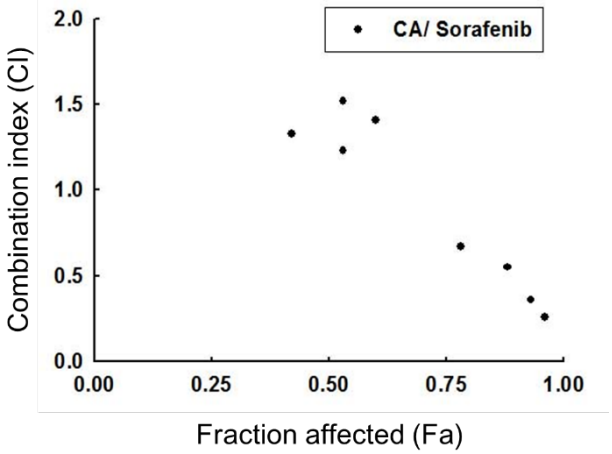

CA (μM)	Sorafenib (μM)	(CI)	(Fa)
1	4	0.55	0.88
2	4	0.36	0.93
4	4	0.26	0.96
2	2	0.67	0.78

Figure 37. Combinatorial effects of corosolic acid and sorafenib on migration activity of Huh7 cells (A) Dose dependent migration inhibitory effects of corosolic acid and sorafenib on Huh7 cells. The control group was treated with 0.1% DMSO and the experimental groups were treated with indicated compounds. (n = 3, **P < 0.01, ***P < 0.001 compared with the DMSO treated group) (B) Transwell assay were performed to determine anti-migration effect of corosolic acid and sorafenib. The combination index (CI) values were examined at different levels of migration inhibition effect (fa), and the effective combination treatments between corosolic acid and sorafenib (CI < 1) were displayed.

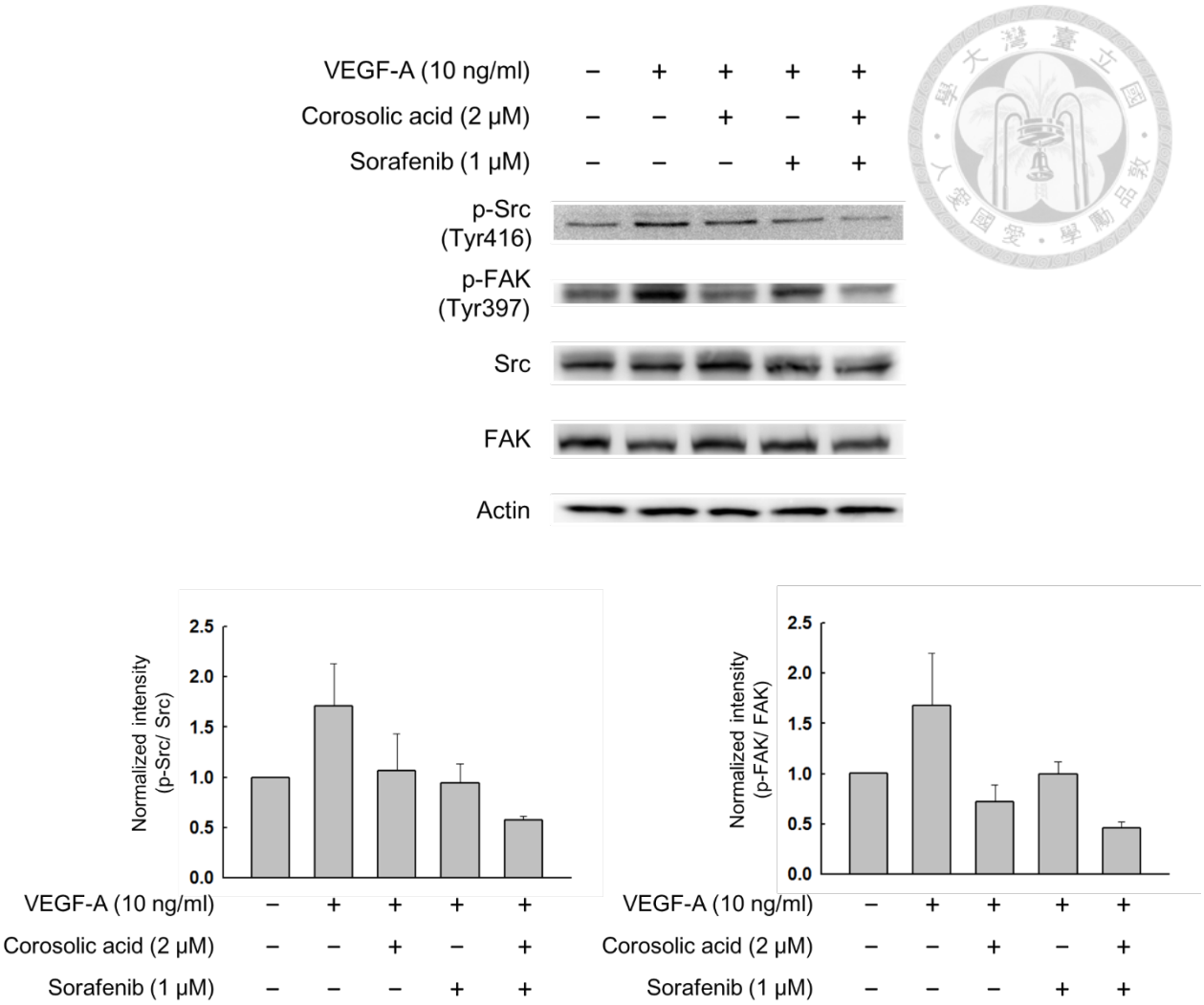

Figure 38. Combinatorial effects of corosolic acid and sorafenib on signaling molecules of Huh7 cells

Huh7 cells were treated with 0.1% DMSO (control), corosolic acid, sorafenib, or combination of corosolic acid and sorafenib for 30 min, and the lysates were analyzed by western blot. (n=3)

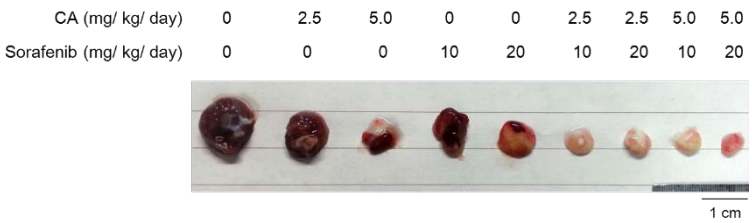

CA (mg/ kg/ day)	Sorafenib (mg/ kg/ day)	(Fa)	(CI)
2.5	10.0	0.82	0.92
2.5	20.0	0.96	0.66
5.0	10.0	0.89	1.20
5.0	20.0	0.88	1.52

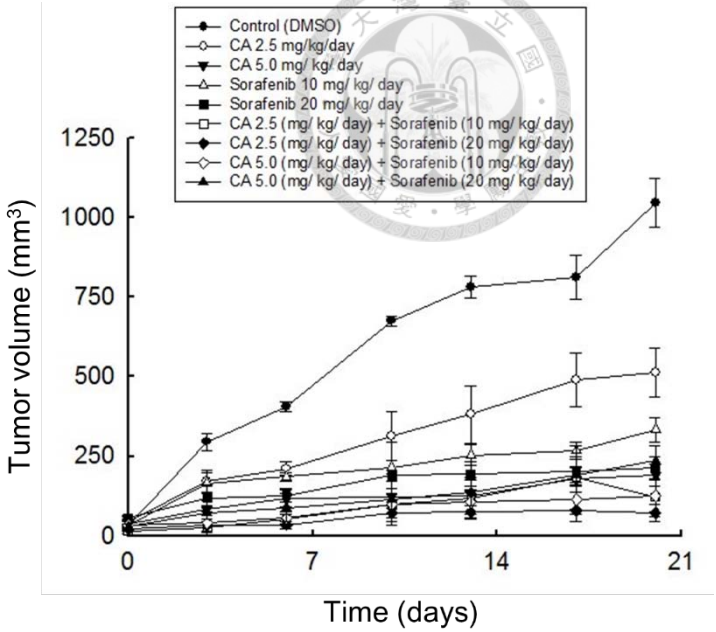

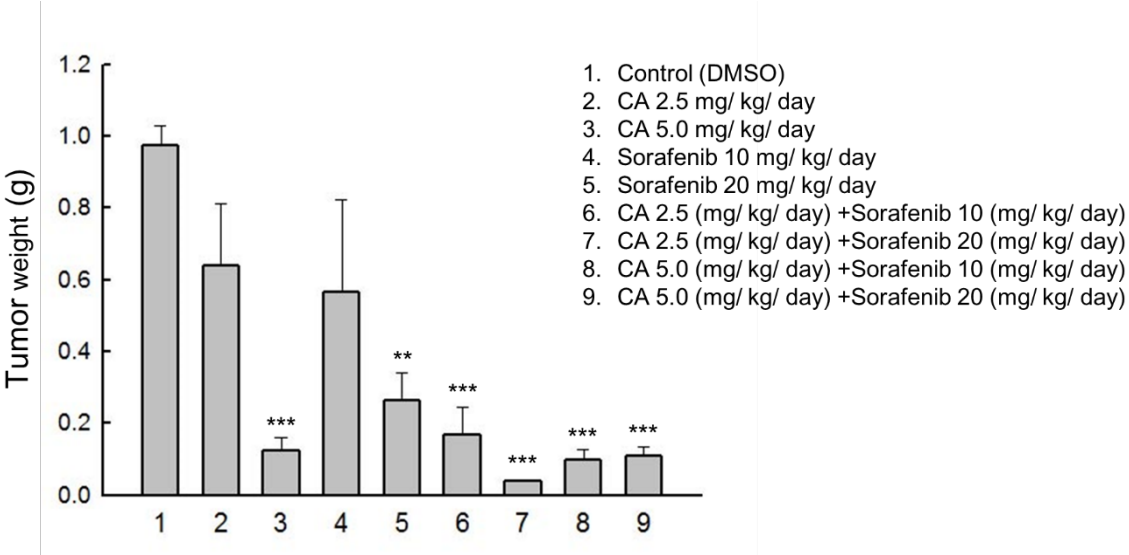

Figure 39. Combinatorial effects of corosolic acid and sorafenib on Huh7 cells by *in vivo* xenograft model

For the *in vivo* combinatorial study, Huh7 cells (5×10^6) were subcutaneously injected into each mouse. After 7 days, when the tumors reached 50 mm^3, the mice were randomized into different groups. CA (2.5, 5 mg/kg), sorafenib (10, 20 mg/kg), or a combination of the two was administrated daily via intraperitoneal injection for 20 days the tumor volume was recorded every 3 to 4 days. Weight of tumor mass (n = 5, **P < 0.01, ***P < 0.001 compared with the DMSO treated control group) and synergistic effects (CI < 1) between different combination group.

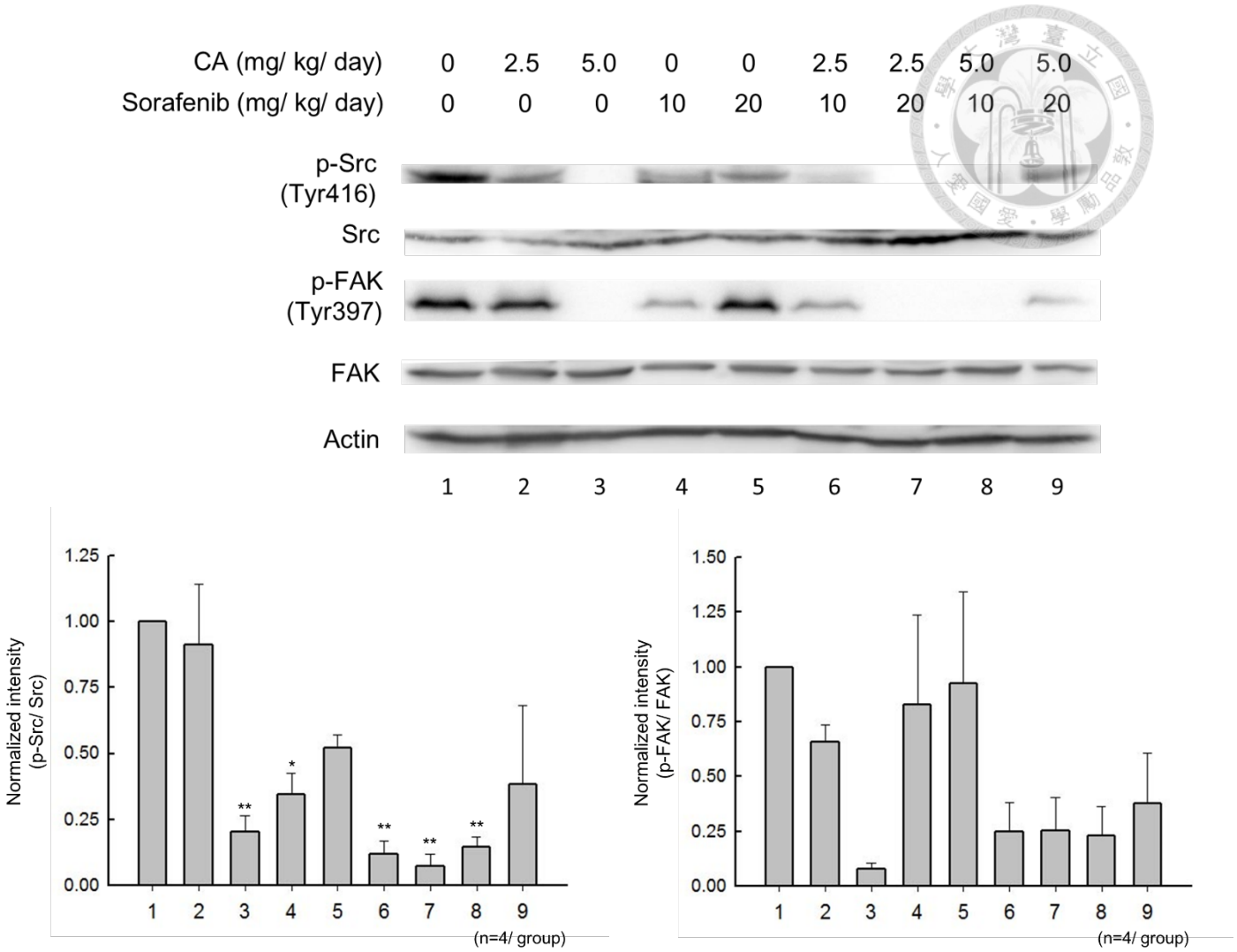

Figure 40. Inhibitory effects of corosolic acid combined with sorafenib on Src and FAK kinases *in vivo*

Xenograft tumors excised from mice were homogenized in RIPA buffer and analyzed by western blotting. (n = 4 for each group, *P < 0.05, **P < 0.01 compared with the DMSO treated control group)

(A)

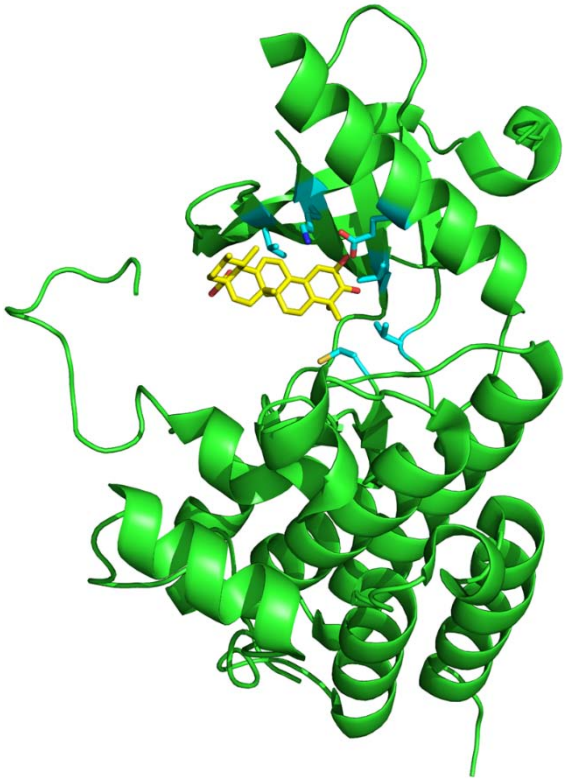

(B)

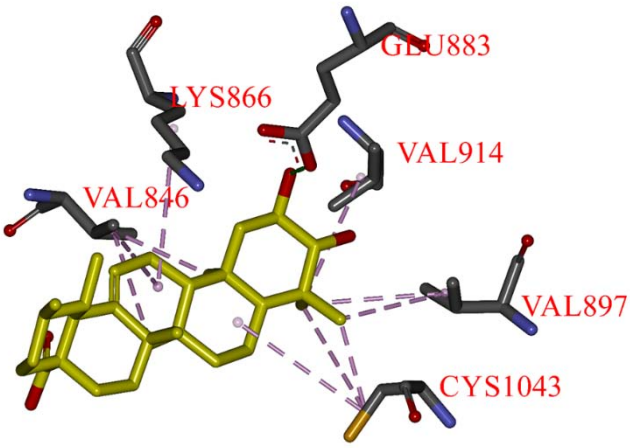

Figure 41. Corosolic acid interacts with the ATP-binding site of VEGFR2 kinase domain by molecular docking analysis

(A) The three-dimensional diagram displays the interaction of corosolic acid to the ATP binding site of VEGFR2 (PDB code: 1YWN). (B) The interaction of corosolic acid with the amino acid residues in the ATP-binding site; Glu883 significantly contributes to binding.

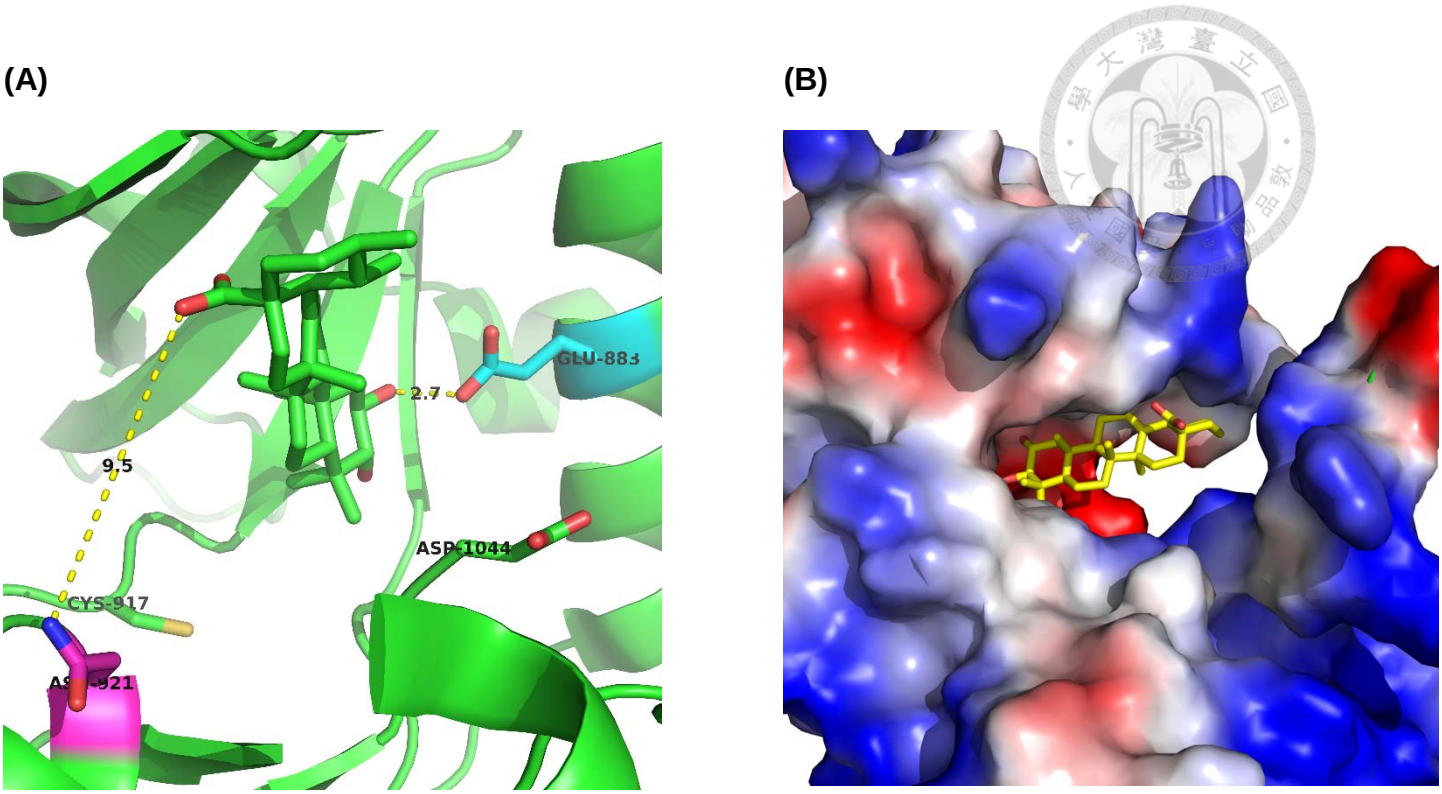

Figure 42. Analysis of relative distance and surface charge distribution between corosolic acid and VEGFR2 ATP binding pocket

(A) The Glu883 residue was represented by cyan color, and Asn921 residue was showed by pink color. The yellow dotted line means the distance between corosolic acid with these two residues. (B) The surface charge distribution was displayed by PyMOL software. The negative charge, positive charge, and hydrophobic area were represented by red, blue, and white color, respectively.

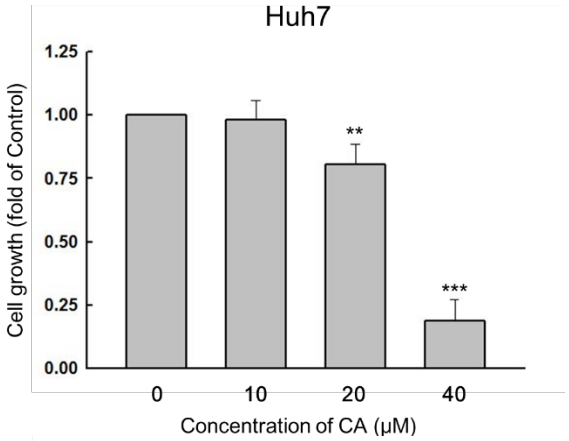

Sorafenib (μM)	CA (μM)	(Fa)	(CI)
2.5	10.0	0.46	0.67
2.5	20.0	0.55	0.90
2.5	40.0	0.75	1.23
5.0	10.0	0.50	0.92
5.0	20.0	0.59	1.10
5.0	40.0	0.81	1.24
10.0	10.0	0.61	1.22
10.0	20.0	0.62	1.50
10.0	40.0	0.83	1.45

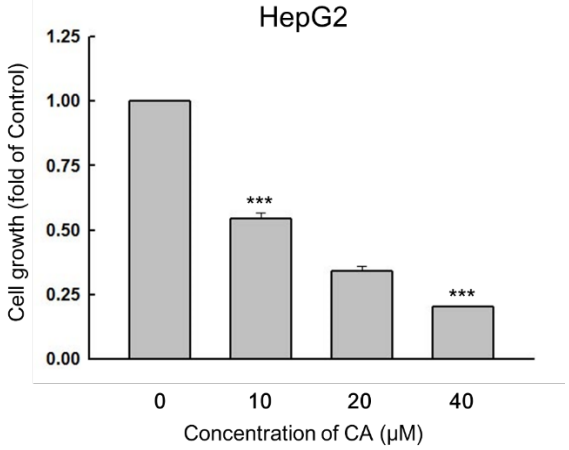

Sorafenib (μM)	CA (μM)	(Fa)	(CI)
2.5	10.0	0.21	0.96
2.5	20.0	0.61	0.76
2.5	40.0	0.82	1.00
5.0	10.0	0.44	0.97
5.0	20.0	0.68	0.88
5.0	40.0	0.84	1.09
10.0	10.0	0.67	1.03
10.0	20.0	0.73	1.14
10.0	40.0	0.85	1.28

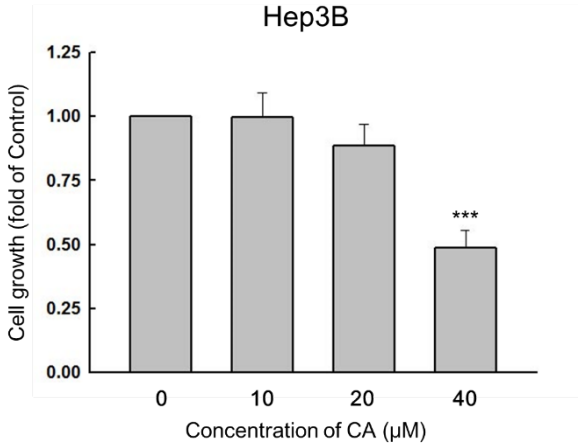

Sorafenib (μM)	CA (μM)	(Fa)	(CI)
2.5	10.0	0.01	5.70
2.5	20.0	0.38	0.70
2.5	40.0	0.61	0.93
5.0	10.0	0.10	1.29
5.0	20.0	0.47	0.68
5.0	40.0	0.63	0.95
10.0	10.0	0.30	0.87
10.0	20.0	0.41	0.94
10.0	40.0	0.68	0.95

Figure 43. Corosolic acid inhibits growth of Huh7, HepG2, and Hep3B cells

Cells were treated with 0.1% DMSO (control) or varying concentrations of corosolic acid for 24 h, and the growth inhibition effect of corosolic acid was determined by SRB assay. Results are presented as mean value ± SE. (**P < 0.01, ***P < 0.001 compared with the DMSO treated group); combinatorial effects of corosolic acid and sorafenib on HCC cell growth are displayed on the right side of each chart.

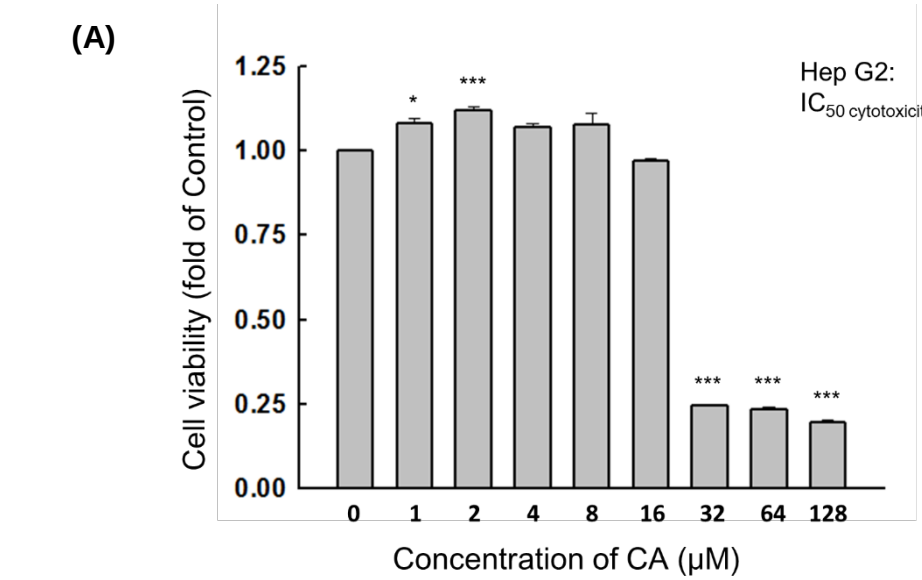

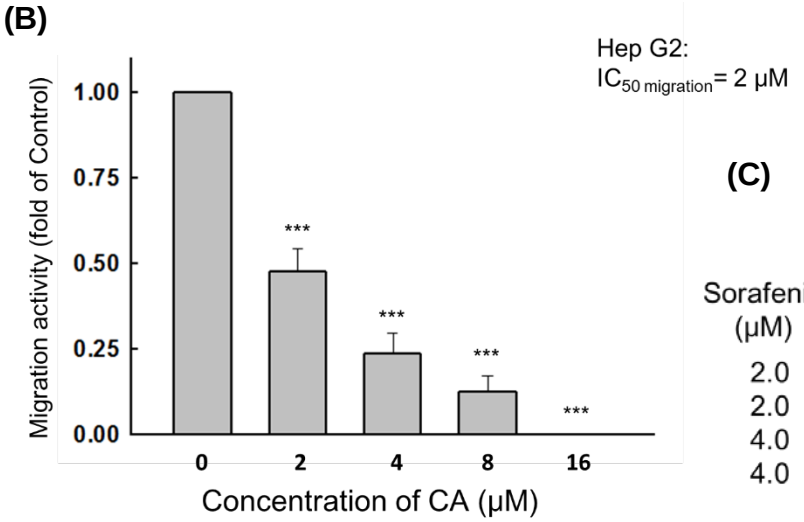

(C)

HepG2

Sorafenib (μM)	CA (μM)	(Fa)	(CI)
2.0	2.0	0.49	6.99
2.0	4.0	0.65	0.95
4.0	2.0	0.71	1.21
4.0	4.0	0.87	0.68

Figure 44. Cytotoxicity and migration-inhibitory effects of corosolic acid on HepG2 cells

(A) HepG2 cells were treated with 0.1% DMSO (control) or various concentrations of corosolic acid for 24 h and cell viability was determined with an MTT assay. Results are presented as mean value ± SE. (*P < 0.05, ***P < 0.001 compared with the DMSO treated group) (B) The migration activity of HepG2 cells was inhibited by corosolic acid in a dose-dependent manner. Results are presented as mean value ± SE. (***P < 0.001 compared with the DMSO treated group) (C) Combinatorial effects of corosolic acid and sorafenib on HepG2 cell migration are displayed by CI value.

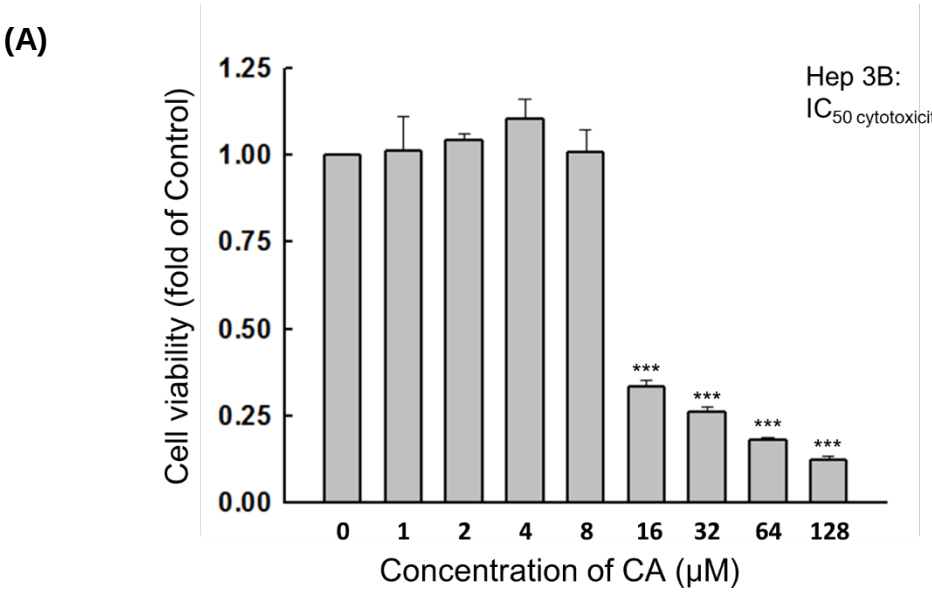

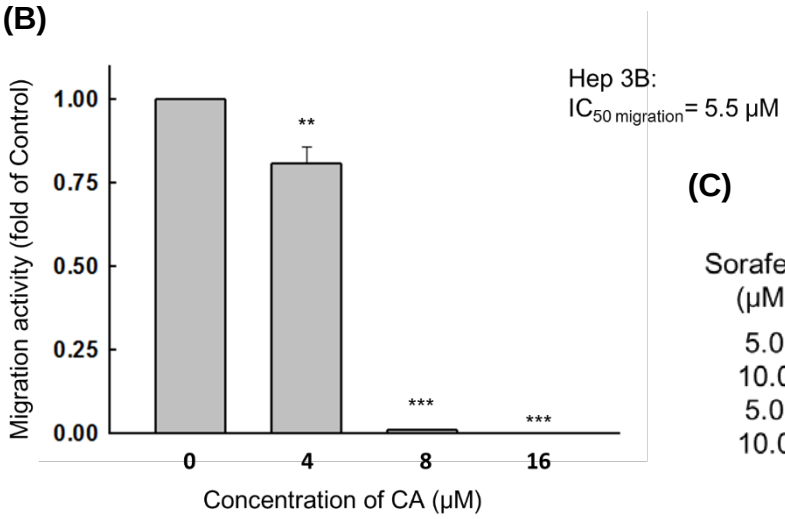

(C)

Hep3B

Sorafenib (μM)	CA (μM)	(Fa)	(CI)
5.0	5.0	0.94	0.44
10.0	5.0	0.97	0.34
5.0	10.0	0.97	0.65
10.0	10.0	0.99	0.50

Figure 45. Cytotoxicity and migration-inhibitory effects of corosolic acid on Hep3B cells

(A) Hep3B cells were treated with 0.1% DMSO (control) or various concentrations of corosolic acid for 24 h and cell viability was determined with an MTT assay. Results are presented as mean value ± SE. (***P < 0.001 compared with the DMSO treated group) (B) The migration activity of Hep3B cells was inhibited by corosolic acid in a dose-dependent manner. Results are presented as mean value ± SE. (**P < 0.01, ***P < 0.001 compared with the DMSO treated group) (C) Combinatorial effects of corosolic acid and sorafenib on Hep3B cell migration are displayed by CI value.

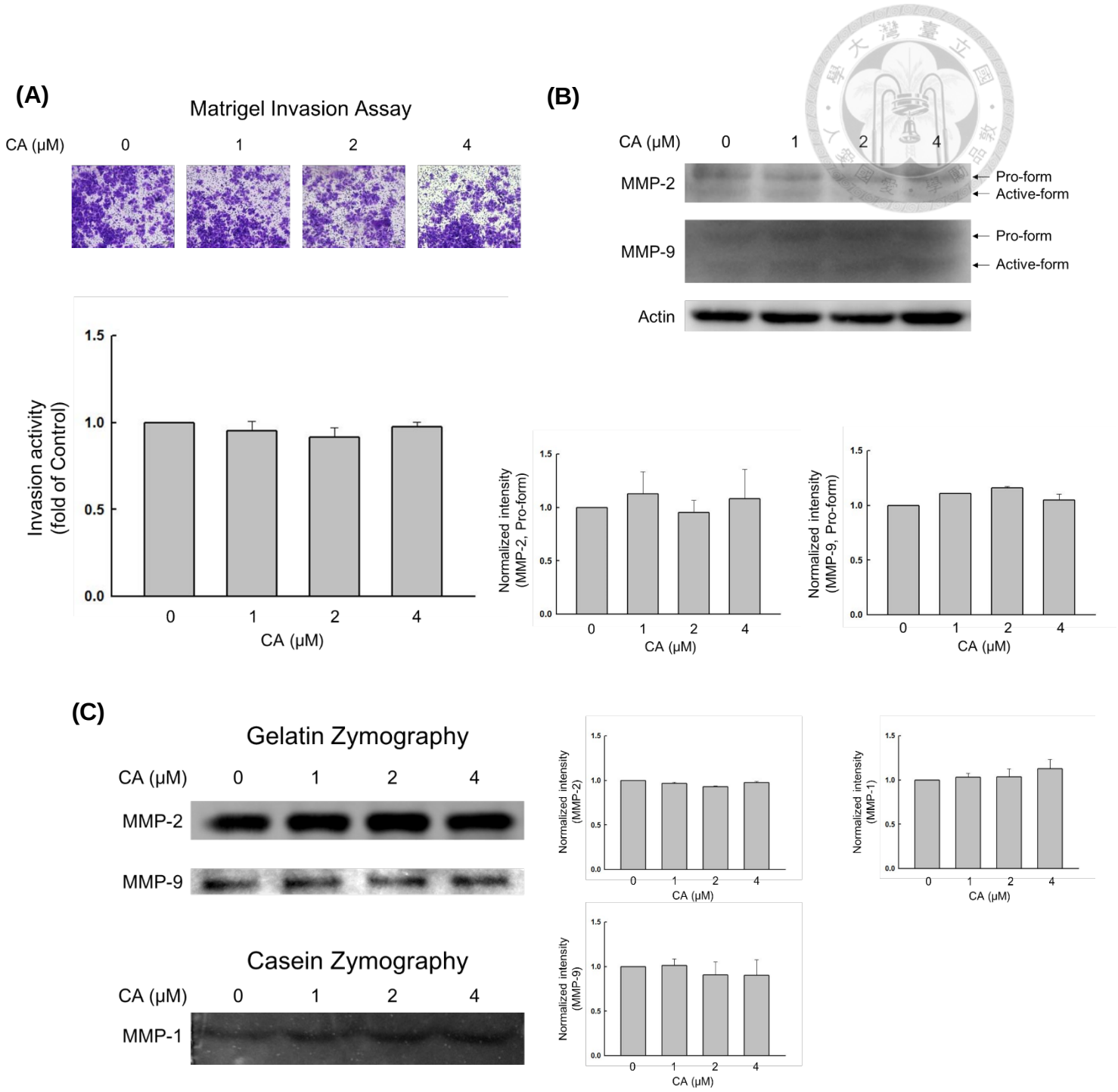

Figure 46. Corosolic acid doesn't exhibit significant inhibitory effect on invasion activity of Huh7 cells

(A) Matrigel invasion assay was used to analyze the invasion activity of Huh7 cells. (B) Expression levels of MMP-2 and MMP-9 were carried out by western blot analysis. (C) Zymography assay was used to examine the activity of MMP-1, MMP-2 and MMP-9.

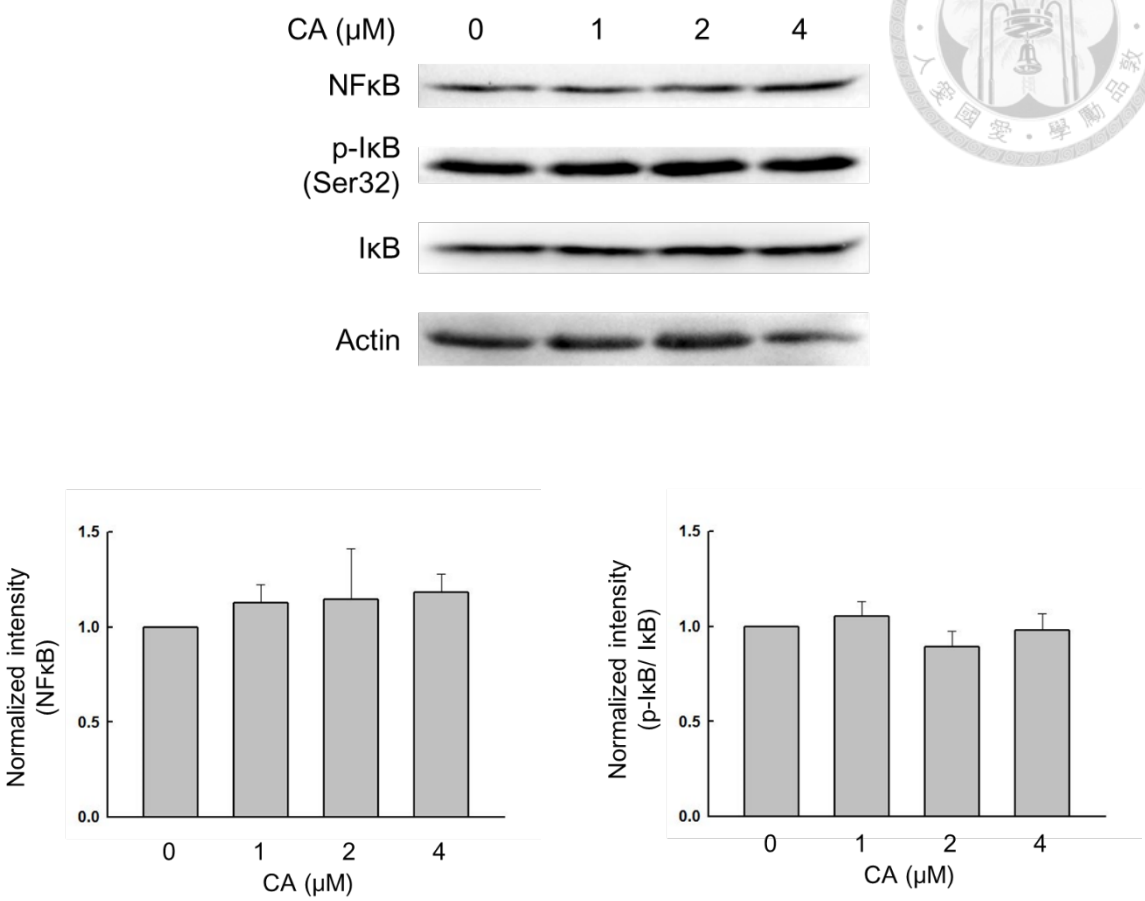

Figure 47. Corosolic acid shows no inhibitory effect on NFκB signaling

Huh7 cells were treated with 0.1% DMSO (control) or corosolic acid for 12 h, and The lysates were examined by western blot analysis.

Table 1. Correlation between L-FABP and VEGF-A protein expression in tissue pairs from 90 HCC patients

Intensity [a]		NAT, N (%)	HCC without cirrhosis, N (%)	HCC with cirrhosis, N (%)	P value [b]	P value [c]	P value [d]	P value [e]	P value [f]
L-FABP	1	15 (44.1)	8 (23.5)	11 (32.4)	0.012	0.028	0.027	0.040	0.086
	2	72(55.0)	40 (30.5)	19 (14.5)					
	3	3 (20.0)	9 (60.0)	3 (20.0)					
VEGF-A	1	25 (48.1)	12 (23.1)	15 (28.8)	0.025	0.563	0.360	0.037	0.017
	2	65 (51.2)	45 (35.4)	17 (13.4)					
	4	0 (0.0)	0 (0.0)	1 (100.0)					

Abbreviations: HCC, hepatocellular carcinoma; OR, odds ratios; CI, confidence interval; N, number.
[a] Intensity: 0, negative; 1, weak positive; 2, moderate positive; 3, strong positive.
[b] Chi-square test, NAT vs HCC without cirrhosis vs HCC with cirrhosis.
[c] Chi-square test, NAT vs HCC with or without cirrhosis.
[d] Chi-square test, NAT vs HCC without cirrhosis.
[e] Chi-square test, NAT vs HCC with cirrhosis.
[f] Chi-square test, HCC without cirrhosis vs HCC with cirrhosis.

Table 2. Clinical characteristics of the cases included in analyses of L-FABP protein expression evaluated by immunohistochemistry

Characteristics	NAT, N = 90	HCC without cirrhosis, N = 57	HCC with cirrhosis, N = 33	P value
Age (years), Mean ± SD	53.5 ± 10.0	54.2 ± 10.3	52.2 ± 9.6	0.650 [a]
Sex, N (%)				
Female	8 (13.3)	6 (10.5)	6 (18.2)	0.589 [b]
Male	78 (86.7)	51 (89.5)	27 (81.8)	

Abbreviations: HCC, hepatocellular carcinoma; N, number.
a. ANOVA test.
b. Chi-square test.
c. One age miss data.

Table 3. Association of L-FABP protein expression with clinical pathologic characteristics in patients with HCC

Characteristics	Low (1)	Intermediate (2)	High (3)	P value
Age (years) Mean ±SD	53.2 ± 8.5	52.4 ± 10.6	59.3 ± 8.2	0.089 [a]
Age >= 53.5	9 (47.4)	30 (51.7)	8 (66.7)	0.555 [b]
Sex				
Female	4 (21.1)	7 (11.9)	1 (8.3)	0.509 [b]
Male	15 (78.9)	52 (88.1)	11 (91.7)	
Grade				0.484 [b]
G1	2 (10.5)	3 (5.1)	1 (8.3)	
G2	15 (78.5)	46 (78.0)	7 (58.3)	
G3	2 (10.5)	10 (16.9)	4 (33.3)	
pT (invasion depth)				0.169 [b]
T1	2 (10.5)	8 (14.3)	2 (16.7)	
T2	9 (47.4)	20 (35.7)	2 (16.7)	
T3	6 (31.6)	28 (50.0)	7 (58.3)	
T4	2 (10.5)	0 (0.0)	1 (8.3)	
pN (lymph node metastasis)				0.759 [b]
N0	19 (100.0)	54 (98.2)	11 (100.0)	
N1	0 (0.0)	1 (1.8)	0 (0.0)	
pM (distant metastasis)				0.578 [b]
M0	19 (100.0)	54 (96.4)	11 (100.0)	
M1	0 (0.0)	2 (3.6)	0 (0.0)	
TNM stage				0.546 [b]
I	2 (10.5)	8 (14.3)	2 (16.7)	
II	9 (47.4)	20 (35.7)	2 (16.7)	
III	8 (42.1)	25 (44.6)	8 (66.7)	
IV	0 (0.0)	3 (5.4)	0 (0.0)	

Abbreviations: HCC, hepatocellular carcinoma; N, number.

a. ANOVA test.

b. Chi-square test.

Supplementary data, Table 1.

Primers (5’ to 3’):

pcDNA 3.1/L-FABP cloning:

1. L-FABP TOPO PCR primer (Forward): CAC CAT GAG TTT CTC CGG CAA G
2. L-FABP TOPO PCR primer (Reverse): AAT TCT CTT GCT GAT TCT C

qRT-PCR:

1. L-FABP primer (Forward): ATG AGT TTC TCC GGC AAG TAC
2. L-FABP primer (Reverse): TCC TTC CCC TTC TGG ATG AGC
3. VEGF-A primer (Forward): CAT GAA CTT TCT GCT GTC TTG G
4. VEGF-A primer (Reverse): CCT GGT GAG AGA TCT GGT TCC
5. 18S rRNA primer (Forward): GCT TAA TTT GAC TCA ACA CGG GA
6. 18S rRNA primer (Reverse): AGC TAT CAA TCT GTC AAT CCT GTC

VEGF-A promoter cloning:

1. D1 primer (Forward): GGG GTA CCC CGC TCC ACA AAC TTG GTG CC
2. D2 primer (Forward): GGG GTA CCC CGA GGG CTC CAG ATG GCA
3. D3 primer (Forward): GGG GTA CCC CGT CGA GCT TCC CCT TCA TTG
4. Reverse primer(~+73): CCC TCG AGG GCG CCT CCC GAC AGA GCG CT

Site-directed mutagenesis cloning:

1. L-FABP F3W primer (Forward):
   ATG AGT TGG TCC GGC AAG TGG CAA CTG CAG
2. L-FABP F3W primer (Reverse):
   CTG CAG TTG CCA CTT GCC GGA CCA ACT CAT
3. L-FABP K31E primer (Forward):
   GAG CTC ATC CAG GAG GGG GAG GAT ATC AAG
4. L-FABP K31E primer (Reverse):
   CTT GAT ATC CTC CCC CTC CTG GAT GAG CTC
5. L-FABP T94A primer (Forward):
   CTG GTG ACA GCT TTC AAA AAC ATC
6. L-FABP T94A primer (Reverse):
   GAT GTT TTT GAA AGC TGT CAC CAG

siRNA & shRNA (5’to 3’)

L-FABP siRNA (Invitrogen, FABP1HSS141976)

Primer number: 228624A01

(RNA)-GGU UCA GUU GGA AGG UGA CAA UAA A

Primer number: 228624A02

(RNA)-UUU AUU GUC ACC UUC CAA CUG AAC C

L-FABP shRNA (Acdemia Sinica, RNAi Core Lab)

Clone ID: TRCN0000059643

NM ID: NM_001443

Vector: pLKO.1

Target sequence: GTG ACA ATA AAC TGG TGA CAA

Hairpin sequence:

CCGG-GTGACAATAAACTGGTGACAA-CTCGAG-TTGTCACCAGTTTATTGTCA
C-TTTTTG

Supplementary data, Figure 1.

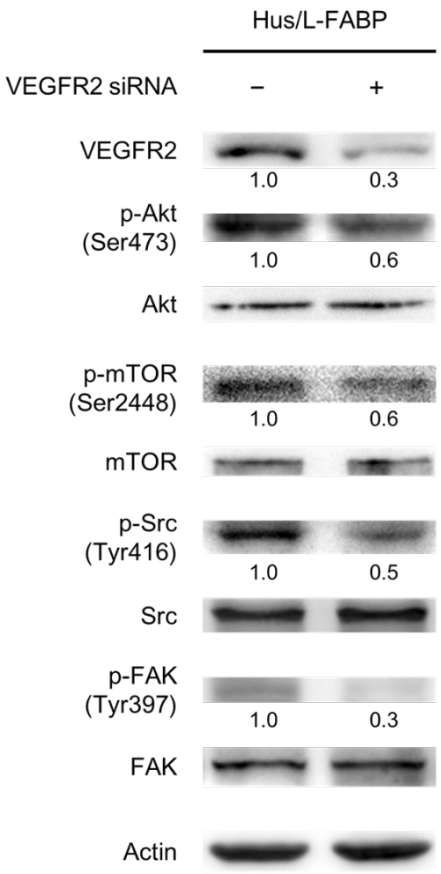

Figure S1. Knockdown of VEGFR2 in Hus/L-FABP cells decreased the activation of down-stream signaling molecules.

Western blot analysis of the phosphorylation level of signaling molecules including Akt, mTOR, Src and FAK in Hus/L-FABP cells transfected with control siRNA or VEGFR2-targeting siRNA for 24 h.

Supplementary data, Figure 2.

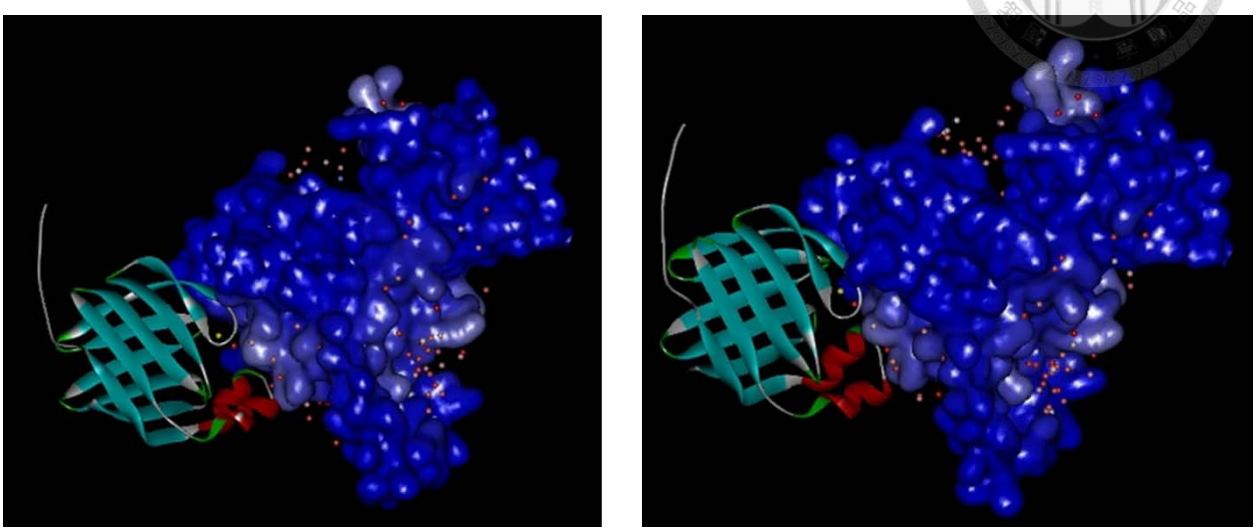

Figure S2. Prediction of the interaction models of L-FABP and VEGFR2 kinase domain

The predicted docking models of L-FABP and VEGFR2 kinase domain were performed by MEGADOCK 3.0 software. L-FABP protein was showed by sheet form, and VEGFR2 kinase domain was exhibited by 3D structure in blue color.

Supplementary data, Figure 3.

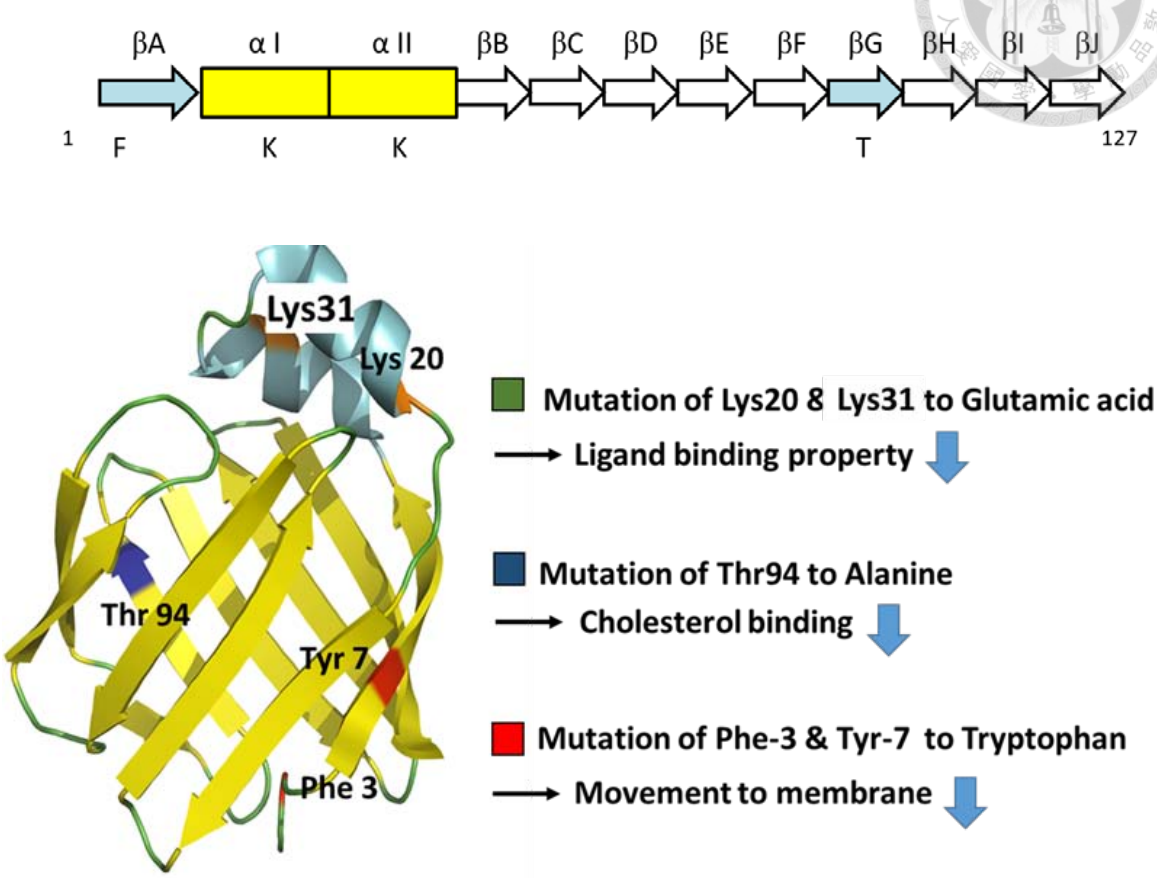

Figure S3. Amino acid substitution of L-FABP in present studies

The position of substituted amino acids in mutant L-FABP were presented in secondary and tertiary structure. We substituted four different amino acids including F3 to W (β sheet A, N-terminal), K20 to E (α-helix I), K30 to E (α-helix II), T94 to A (β sheet G, C-terminal) to examine the mechanisms of L-FABP in its oncogenic role.

References:

1. Kaseb AO, Hanbali A, Cotant M, Hassan MM, Wollner I and Philip PA. Vascular endothelial growth factor in the management of hepatocellular carcinoma: a review of literature. Cancer. 2009; 115(21):4895-4906.
2. Moeini A, Cornellà H and Villanueva A. Emerging signaling pathways in hepatocellular carcinoma. Liver Cancer. 2012; 1(2):83-93.
3. Olsen SK, Jr RSB and Siegel AB. Hepatocellular carcinoma: review of current treatment with a focus on targeted molecular therapies. Therap Adv Gastroenterol. 2010; 3(1):55-66.
4. Semela D and Dufour J-Fo. Angiogenesis and hepatocellular carcinoma. J Hepatol. 2004; 41(5):864-880.
5. Villanueva A, Hernandez-Gea V and Llovet JM. Medical therapies for hepatocellular carcinoma: a critical view of the evidence. Nat Rev Gastroenterol Hepatol. 2013; 10(1):34-42.
6. Romanque P, Piguet AC and Dufour JF. Targeting vessels to treat hepatocellular carcinoma. Clin Sci (Lond). 2008; 114(7):467-477.
7. Aucejo F, Kim R, Zein N, Quintini C, Uso TD, Lopez R, Eghtesad B, Fung J, Miller C and Yerian L. Vascular endothelial growth factor receptor 2 expression in non-tumorous cirrhotic liver is higher when hepatoma is beyond Milan criteria.

Liver Transpl. 2009; 15(2):169-176.

8. Huang J, Zhang X, Tang Q, Zhang F, Li Y, Feng Z and Zhu J. Prognostic significance and potential therapeutic target of VEGFR2 in hepatocellular carcinoma. J Clin Pathol. 2011; 64(4):343-348.

9. Zhu AX, Duda DG, Sahani DV and Jain RK. HCC and angiogenesis: possible targets and future directions. Nat Rev Clin Oncol. 2011; 8(5):292-301.

10. Storch J and McDermott L. Structural and functional analysis of fatty acid-binding proteins. J Lipid Res. 2009; 50(Suppl):S126-131.

11. Woodford JK, Behnke WD and Schroeder F. Liver fatty acid binding protein enhances sterol transfer by membrane interaction. Mol Cell Biochem. 1995; 152(1):51-56.

12. Dong LH, Li H, Wang F, Li FQ, Zhou HY and Yang HJ. Expression of liver-type fatty acid-binding protein and vascular endothelial growth factor and their correlation in human hepatocellular carcinoma. Nan Fang Yi Ke Da Xue Xue Bao. 2007; 27(3):318-321.

13. Kawamura T, Kanno R, Fujii H and Suzuki T. Expression of liver-type fatty-acid-binding protein, fatty acid synthase and vascular endothelial growth factor in human lung carcinoma. Pathobiology. 2005; 72(5):233-240.

14. Hashimoto T, Kusakabe T, Watanabe K, Sugino T, Fukuda T, Nashimoto A, Honma

K, Sato Y, Kimura H, Fujii H and Suzuki T. Liver-type fatty acid-binding protein is highly expressed in intestinal metaplasia and in a subset of carcinomas of the stomach without association with the fatty acid synthase status in the carcinoma. Pathobiology. 2004; 71(3):115-122.

15. Sharaf RN, Butte AJ, Montgomery KD, Pai R, Dudley JT and Pasricha PJ. Computational prediction and experimental validation associating FABP-1 and pancreatic adenocarcinoma with diabetes. BMC Gastroenterol. 2011; 11:5.
16. Li H, Lu Q, Dong LH, Xue H, Zhou HY and Yang HJ. Expression of fatty acid binding protein in human breast cancer tissues. Xi Bao Yu Fen Zi Mian Yi Xue Za Zhi. 2007; 23(4):312-316.
17. Hammamieh R, Chakraborty N, Barmada M, Das R and Jett M. Expression patterns of fatty acid binding proteins in breast cancer cells. J Exp Ther Oncol. 2005; 5(2):133-143.
18. Wang B, Tao X, Huang CZ, Liu JF, Ye YB and Huang AM. Decreased expression of liver-type fatty acid-binding protein is associated with poor prognosis in hepatocellular carcinoma. Hepatogastroenterology. 2014; 61(133):1321-1326.
19. Li J, Dong L, Wei D, Wang X, Zhang S and Li H. Fatty acid synthase mediates the epithelial-mesenchymal transition of breast cancer cells. Int J Biol Sci. 2014; 10(2):171-180.

20. Sonnino S and Prinetti A. Membrane domains and the "lipid raft" concept. Curr Med Chem. 2013; 20(1):4-21.

21. Lingwood D and Simons K. Lipid rafts as a membrane-organizing principle. Science. 2010; 327(5961):46-50.

22. Pike LJ. Growth factor receptors, lipid rafts and caveolae: an evolving story. Biochim Biophys Acta. 2005; 1746(3):260-273.

23. Arcaro A, Aubert M, Hierro MEEd, Khanzada UK, Angelidou S, Tetley TD, Bittermann AG, Frame MC and Seckl MJ. Critical role for lipid raft-associated Src kinases in activation of PI3K-Akt signalling. Cell Signal. 2007; 19(5):1081-1092.

24. Chen X and Resh MD. Cholesterol depletion from the plasma membrane triggers ligand-independent activation of the epidermal growth factor receptor. J Biol Chem. 2002; 277(51):49631-49637.

25. Patwardhan P and Resh MD. Myristoylation and membrane binding regulate c-Src stability and kinase activity. Mol Cell Biol. 2010; 30(17):4094-4107.

26. Jiang M, Yang J, Zhang C, Liu B, Chan K, Cao H and Lu A. Clinical studies with traditional Chinese medicine in the past decade and future research and development. Planta Med. 2010; 76(17):2048-2064.

27. Youns M, Hoheisel JD and Efferth T. Traditional Chinese medicines (TCMs) for molecular targeted therapies of tumours. Curr Drug Discov Technol. 2010;

7(1):37-45.

28. Zuo LL, Wang ZY, Fan ZL, Tian SQ and Liu JR. Evaluation of antioxidant and antiproliferative properties of three *Actinidia* (*Actinidia kolomikta*, *Actinidia arguta*, *Actinidia chinensis*) extracts *in vitro*. Int J Mol Sci. 2012; 13(5):5506-5518.

29. Zhu WJ, Yu DH, Zhao M, Lin MG, Lu Q, Wang QW, Guan YY, Li GX, Luan X, Yang YF, Qin XM, Fang C, Yang GH and Chen HZ. Antiangiogenic triterpenes isolated from Chinese herbal medicine *Actinidia chinensis* planch. Anticancer Agents Med Chem. 2013; 13(2):195-198.

30. Fujiwara Y, Takeya M and Komohara Y. A novel strategy for inducing the antitumor effects of triterpenoid compounds: blocking the protumoral functions of tumor-associated macrophages via STAT3 inhibition. Biomed Res Int. 2014; 2014:348539.

31. Fujiwara Y, Takaishi K, Nakao J, Ikeda T, Katabuchi H, Takeya M and Komohara Y. Corosolic acid enhances the antitumor effects of chemotherapy on epithelial ovarian cancer by inhibiting signal transducer and activator of transcription 3 signaling. Oncol Lett. 2013; 6(6):1619-1623.

32. Fujiwara Y, Komohara Y, Ikeda T and Takeya M. Corosolic acid inhibits glioblastoma cell proliferation by suppressing the activation of signal transducer and activator of transcription-3 and nuclear factor-kappa B in tumor cells and

tumor-associated macrophages. Cancer Sci. 2011; 102(1):206-211.

33. Horlad H, Fujiwara Y, Takemura K, Ohnishi K, Ikeda T, Tsukamoto H, Mizuta H, Nishimura Y, Takeya M and Komohara Y. Corosolic acid impairs tumor development and lung metastasis by inhibiting the immunosuppressive activity of myeloid-derived suppressor cells. Mol Nutr Food Res. 2013; 57(6):1046-1054.

34. Aranda E and Owen GI. A semi-quantitative assay to screen for angiogenic compounds and compounds with angiogenic potential using the EA.hy926 endothelial cell line. Biol Res. 2009; 42(3):377-389.

35. Wang D, Stockard CR, Harkins L, Lott P, Salih C, Yuan K, Buchsbaum D, Hashim A, Zayzafoon M, Hardy R, Hameed O, Grizzle W and Siegal GP. Immunohistochemistry in the evaluation of neovascularization in tumor xenografts. Biotech Histochem. 2008; 83(3-4):179-189.

36. Rosner M, Siegel N, Fuchs C, Slabina N, Dolznig H and Hengstschläger M. Efficient siRNA-mediated prolonged gene silencing in human amniotic fluid stem cells. Nat Protoc. 2010; 5(6):1081-1095.

37. Kim KB, Lee JS and Ko YG. The isolation of detergent resistant lipid rafts for two dimensional electrophoresis. Methods Mol Biol. 2008; 424:413-422.

38. Chang YC, Tien SC, Tien HF, Zhang H, Bokoch GM and Chang ZF. p210Bcr-Abl desensitizes Cdc42 GTPase signaling for SDF-1a-directed migration in chromic

myeloid leukemia cells. Oncogene. 2009; 28(46):4105-4115.

39. Tang SW, Yang TC, Lin WC, Chang WH, Wang CC, Lai MK and Lin JY. Nicotinamide N-methyltransferase induces cellular invasion through activating matrix metalloproteinase-2 expression in clear cell renal cell carcinoma cells. Carcinogenesis. 2011; 32(2):138-145.

40. Wang SC, Tang SW, Lam SH, Wang CC, Liu YH, Lin HY, Lee SS and Lin JY. Aqueous extract of *Paeonia suffruticosa* inhibits migration and metastasis of renal cell carcinoma cells via suppressing VEGFR-3 pathway. Evid Based Complement Alternat Med. 2012; 2012:409823.

41. Sackton KL, Dimova N, Zeng X, Tian W, Zhang M, Sackton TB, Meaders J, Pfaff KL, Sigoillot F, Yu H, Luo X and King RW. Synergistic blockade of mitotic exit by two chemical inhibitors of the APC/C. Nature. 2014; 514:646-649.

42. Asnaghi L, Vass WC, Quadri R, Day PM, Qian X, Braverman R, Papageorge AG and Lowy DR. E-cadherin negatively regulates neoplastic growth in non-small cell lung cancer: role of Rho GTPases. Oncogene. 2010; 29(19):2760-2771.

43. Shum WW, Silva ND, Belleannée C, McKee M, Brown D and Breton S. Regulation of V-ATPase recycling via a RhoA- and ROCKII-dependent pathway in epididymal clear cells. Am J Physiol Cell Physiol. 2011; 301(1):C31-43.

44. Tsubouchi T, Soza-Ried J, Brown K, Piccolo FM, Cantone I, Landeira D, Bagci H,

Hochegger H, Merkenschlager M and Fisher AG. DNA synthesis is required for reprogramming mediated by stem cell fusion. Cell. 2013; 152(4):873-883.

45. Bennett SM, Jiang M and Imperiale MJ. Role of cell-type-specific endoplasmic reticulum-associated degradation in polyomavirus trafficking. J Virol. 2013; 87(16):8843-8852.

46. Gottwein JM, Jensen SB, Li Y-P, Ghanem L, Scheel TKH, Serre SBN, Mikkelsen L and Bukh J. Combination treatment with hepatitis C virus protease and NS5A inhibitors is effective against recombinant genotype 1a, 2a, and 3a Viruses. Antimicrob Agents Chemother. 2013; 57(3):1291-1303.

47. Nevo J, Mai A, Tuomi S, Pellinen T, Pentikäinen OT, Heikkilä P, Lundin J, Joensuu H, Bono P and Ivaska J. Mammary-derived growth inhibitor (MDGI) interacts with integrin α-subunits and suppresses integrin activity and invasion. Oncogene. 2010; 29(49):6452-6463.

48. Takeuchi Y and Fukunaga K. Differential subcellular localization of two dopamine D2 receptor isoforms in transfected NG108-15 cells. J Neurochem. 2003; 85(4):1064-1074.

49. Shioda N, Takeuchi Y and Fukunaga K. Advanced research on dopamine signaling to develop drugs for the treatment of mental disorders: proteins interacting with the third cytoplasmic loop of dopamine D2 and D3 receptors. J Pharmacol Sci. 2010;

114(1):25-31.

50. Storch J and Thumser AE. Tissue-specific functions in the fatty acid-binding protein family. J Biol Chem. 2010; 285(43):32679-32683.

51. Rousseau S, Houle F, Kotanides H, Witte L, Waltenberger J, Landry J and Huot J. Vascular endothelial growth factor (VEGF)-driven actin-based motility is mediated by VEGFR2 and requires concerted activation of stress-activated protein kinase 2 (SAPK2/p38) and geldanamycin-sensitive phosphorylation of focal adhesion kinase. J Biol Chem. 2000; 275(14):10661-10672.

52. Koch S, Tugues S, Li X, Gualandi L and Claesson-Welsh L. Signal transduction by vascular endothelial growth factor receptors. Biochem J. 2011; 437(2):169-183.

53. Claesson-Welsh L and Welsh M. VEGFA and tumour angiogenesis. J Intern Med. 2013; 273(2):114-127.

54. Dodd KM, Yang J, Shen MH, Sampson JR and Tee AR. mTORC1 drives HIF-1α and VEGF-A signalling via multiple mechanisms involving 4E-BP1, S6K1 and STAT3. Oncogene. 2015; 34(17):2239-2250.

55. Chatterjee S, Heukamp LC, Siobal M, Schöttle J, Wieczorek C, Peifer M, Frasca D, Koker M, König K, Meder L, Rauh D, Buettner R, Wolf J, Brekken RA, Neumaier B, Christofori G, et al. Tumor VEGF:VEGFR2 autocrine feed-forward loop triggers angiogenesis in lung cancer. J Clin Invest. 2013; 123(4):1732-1740.

56. Segrelles C, Ruiz S, Santos M, Martínez-Palacio J, Lara MF and Paramio JM. Akt mediates an angiogenic switch in transformed keratinocytes. Carcinogenesis. 2004; 25(7):1137-1147.

57. Davies JK, Thumser AEA and Wilton DC. Binding of recombinant rat liver fatty acid-binding protein to small anionic phospholipid vesicles results in ligand release: a model for interfacial binding and fatty acid targeting. Biochemistry. 1999; 38(51):16932-16940.

58. Davies JK, Hagan RM and Wilton DC. Effect of charge reversal mutations on the ligand- and membrane-binding properties of liver fatty acid-binding protein. J Biol Chem. 2002; 277(50):48395-48402.

59. Huang H, McIntosh AL, Martin GG, Landrock KK, Landrock D, Gupta S, Atshaves BP, Kier AB and Schroeder F. Structural and functional interaction of fatty acids with human liver fatty acid-binding protein (L-FABP) T94A variant. FEBS J. 2014; 281(9):2266-2283.

60. Martin GG, McIntosh AL, Huang H, Gupta S, Atshaves BP, Landrock KK, Landrock D, Kier AB and Schroeder F. The human liver fatty acid binding protein T94A variant alters the structure, stability, and interaction with fibrates. Biochemistry. 2013; 52(51):9347-9357.

61. Gao N, Qu X, Yan J, Huang Q, Yuan HY and Ouyang DS. L-FABP T94A decreased

fatty acid uptake and altered hepatic triglyceride and cholesterol accumulation in Chang liver cells stably transfected with L-FABP. Mol Cell Biochem. 2010; 345(1-2):207-214.

62. Chiang AC and Joan Massagué. Molecular Basis of Metastasis. N Engl J Med. 2008; 359(26):2814-2823.

63. Zhang L, Wang JN, Tang JM, Kong X, Yang JY, Zheng F, Guo LY, Huang YZ, Zhang L, Tian L, Cao SF, Tuo CH, Guo HL and Chen SY. VEGF is essential for the growth and migration of human hepatocellular carcinoma cells. Mol Biol Rep. 2012; 39(5):5085-5093.

64. Llovet JM, Ricci S, Mazzaferro V, Hilgard P, Gane E, Blanc JF, Oliveira ACd, Santoro A, Raoul JL, Forner A, Schwartz M, Porta C, Zeuzem S, Bolondi L, Greten TF, Galle PR, et al. Sorafenib in advanced hepatocellular carcinoma. N Engl J Med. 2008; 359(4):378-390.

65. Kim JH, Kim YH, Song GY, Kim DE, Jeong YJ, Liu KH, Chung YH and Oh S. Ursolic acid and its natural derivative corosolic acid suppress the proliferation of APC-mutated colon cancer cells through promotion of β-catenin degradation. Food Chem Toxicol. 2014; 67:87-95.

66. Lee K, Jeong KW, Lee Y, Song JY, Kim MS, Lee GS and Kim Y. Pharmacophore modeling and virtual screening studies for new VEGFR-2 kinase inhibitors. Eur J

Med Chem. 2010; 45(11):5420-5427.

67. Ogasawara S, Yano H, Momosaki S, Nishida N, Takemoto Y, Kojiro S and Kojiro M. Expression of matrix metalloproteinases (MMPs) in cultured hepatocellular carcinoma (HCC) cells and surgically resected HCC tissues. Oncol Rep. 2005; 13(6):1043-1048.

68. Wang G, Gong Y, Anderson J, Sun D, Minuk G, Roberts MS and Burczynski FJ. Antioxidative function of L-FABP in L-FABP stably transfected Chang liver cells. Hepatology. 2005; 42(4):871-879.

69. Yan J, Gong Y, She YM, Wang G, Roberts MS and Burczynski FJ. Molecular mechanism of recombinant liver fatty acid binding protein's antioxidant activity. J Lipid Res. 2009; 50(12):2445-2454.

70. Furuhashi M and Hotamisligil GS. Fatty acid-binding proteins: role in metabolic diseases and potential as drug targets. Nat Rev Drug Discov. 2008; 7(6):489-503.

71. Simons K and Toomre D. Lipid rafts and signal transduction. Nat Rev Mol Cell Biol. 2000; 1(1):31-39.

72. Laurentiis Ad, Donovan L and Arcaro A. Lipid rafts and caveolae in signaling by growth factor receptors. Open Biochem J. 2007; 1:12-32.

73. Staubach S and Hanisch FG. Lipid rafts: signaling and sorting platforms of cells and their roles in cancer. Expert Rev Proteomics. 2011; 8(2):263-277.

74. Besnard P, Niot I, Poirier H, Clément L and Bernard A. New insights into the fatty acid-binding protein (FABP) family in the small intestine. Mol Cell Biochem. 2002; 239(1-2):139-147.

75. Hostetler HA, McIntosh AL, Atshaves BP, Storey SM, Payne HR, Kier AB and Schroeder F. L-FABP directly interacts with PPARalpha in cultured primary hepatocytes. J Lipid Res. 2009; 50(8):1663-1675.

76. Atshaves BP, Martin GG, Hostetler HA, McIntosh AL, Kier AB and Schroeder F. Liver fatty acid-binding protein and obesity. J Nutr Biochem. 2010; 21(11):1015-1032.

77. Cohen AW, Combs TP, Scherer PE and Lisanti MP. Role of caveolin and caveolae in insulin signaling and diabetes. Am J Physiol Endocrinol Metab. 2003; 285(6):E1151-1160.

78. Chen A, Tang Y, Davis V, Hsu FF, Kennedy SM, Song H, Turk J, Brunt EM, Newberry EP and Davidson NO. Liver fatty acid binding protein (L-Fabp) modulates murine stellate cell activation and diet-induced nonalcoholic fatty liver disease. Hepatology. 2013; 57(6):2202-2212.

79. Brodsky SV, Mendelev N, Melamed M and Ramaswamy G. Vascular density and VEGF expression in hepatic lesions. J Gastrointestin Liver Dis. 2007; 16(4):373-377.

80. Heindryckx F and Gerwins P. Targeting the tumor stroma in hepatocellular carcinoma. World J Hepatol 2015 Feb 27;7(2):165-76. 2015; 7(2):165-176.

81. Ferrara N. Vascular endothelial growth factor as a target for anticancer therapy. Oncologist. 2004; 9 Suppl 1:2-10.

82. Alkozai EM, Porte RJ, Adelmeijer J, Zanetto A, Simioni P, Senzolo M and Lisman T. Levels of angiogenic proteins in plasma and platelets are not different between patients with hepatitis B/C-related cirrhosis and patients with cirrhosis and hepatocellular carcinoma. Platelets. 2014:1-6.